(4)

SOURCES OF AMBIENT NOISE IN THE OCEAN:
AN EXPERIMENTAL INVESTIGATION

National Center for Physical Acoustics

The University of Mississippi

Institute for Technology Development

A joint venture

(4)

SOURCES OF AMBIENT NOISE IN THE OCEAN: AN EXPERIMENTAL INVESTIGATION

BY

HUGH C. PUMPHREY
and
LAWRENCE A. CRUM

May 1989

Technical Report
prepared for:

Office of Naval Research
Ocean Acoustics Division
Contract # N0014 - 87 - K - 0019

Previously issued as
A Dissertation
Submitted to the Faculty of
the University of Mississippi
in Partial Fulfillment of the Requirements
for the Degree of Doctor of Philosophy
in the Department of Physics and Astronomy

UNCLASSIFIED
SECURITY CLASSIFICATION OF THIS PAGE

REPORT DOCUMENTATION PAGE

Form Approved
OMB No. 0704-0188

1a. REPORT SECURITY CLASSIFICATION Unclassified	1b. RESTRICTIVE MARKINGS
2a. SECURITY CLASSIFICATION AUTHORITY	3. DISTRIBUTION / AVAILABILITY OF REPORT Approved for public release Distribution unlimited
2b. DECLASSIFICATION / DOWNGRADING SCHEDULE	
4. PERFORMING ORGANIZATION REPORT NUMBER(S) NCPA-LC-01-1989 ✓	5. MONITORING ORGANIZATION REPORT NUMBER(S)
6a. NAME OF PERFORMING ORGANIZATION National Center for Physical Acoustics 6b. OFFICE SYMBOL (If applicable) LC	7a. NAME OF MONITORING ORGANIZATION Office of Naval Research
6c. ADDRESS (City, State, and ZIP Code) NCPA P. O. Box 847 University MS 38677	7b. ADDRESS (City, State, and ZIP Code) Department of the Navy Arlington VA 22217
8a. NAME OF FUNDING / SPONSORING ORGANIZATION 8b. OFFICE SYMBOL (If applicable)	9. PROCUREMENT INSTRUMENT IDENTIFICATION NUMBER
8c. ADDRESS (City, State, and ZIP Code)	10. SOURCE OF FUNDING NUMBERS PROGRAM ELEMENT NO. / PROJECT NO. / TASK NO. / WORK UNIT ACCESSION NO.

11. TITLE (Include Security Classification)
Sources of Ambient Noise in the Ocean: an Experimental Investigation

12. PERSONAL AUTHOR(S)
Pumphrey, Hugh C.; Crum, L. A.

13a. TYPE OF REPORT	13b. TIME COVERED	14. DATE OF REPORT (Year, Month, Day)	15. PAGE COUNT
Technical	FROM 86/7/1 TO 89/5/31	1989 May 12	96

16. SUPPLEMENTARY NOTATION

17. COSATI CODES			18. SUBJECT TERMS (Continue on reverse if necessary and identify by block number)
FIELD	GROUP	SUB-GROUP	Physical Acoustics Rain noise Fluid Mechanics Sea Surface Noise Drop impacts

19. ABSTRACT (Continue on reverse if necessary and identify by block number)

The general characteristics of underwater sound produced at the ocean surface have been known for many years and recent measurements have also described the sound of rainfall. The mechanisms which produce these sounds have remained a mystery. This report describes a series of laboratory experiments in which various simple mechanisms in the 0.5-100 kHz frequency range were examined.

A large part of the work describes the sounds made by the impact of a drop of water on the water surface. It is found that two types of sound are emitted: first, a sharp spike radiated when the drop first strikes the surface and second, a damped sinewave emitted when a bubble is entrained below the water surface. Previous authors thought that bubbles were unimportant because the initial impact sound occurs for every drop impactwhile bubbles are only entrained occasionally. This report shows that for a certain range of drop sizes and velocities a bubble will always be entrained; this phenomenen has been named regular entrainment.

20. DISTRIBUTION / AVAILABILITY OF ABSTRACT	21. ABSTRACT SECURITY CLASSIFICATION
☐ UNCLASSIFIED/UNLIMITED ☒ SAME AS RPT. ☐ DTIC USERS	Unclassified
22a. NAME OF RESPONSIBLE INDIVIDUAL Lawrence A. Crum	22b. TELEPHONE (Include Area Code) (601) 232-5815
	22c. OFFICE SYMBOL LC

DD Form 1473, JUN 86 *Previous editions are obsolete.* SECURITY CLASSIFICATION OF THIS PAGE

Unclassified

The hydrodynamics of a drop impact are discussed in an attempt to show why regular entrainment occurs; a qualitative explanation is described but it was found that the process was too complicated to be explained in terms of simple analysis and that it would be necessary to use computer modelling.

The sound of rainfall on water is studied in detail; an important feature of the acoustic spectrum is a peak at about 14 kHz. It is shown that this peak is caused by regular entrainment and not by initial impacts as one author has suggested. Experimental results enable us to predict the spectrum levels which rain of a given intensity would produce; the predictions compare reasonably well with real rain data.

Other experiments examined the sounds of a breaking wave and of bubbles interacting with a submerged jet of water. The results are helpful in selecting which of the many published theories of sea surface noise is the most likely. It is suggested that free oscillations of bubbles which have just been entrained or broken up cause most of the sound at frequencies above 500 Hz.

SOURCES OF AMBIENT NOISE IN THE OCEAN:
AN EXPERIMENTAL INVESTIGATION

BY

HUGH CHARLES PUMPHREY

H. E. Bass

Dr. H. E. Bass,
F. A. P. Barnard Distinguished Professor

L. A. Crum

Dr. L. A. Crum,
F. A. P. Barnard Distinguished Professor

R. R. Goodman

Dr. R. R. Goodman,
Professor of physics

K. E. Gilbert

Dr. K. E. Gilbert,
NCPA Senior Scientist

Dr. R. Hickling,
Research Professor of Engineering

J. A. Roux

Dr. J. A. Roux,
Professor of Mechanical Engineering

Dr. M. R. Dingerson,
Dean of the Graduate School

ACKNOWLEDGEMENTS

I would like to thank everyone who has helped me to complete this dissertation, especially the following:

Dr L. A. Crum for directing the dissertation and for being a constant source of help and guidance.

Dr A. Prosperetti for supplying an endless stream of ideas.

The faculty and graduate students of the Physics Department and the National Center for Physical Acoustics for their help, advice and friendship, especially Dr Henry E. Bass, Dr Ron Roy, Dr Charles Church, Dr Brian Fowlkes, Dr Glynn Holt, Steve Horsburgh and Felipe Gaitan.

The secretarial staff of the said institutions for their patience, especially Mrs Sandra Smith and Mrs Linnea Weddington.

My dissertation committee for their helpful suggestions

Steve Horsburgh (again) for rescuing various computers from the trouble which I got them into.

Dr Alan J. Walton for directing my undergraduate research, and thereby getting me interested in water noises in the first place.

Lastly to my wife Lucy for her love, patience, and tolerance of the ill humor which the writing of this dissertation has caused.

This work was supported by the National Center for Physical Acoustics, The Johns Hopkins University and the Office of Naval Research.

ABSTRACT

SOURCES OF AMBIENT NOISE IN THE OCEAN: AN EXPERIMENTAL INVESTIGATION

PUMPHREY, HUGH CHARLES. B.A., Jesus College, Cambridge, 1986. Ph.D., University of Mississippi, 1989. Dissertation directed by Dr. L. A. Crum, F. A. P. Barnard Distinguished Professor.

The general characteristics of underwater sound produced at the ocean surface have been known for many years and recent measurements have also described the sound of rainfall. The mechanisms which produce these sounds have remained a mystery. This dissertation describes a series of laboratory experiments in which various simple mechanisms in the 0.5-100 kHz frequency range were examined.

A large part of the work describes the sounds made by the impact of a drop of water on the water surface. It is found that two types of sound are emitted: first, a sharp spike radiated when the drop first strikes the surface, and second, a damped sinewave emitted when a bubble is entrained below the water surface. Previous authors thought that bubbles were unimportant because the initial impact sound occurs for every drop impact while bubbles are only entrained occasionally. This dissertation shows that for a certain range of drop sizes and velocities a bubble will always be entrained; this phenomenon has been named regular entrainment.

The hydrodynamics of a drop impact are discussed in an attempt to show why regular entrainment occurs; a qualitative explanation is described but it was found that the process was too complicated to be explained in terms of simple analysis and that it would be necessary to use computer modelling.

The sound of rainfall on water is studied in detail; an important feature of the acoustic spectrum is a peak at about 14 kHz. It is shown that this peak is caused by regular entrainment and not by initial impacts as one author has suggested. Experimental results

enable us to predict the spectrum levels which rain of a given intensity would produce; the predictions compare reasonably well with real-rain data.

Other experiments examined the sounds of a breaking wave and of bubbles interacting with a submerged jet of water. The results are helpful in selecting which of the many published theories of sea surface noise is the most likely. It is suggested that free oscillations of bubbles which have just been entrained or broken up cause most of the sound at frequencies above 500 Hz.

TABLE OF CONTENTS

LIST OF TABLES

LIST OF FIGURES

CHAPTER I: INTRODUCTION

A Historical review

It was known to Leonardo daVinci [1,2] that the sounds made by ships travel for large distances through the water, but the widespread use of this fact to detect enemy shipping did not begin until the First World War. During the Second World War, with the advent of sensitive hydrophones and electronic amplification, it became clear that the ocean had a distinctive background noise of its own. The first extensive study of this ambient noise was made during the war, by Knudsen [3] et al., and published in 1948; the paper contains many interesting details of the sounds produced by ships and marine life. More importantly for our purposes, it describes the sound produced by the ocean surface due to the action of the wind and waves, the famous Knudsen spectrum. This spectrum always has a slope of about -5 dB / octave; the intensity increases with the wind speed. Knudsen did not have directional hydrophone arrays and he seems to have thought the ambient noise field to have been isotropic. He did, however, recognize that the sound was intermittent, describing how it was possible to hear noises from individual whitecaps if the hydrophone was near the surface. The fact that the sound is largely produced by breaking waves is the first step to understanding the exact mechanism of its production, but Knudsen did not speculate further on the matter.

Knudsen's results only cover the frequency range 100 Hz to 25 kHz, but by 1962, when Wenz [4] published his extensive review paper on ambient noise, a more complete picture had emerged. Wenz divided the acoustic spectrum into three overlapping regions, each of which he thought corresponded to a different source mechanism; the regions were: I) 1 Hz to 100 Hz, II) 10 Hz to 1 kHz, III) 100 Hz to 20 kHz. These divisions have been largely corroborated by later studies [5,6].

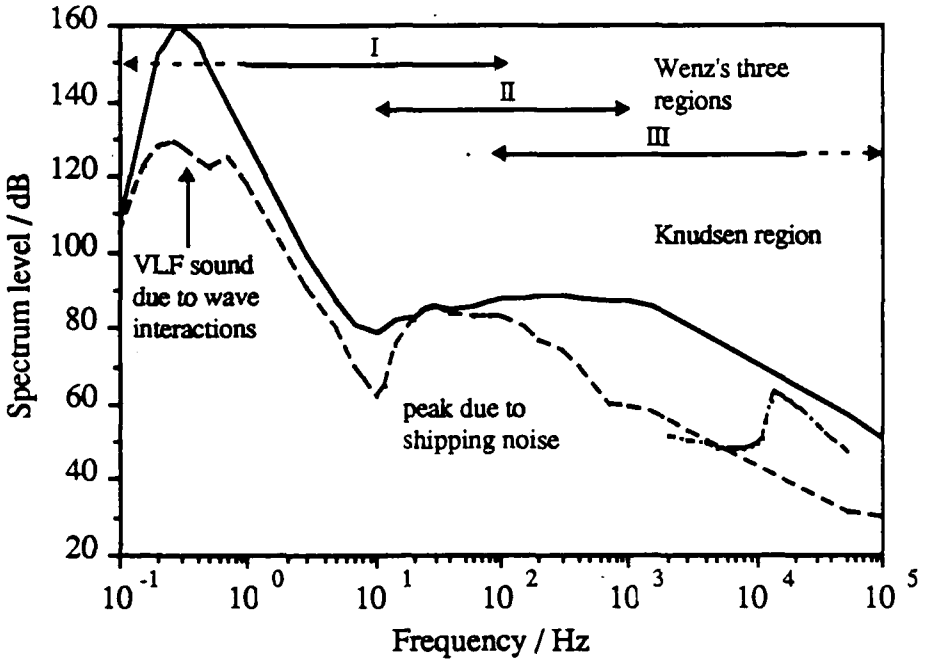

Fig. 1. This graph shows the general form of ambient noise spectra at two different wind speeds: 5 m/s (Force 3); dashed line and 30 m/s (Storm force 11); solid line. These spectra were drawn with the aid of figures in papers by both Wenz and Kibblewhite. Note how the 5 m/s spectrum changes character at about 500 Hz, the Knudsen spectrum peaking out and being replaced at lower frequencies with shipping noise. Only at very high wind speeds does some sort of sea noise swamp out the shipping in region II. The figure also shows the spectrum of rainfall in calm conditions (dot-dash line). The dB reference level is 1 μPa^2/ Hz.

Measurements from region I were scanty in Wenz's day and even nowadays tend to be conflicting and confusing. Wenz describes the spectrum as having a slope of -8 to -10 dB / octave and suggests that the main cause is local pressure fluctuations caused by turbulence and that the spectrum is therefore not really acoustic in nature. Additional sources which he thought to be significant were earthquakes and waves. The first order pressure variation under a wave due to its height is sharply attenuated with depth and is therefore only significant at very low frequencies in very shallow water. If, however, there are two waves travelling in opposite directions which interact, they produce a second order pressure variation which is not attenuated with depth [7]. Subsequent work [8] suggests that

this mechanism is in fact more important than turbulence effects, especially for frequencies below 5 Hz, and may also be the cause of the seismic background noise known as microseisms. It is perhaps worth mentioning that Marsh [9] (writing at the same time as Wenz) explained the entire Knudsen spectrum in terms of this wave-wave interaction mechanism, but his conclusion is at variance with all subsequent writing on the subject and must be regarded as suspect. In fact, Kerman [10] has asserted that Marsh's analysis is only valid for frequencies below 10 Hz. It is also not in agreement with the experimental observation that the sound is associated with breaking waves.

Region II is a transition region between regions I and III but in many parts of the ocean it is dominated by the sounds of distant shipping. These sounds may travel very large distances along an acoustic waveguide formed by the change with depth of the speed of sound in the ocean. Directionality measurements [11,12] show that noise in this frequency range tends to arrive at the hydrophone in a horizontal direction, especially in calm weather, although there is a wind-dependent component which arrives vertically, due to the overlap with region III.

Region III is the Knudsen region: Wenz's survey confirms the general form of Knudsen's results but adds the fact that they are applicable to shallow seas and that the levels in the deep oceans are 5 dB lower on average. This effect seems to be largely due to the greater reverberation which occurs in shallow water. Wenz also showed that there is a peak at about 500 Hz in this part of the spectrum and that at lower frequencies the mechanism responsible for the Knudsen spectrum is masked by shipping noises; below 100 Hz it is not significant at all. Later work with directional arrays [11-13] has shown that the sound not only comes from the surface, but from sporadic, localized events at the surface, much as Knudsen had suspected. These events are presumably breaking waves,

which, like the sound spectrum, are known to be highly dependent on wind speed and sea state but the actual mechanism by which a breaking wave generates sound remains unclear. Wenz suggests several possibilities: free oscillations of air bubbles, cavitation, i.e. the violent collapse of a vapor-filled bubble and the impact of water droplets and spray. Subsequent work has discussed these mechanisms in great detail but there has been no agreement about which is the most important. Ffowcs Williams and Guo [14,15] have proposed the idea that momentum fluctuations associated with splashing water sprays are the dominant mechanism, and that bubbles near the surface cannot radiate because reflections from the surface cancel out the wave. This argument is not entirely valid, as I shall demonstrate and indeed Ffowcs Williams has included bubbles as a significant source in a more recent paper [16]. Prosperetti and Kerman are in favour of bubble related theories as are Shang and Anderson, who suggest both cavitation and the sound of bubbles bursting at the surface as possibilities. Prosperetti and Lu [17], however, have pointed out that the necessary conditions for cavitation, i.e. for the violent collapse of a vapor-filled cavity, are never satisfied in the ocean. They also argue against the bursting bubble theory, Prosperetti [18] preferring one involving the free oscillations of bubbles, excited by formation, coalescence, fission and so on; this is similar to the theory of Hollet and Heitmeyer [19].

In order to make further progress in understanding the Knudsen spectrum it is necessary to study some of the above processes in the laboratory. The first attempts to do this kind of experiment were made by Franz [20], who studied the sounds produced by a drop of water striking a water surface. He discovered that a drop impact may produce two sorts of sound: a sharp pulse when the drop touches the surface and a decaying sinewave when a bubble is formed. The sharp pulse occurs with every drop but bubbles are only

entrained occasionally so Franz was unsure of their importance. He attempted to model the noise made by rain falling onto the ocean by studying the sound produced by a shower of drops falling onto the surface of a large tank. Franz concluded that rain should produce a spectrum rather similar to the Knudsen curves at high frequencies, with a broad peak at 2-3 kHz, and that the sound made by the drops striking the water was more important than the sounds emitted by any bubbles which chanced to be entrained. Unfortunately, he had no good field measurements with which to make a comparison. The first suitable measurements were made by Bom [21] in a small lake in Italy; the agreement with Franz's predictions was not very good. Bom's measurements were only made for frequencies below 10 kHz, which was rather unfortunate (for him) because it meant that he missed the most remarkable and persistent feature of rain noise, namely a peak at a frequency of about 14 kHz with a steep slope on the low frequency side and a less steep one of -9 dB / octave on the high frequency side. This peak was not discovered until 1985, when two independent groups [22, 23] reported the effect; it has been observed several times since then [24, 25]. The peak must be caused by one or other of Franz's two mechanisms; a theoretical investigation by Nystuen [23, 26] suggests that the initial impact is the source and that bubbles may be ignored because they are not produced by every drop.

The idea of this project was to carry out a series of simple laboratory experiments in order to gain a better understanding of how the ocean surface produces sound, particularly in the Knudsen region of the spectrum. Because of the relative simplicity of the process, the first experiments studied the sound produced by a drop of water impacting the water surface. These experiments confirm Franz's work but also show some interesting new effects, which have permitted the explanation in terms of bubble sounds of the peak in the rain noise spectrum. This work makes up a large part of this dissertation, but it does not

help much in understanding the Knudsen curves, so various other experiments were carried out to study the sound produced by breaking waves, bursting bubbles and bubbles interacting with turbulence. The results were not as clear-cut as those from the single-drop work, but they should nevertheless be useful in future studies of ambient ocean sound. First, since they are obviously of some importance, a brief review of some bubble dynamics and acoustics is included.

B. Review of necessary bubble dynamics and acoustics.

We shall begin by considering bubble oscillations which are small and radial, i.e. the bubble remains spherical but its volume varies slightly. We give the bubble a radius a, an equilibrium radius a_0 and let the wall displacement, $a - a_0$, be x. Since the displacement is small we can regard the bubble as a damped harmonic oscillator with the following equation of motion:

$$\ddot{x}+2\beta\dot{x}+\omega_o^2 x=0 , \tag{1}$$

where ω_0 is the natural angular frequency in the absence of damping, β is a damping parameter and the dots denote differentiation with respect to time. This means that x oscillates sinuosoidally with an exponentially decaying amplitude thus:

$$x = x_i e^{-\beta t} \cos(\omega t+\phi), \tag{2}$$

where ω is the angular frequency and ϕ is an arbitrary phase constant. The subscript i will be used throughout to mean an initial value. The wall velocity, U, is given by

$$U = -U_i e^{-\beta t} \sin(\omega t+\phi), \tag{3}$$

with $U_i = \omega x_i$. We will follow standard practice and define a damping constant $\delta = 2\beta / \omega_0$ and a quality factor $Q = 1 / \delta$. For frequencies relevant to this study,

bubbles have Q values greater than 6, which means that we may ignore the small difference between ω and ω_0.

The first attempt to calculate the resonance frequency as a function of the bubble radius was made by Minnaert [27] in 1933. He calculated the maximum kinetic energy of the water outside the bubble and set it equal to the maximum potential energy of the compressed gas inside, on the basis that in any simple harmonic oscillator the energy moves from being all potential to being all kinetic and then back again. The end result is the famous Minnaert formula:

$$\omega = \frac{1}{a_0}\left(\frac{3\kappa P_o}{\rho}\right)^{\frac{1}{2}}, \qquad (4)$$

in which P_0 is the pressure inside the bubble, ρ is the density of water and κ is the polytropic exponent of the gas in the bubble. Unless the bubble is very small, we can assume for practical purposes that P_0 is close to the atmospheric pressure P_A. Minnaert assumed that the gas was compressed and expanded adiabatically so that $\kappa = \gamma$, the ratio of the specific heats.

Minnaert made no attempt to study the damping of a bubble, but subsequent authors have identified three different damping mechanisms, which were first combined and compared with experimental results by Devin [28]; his results have since been confirmed by other theoretical studies [29-31]. The first mechanism results from the fact that the gas inside the bubble does not behave quite adiabatically, in fact the thin layer of gas which is close to the bubble wall behaves almost isothermally. The time taken for heat to diffuse from this layer into the rest of the bubble introduces a phase difference between the pressure in the

bubble and its volume and hence a certain amount of hysteresis. The end result is that mechanical energy is converted to thermal energy and diffuses away into the water.

An oscillating bubble is an acoustic source and therefore some of its energy is lost in the form of sound waves; this mechanism is most important if the bubble is large. If it is very small some additional damping may be caused by viscous losses. If we call the thermal damping constant δ_{th}, the acoustic δ_{ac} and the viscous δ_{vs}, then the total damping constant δ is given by $\delta = \delta_{ac} + \delta_{th} + \delta_{vs}$. Figure 2 shows how the various damping constants vary with resonance frequency.

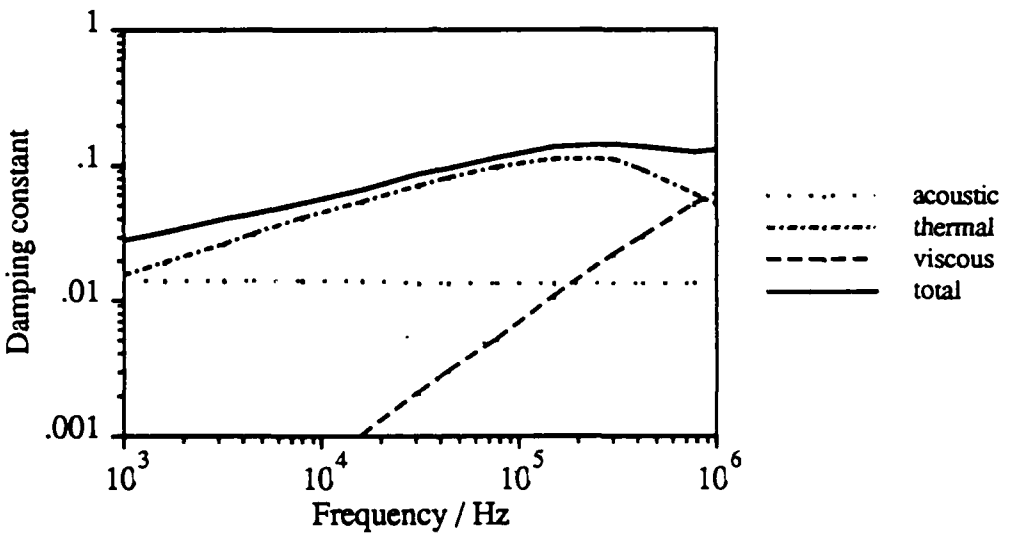

Fig. 2. This graph shows the total damping constant δ (solid line) and its three components δ_{ac} (dots), δ_{th} (dot-dash) and δ_{vs} (dashes).

So far, we have assumed that the bubble is in an infinite volume of water, but for ambient noise applications we often need to consider a bubble which is very close to the surface. Strasberg [32] has calculated the effect that this has on the resonance frequency, in general this is not large: if a bubble has its center four radii below the surface, the frequency will be raised by 7%. The surface has a greater effect on the damping constant

because it effectively changes the bubble from a monopole source to a dipole. This greatly reduces the energy which is lost as sound and hence reduces the acoustic damping essentially to zero at low frequencies. Crowther [33] has shown that δ_{ac} is in fact reduced to a dipole damping constant, δ_{dip}, given by:

$$\delta_{dip} = \frac{2}{3}\left(\frac{2\pi f l}{c}\right)^2 \delta_{ac} \quad , \tag{5}$$

provided that l is much smaller than the wavelength λ. In this expression l is the depth of the bubble center below the surface, f is its frequency of oscillation and c is the speed of sound.

We now consider the sound field radiated by a freely oscillating bubble. If the bubble is in a large volume of water the far-field acoustic pressure, p, at a distance r from the bubble, is given by

$$p = \frac{i\rho c U_i e^{-\beta(t-r/c)} k a_o^2}{r} e^{i(\omega t - kr)} \quad , \tag{6}$$

where c is the speed of sound and k is the wavenumber, $k = 2\pi / \lambda$. The imaginary number $i = \sqrt{-1}$ simply means that there is a phase shift of 90° between U and p. This is a standard result for a simple spherical source, as described in many acoustics texts [34]. It assumes that $ka_o \ll 1$; for bubbles oscillating at their resonance frequencies $ka_o \sim 0.014$ so the condition is always satisfied.

Since our bubbles will usually be close to the surface, we must include the effect of this on the sound field. The free surface is a pressure release boundary so the acoustic pressure at the surface is always zero. If the bubble is very close to the surface, so that $kl \ll 1$, we can calculate the sound field of a bubble near a free surface by introducing an image source of equal strength and 180° out of phase as shown in Fig. 3.

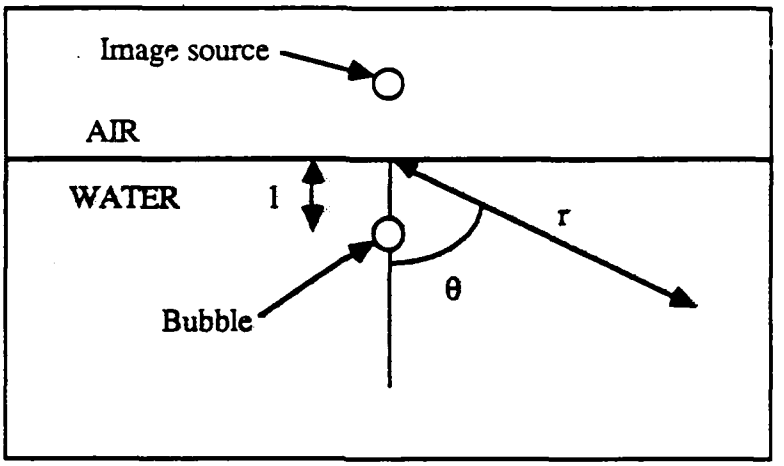

Fig. 3. Sketch showing how a near-surface bubble behaves as a dipole source.

The effect of the image source is to cancel out the sound from the actual bubble to a certain extent. Along the water surface the sounds from the two sources are 180° out of phase, so the total sound field is zero; elsewhere, however, the phase difference is not quite 180° so the sounds do not quite cancel. The largest phase difference occurs in the vertical direction and is equal to 2kl, so it is not surprising that the radiation field for this dipole is obtained (apart from its phase) by multiplying Eq. (6) by 2klcosθ, where θ is the polar angle. The result is that

$$p(r,\theta,t) = \frac{2\rho c U_i e^{-\beta(t-r/c)} k^2 a_o^2 l}{r} \cos\theta \, e^{i(\omega t - kr)} \tag{7}$$

or equivalently

$$p = \frac{D}{r} e^{-\beta(t-r/c)} \cos\theta \, e^{i(\omega t - kr)} \tag{8}$$

where the initial dipole strength D is given by $D = 2\rho c U_i k^2 a_o^2 l$. Note that this is a far-field result; it assumes $kr > 1$. This pressure is smaller than that of a bubble in a large volume of water, as described in Eq. (6), but it is not zero and we shall find that it is not negligible as Ffowcs Williams and Guo [14,15] have implied. Note that to calculate D, we need a value for

U_i, the initial wall velocity of the newly formed bubble. This velocity could be provided by a variety of mechanisms such as the extra internal pressure due to surface tension, the hydrostatic pressure due to the bubble's depth below the surface or possibly distortions of the bubble's shape.

Now that the expected behavior of a bubble has been discussed, the experimental methods used will be described.

CHAPTER II: EXPERIMENTAL METHODS

As stated in the introduction, the aim of this project was to make a laboratory study of processes at the sea surface which might cause ambient noise. The studies were made in a large wooden tank 1m x 1m x 1m in size, or, when photographs were being taken, in a 10 gallon aquarium. The large tank had a time of flight for sound to reach the bottom and return to the surface of about 1.2 ms, which meant that sound pulses shorter than this could be studied without interference from reverberations. The tank had a lowest resonance frequency of approximately 1.5 kHz and many resonances at higher frequencies. Below 10 kHz these could be seen in most of the frequency spectrums which were made, but above 10 kHz they blurred together into a continuum, allowing reasonably good measurements of spectral shape, though not absolute spectrum level.

The process which was examined in the greatest detail was the impact of a water drop on the water surface. Drops with diameters greater than 2.2 mm were produced by allowing water to drip from hypodermic needles of various sizes; the water was fed to the needle from a small reservoir via a tap. Drop sizes were measured either by counting drops into a measuring cylinder or by catching individual drops and drawing them into a microliter syringe; in each case the measured volume was used to calculate the diameter of a sphere with that volume. It was possible to produce drops with a repeatability of about 0.1 mm. Drops with diameters smaller than 2.2 mm are rather difficult to produce one at a time; two alternative methods were used to circumvent this problem. Firstly, single drops were produced by drawing the relevant volume of water into a microliter syringe, expelling it to form a drop on the end of the syringe and persuading it to fall by tapping the apparatus. This is slow and laborious and usually gives the drop some horizontal velocity. As an alternative, a spray of small drops was produced by pumping water through a

hypodermic needle so that it formed a stream which broke up into droplets. The size range of these droplets was monitored by catching samples on a glass plate and measuring their volumes with the microliter syringe. In earlier experiments, a spray which covered a larger area of the tank was also used; this was produced by pumping water into a 1/2" diameter pipe which had a line of small holes drilled in the side and will be referred to as spray #1; the spray produced by the needle will be referred to as spray #2.

The impact velocity, v_I, of the drops was controlled by varying the height of fall, z, and was calculated from the equation [35]

$$v_I = v_T\left[1-\exp\left(\frac{-2gz}{v_T^2}\right)\right]^{\frac{1}{2}}, \qquad (9)$$

where g is the acceleration due to gravity. The terminal velocity v_T was calculated from the drop diameter by a polynomial fit to a set of experimental data. (See appendix A for details).

Various other mechanisms were studied, the most important being a breaking wave and bubbles interacting with turbulence. The wave was a standing wave, made by allowing water to flow along a narrow plexiglass channel with an obstruction halfway along it. A turbulent region was made by pumping water into a tank through a narrow pipe to form an underwater jet, into which bubbles were introduced by pumping air through a hypodermic needle.

In all studies the sound was detected with a miniature hydrophone (B&K 8103) and amplified by a conditioning charge amplifier (B&K 2635). From there, the signal was usually passed to a digital oscilloscope (LeCroy 9400) which was capable of capturing transient signals, doing FFT's and averaging them to give a power spectrum and performing various other signal processing tasks. The oscilloscope was interfaced via a

GPIB bus to a computer (DEC MINC-73) which did additional signal processing. Many of the signals studied were damped sinusoids emitted by oscillating bubbles and the computer was used to make repetitive measurements of the frequencies and damping constants of these signals. The computer also enabled power spectra generated by the oscilloscope to be plotted on a logarithmic frequency axis.

The sound-producing processes were also studied by high-speed movie photography. The camera used was a Photec IV and was usually run at a speed of 1000 or 2000 frames per second. The water was photographed against a brightly lit background and the view was usually horizontal through the glass wall of the tank. In addition to photographing the water an oscilloscope trace was also recorded on the film, providing a simultaneous record of the behavior of the water and the sound which it was producing. Figure 4 shows a sketch of the experimental apparatus.

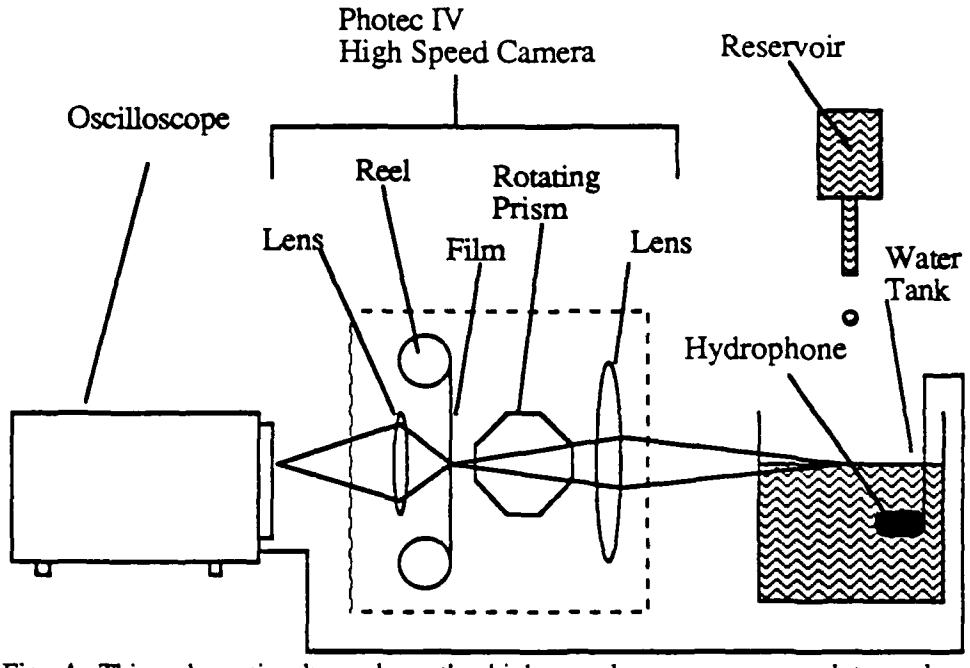

Fig. 4. This schematic shows how the high speed camera was used to make a simultaneous record of the movement of the water and the sound produced. The camera is a rotating prism type, which means that the film moves continuously from reel to reel; the rotating prism makes the image of the water move along with the film. The oscilloscope is set in the x-y mode and the signal is fed to the x input so that it deflects the beam perpendicular to the plane of the schematic. This means that the image of the "spot" moves sideways across the film while the film moves continuously past it.

The film used was either Kodak RAR 2498 monochrome reversal or Kodak ektachrome video news color reversal. The RAR 2498 seemed to give slightly smaller grain but had a slower film speed. We had to switch to the color film because the developing lab ceased developing of black and white reversal. The developed films were studied with a stop-motion projector (L-W 224-S-MK VIII); measurements of drop and bubble sizes, positions, velocities and so on were made by projecting the image onto graph paper. In most films an object of known size was placed in the field of view to provide a scale.

CHAPTER III: RESULTS-SINGLE DROP IMPACTS

A. General observations

Figure 5 shows examples of the acoustic pressure traces produced by the impact of 5.6 mm diameter drops impacting with velocities of 5.2 m/s.

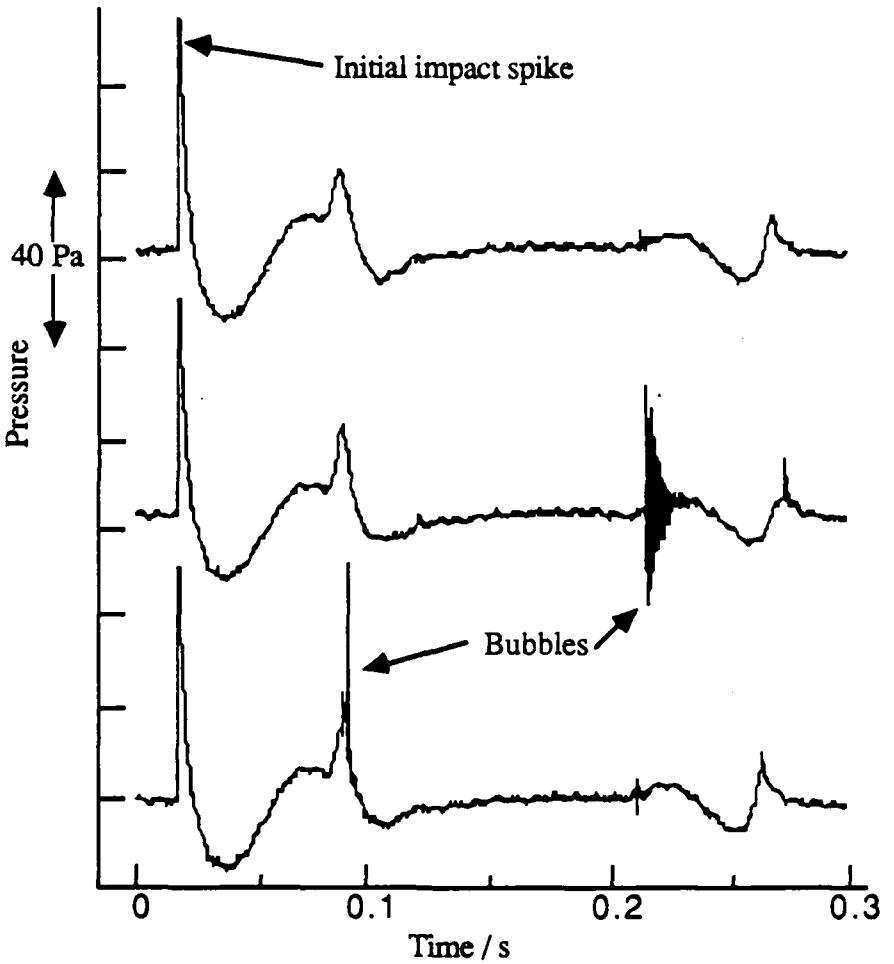

Fig. 5. Three pressure traces caused by drops of 5.6 mm diameter impacting at a speed of 5.2 m/s. The hydrophone is 40 mm below the impact site. The bubble sounds would be damped sinusoids if shown on an expanded timescale. These traces look a little noisy because they are genuine data, taken directly from the digital oscilloscope, without any smoothing.

The results are similar to those of Franz in that there is always a sharp spike followed by a low-frequency oscillation and there are also damped sinusoids produced by bubbles which seem to occur more or less randomly. These results are typical for large drops and high impact velocities [20, 36, 37].

For small enough drops, a slightly different process occurs as shown in Fig. 6.

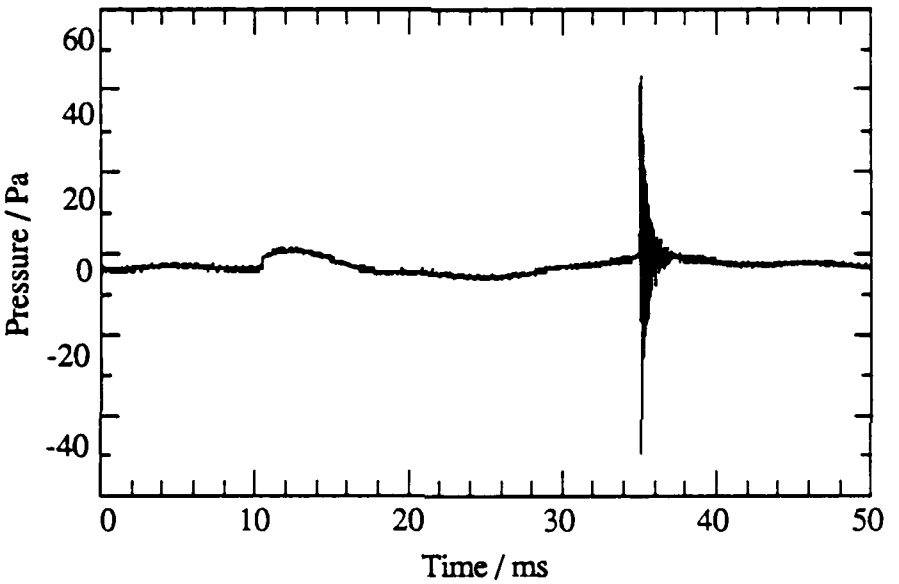

Fig. 6. Pressure trace caused by the impact of a 3.4 mm diameter drop at a velocity of 1.7 m/s. The hydrophone was 25 mm below the point of impact. In this case the bubble entrainment is *repeatable*, unlike that in Fig. 5.

As before, we see the initial impact sound followed by a bubble oscillation but now the bubble occurs predictably, at the same time after the impact, with about the same frequency, for every drop. This process has not been observed before; I have named it regular entrainment [36, 37] and will use the term irregular entrainment to describe the unpredictable bubble formation discovered by Franz and shown in Fig. 5.

Figure 7 shows a sequence of frames from a high speed movie film of the irregular entrainment process. The initial impact sound begins at the top of frame c and is the reason

why the trace is displaced to the right in frame d. In frame f a very small drop is seen falling towards the crater; this drop detached from the dropper at the same time as the main drop. The impact of this little drop causes a small cavity to appear at the bottom of the main crater (frame g), this closes to form a bubble (frame h); note the sound produced by this bubble. Next, a column of water is thrown up and collapses to entrain another bubble some time between frames l and m. By this time the top of the column has detached to form another drop, the impact of this drop could entrain yet another bubble.

Fig. 7. (over page). This is a sequence of frames from a high speed movie of the irregular entrainment process as caused by a drop of 5.8 mm in diameter impacting at a speed of 2.4 m/s. The original movie was taken at a speed of 4000 frames per second but these frames originate from the beginning of the film where it was still accelerating. The frames are in the correct order, of course, but are not necessarily sequential, e.g. there were many frames on the original film between frames h and i, which are not shown in the figure. Times in milliseconds after the initial impact for each frame are as follows: (a): -9 ms, (b): -0.5 ms, (c): 0 ms, (d): 4 ms, (e): 14 ms, (f): 30 ms, (g): 46 ms, (h): 49 ms, (i): 90 ms, (j): 127 ms, (k): 148 ms, (l): 159 ms, (m): 159.3 ms, (n): 177 ms. Note that l and m are consecutive frames; the film had accelerated to about 3000 frames / sec at this point. The bubble in frame h had a measured diameter of 1.2±0.2 mm and a frequency of 5.4±0.3 kHz; Minnaert's equation gives a frequency of 5.5±1 kHz for this bubble size. For the bubble in frame m the values are similar.

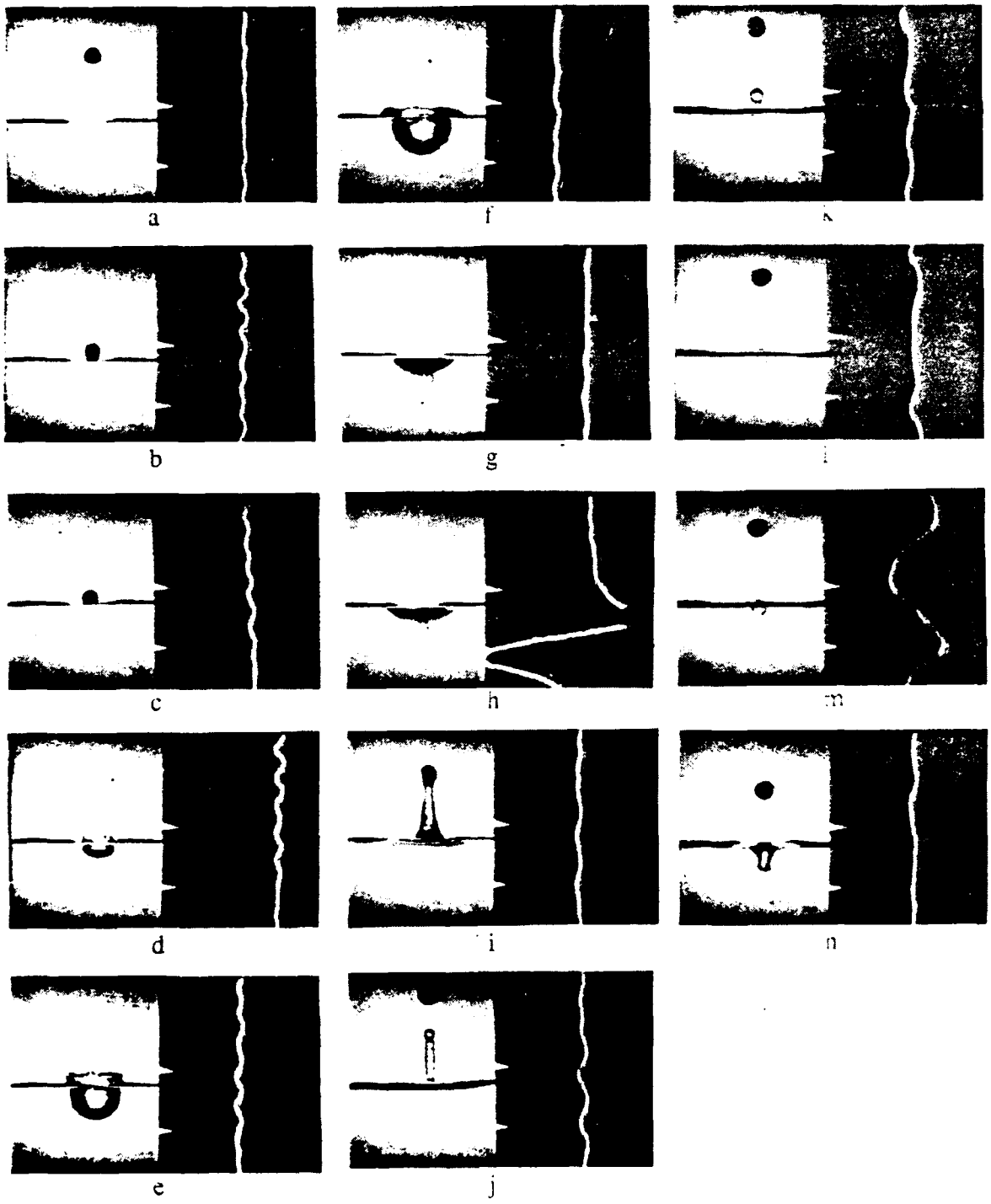

Figure 7.

Fig. 8. (over page) Frames from a high speed movie showing regular entrainment as caused by a drop of 3.2 mm diameter impacting at 1.5 m/s. As in Fig. 7, the frames are in order but are not necessarily consecutive. The black object at the lower edge of the picture is the hydrophone. The camera was running at 950 frames / sec so one frame is slightly greater than 1 ms. Times in milliseconds (correct to 0.5 ms) after the initial impact for each frame are as follows: (a): -3 ms, (b): 0 ms, (c): 1 ms, (d): 2 ms, (e): 4 ms, (f): 6.5 ms, (g): 9.5 ms, (h): 13.5 ms, (i): 16 ms, (j): 18 ms, (k): 19 ms, (l): 20 ms, (m): 21 ms, (n): 22 ms, (o): 26 ms. The entrained bubble had a measured diameter of 0.89±0.08 mm and a frequency of 6.5±0.2 kHz; Minnaert's equation gives a frequency of 7.4±.6 kHz for this bubble size.

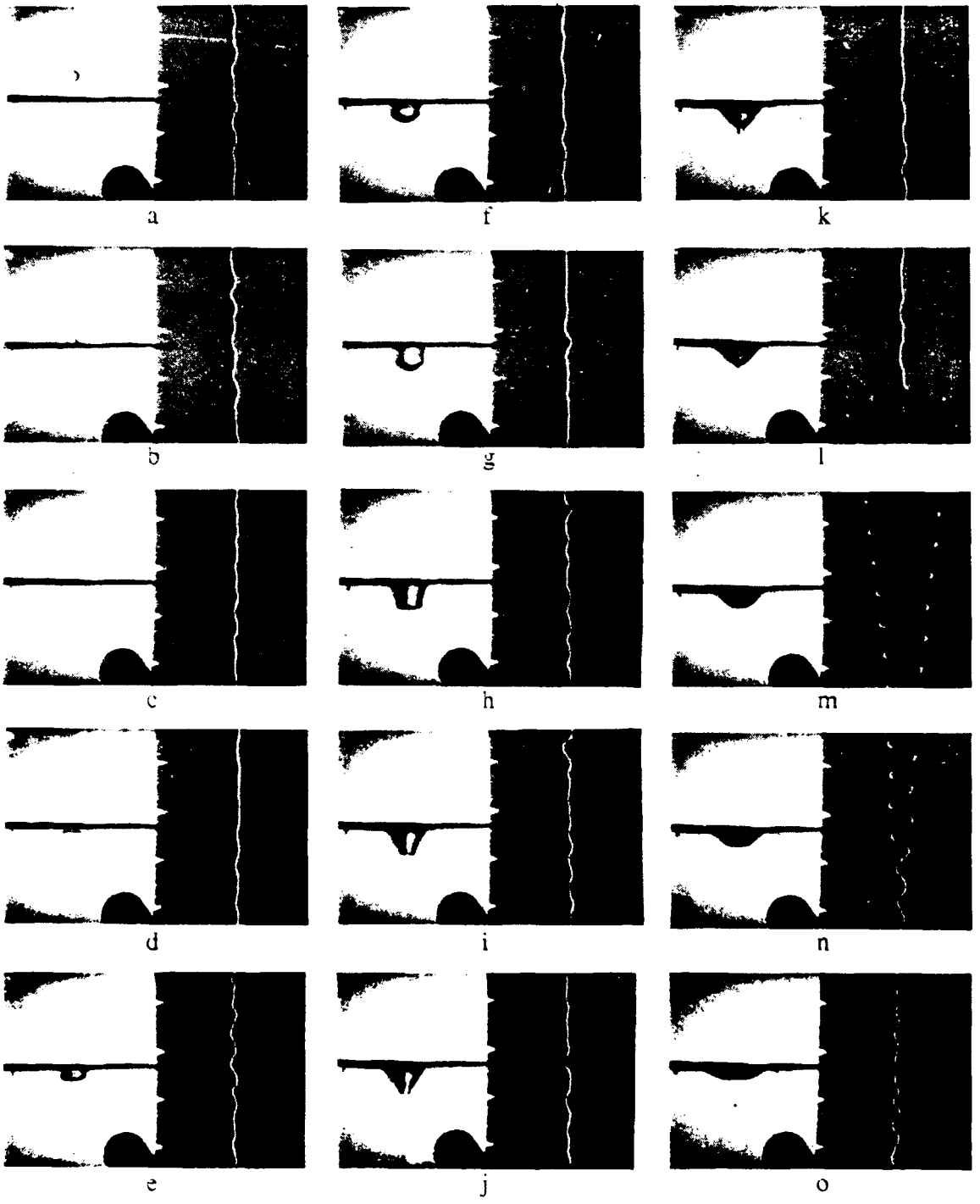

Figure 8.

Regular entrainment is shown in Fig. 8, the initial impact sound in frame b is lost in the noise of the movie camera but the bubble sound in frames l-n is clearly seen. Note that the process is repeatable partly because it does not rely on precise timing of impacts of secondary drops as irregular entrainment seems to. Before studying the bubble processes further we shall describe the initial impact sound in more detail.

B. The initial impact sound

The form of the initial impact sound is shown in detail in Fig. 9. It consists of a low frequency oscillation of about one cycle, with a very steep rise at the beginning.

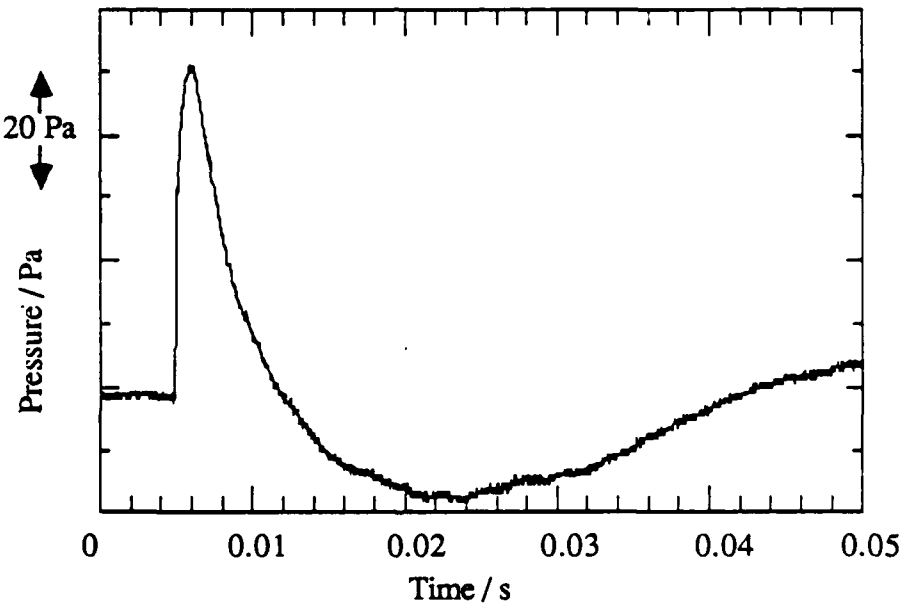

Fig. 9. Initial impact sound of drops of 5.6 mm diameter impacting at a speed of 5.2 m/s. The hydrophone is 40 mm below the impact site.

If we look at the front edge of the pulse on an expanded timescale, as in Fig. 10, we can see that the rise time is very short indeed, in fact it seems to be limited by the

response of the hydrophone, which rolls off quite sharply above 150 kHz. We shall examine the initial "spike" and the rest of the pulse separately.

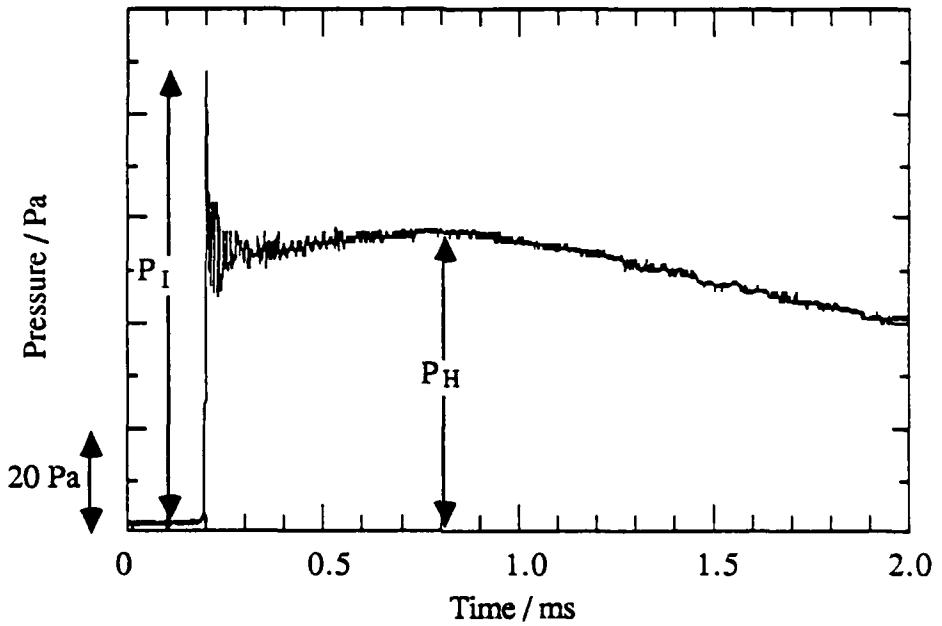

Fig. 10. Like Fig. 9 above but on a smaller timescale to show how sharp the initial impact is. The spike is so narrow that it cannot be seen in Fig. 9. The symbol P_I has been used to denote the maximum pressure of the initial spike, P_H is the maximum pressure which occurs in the rest of the pulse.

For energy to be radiated to large distances, the pressure field must vary as 1 / r, where r is the distance from the source. Figure 11 shows how the magnitude of these two components varies with distance from the source; note that the 'spike' is true radiated sound, because P_I is inversely proportional to r. The rest of the pulse is a near-field hydrodynamic effect, because P_H falls off more rapidly with distance.

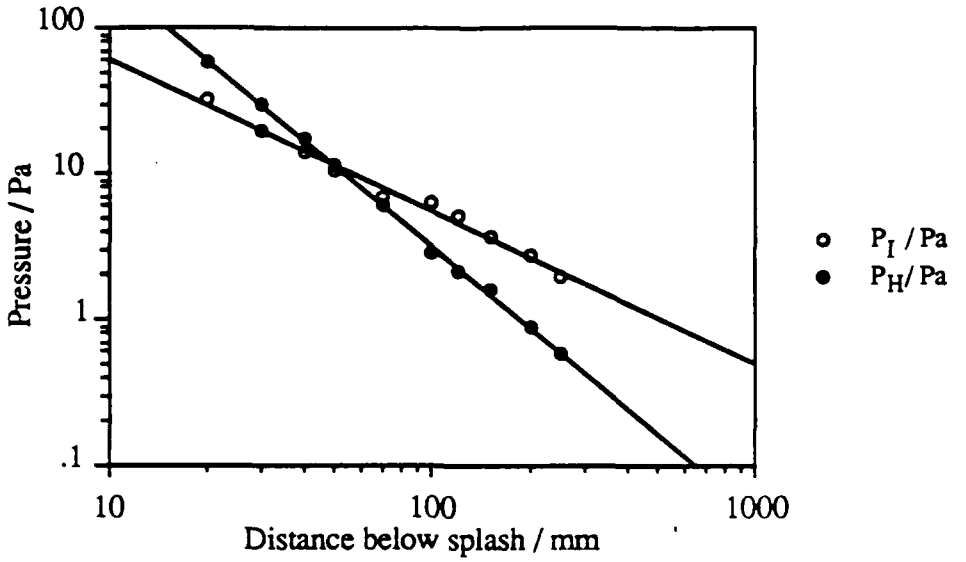

Fig. 11. This graph shows how the hydrodynamic pressure P_H and the impact spike pressure P_I vary with the distance, r, from the impact. P_I varies as $1 / r$ and is therefore radiated sound; P_H varies as $1 / r^{1.8}$ and is therefore a near-field effect. Note that in order to measure P_I it was necessary to use a timebase setting on the oscilloscope which expanded the trace much more than in Fig. 10. The oscilloscope has a maximum sampling rate of 100 MHz so this is not a limiting factor or a source of error.

At larger distances the whole pulse is as shown in Fig. 12, the spike is now dominant and the near-field part has dropped almost to nothing.

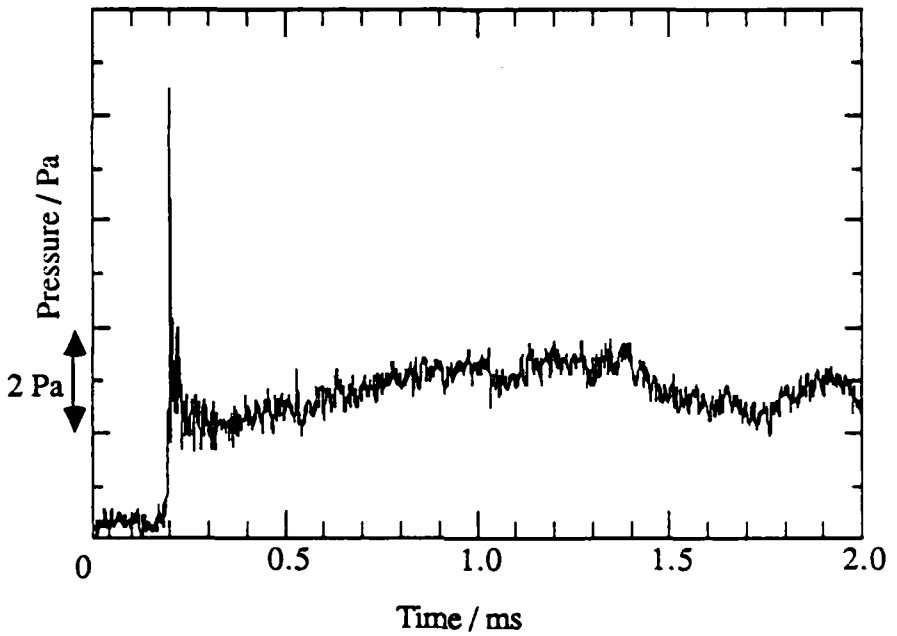

Fig. 12. This is like Fig. 10. above except that the hydrophone has been moved to a larger distance: 0.22 m from the splash. Note how the hydrostatic pressure P_H is now smaller with respect to the impact spike pressure P_I.

The spike is obviously the part we need to study further for ambient noise purposes. Figure 13 shows how the peak pressure P_I varies with impact velocity v_I; it seems to be proportional to $v_I^{2.7}$. This result is at variance with the "water hammer" theory of Nystuen [23, 26], which suggests that P_I should be proportional to v_I.

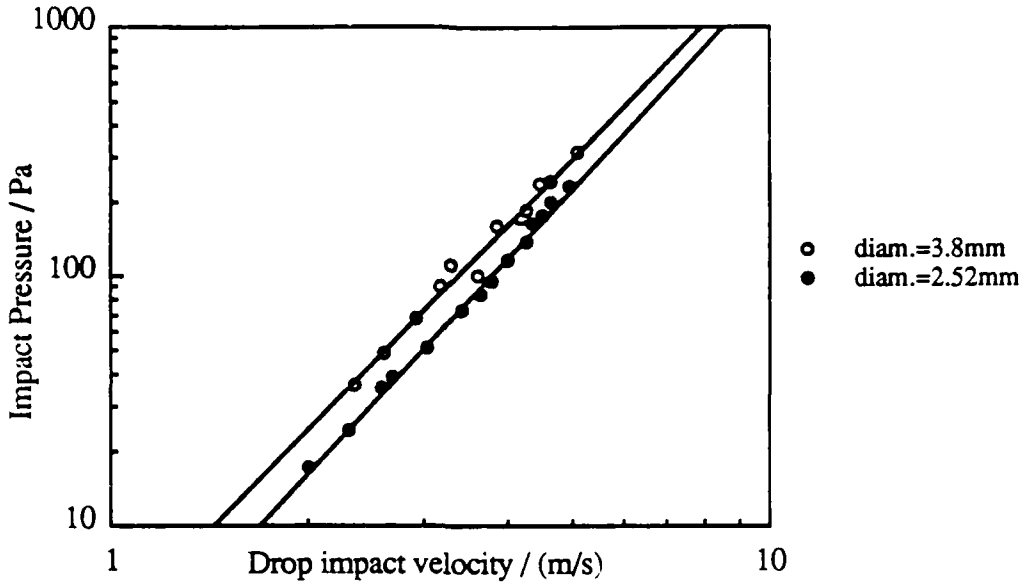

Fig. 13. Shows how the impact spike pressure P_I varies with drop impact velocity. The power law is 2.7 for d = 3.8 mm and 2.8 for d = 2.52 mm.

Figure 14 shows that the pressure is also proportional to the 1.63 power of the drop diameter and hence to a power of about 0.54 of its volume.

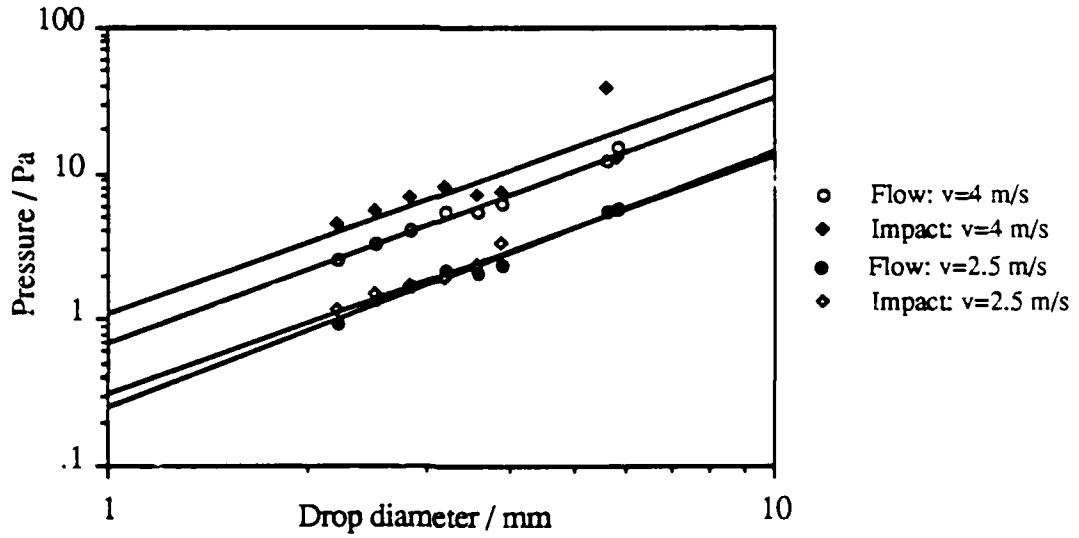

Fig. 14. Shows how the impact spike pressure, P_I and the hydrodynamic pressure P_H vary with drop diameter for two different impact velocities. The power laws are: P_I: 1.6 for both velocities, P_H: 1.7 for v = 4 m/s and 1.8 for v = 2.5 m/s with errors of about 0.1 m/s. The hydrophone was at a depth of 70 mm vertically below the splash.

As was mentioned previously, (Fig. 10), the spike is extremely narrow, it seems to be less than 10 μs wide; the response of the hydrophone prevents a more accurate measurement. The narrowness suggests that the power spectrum of the spike should be rather flat at frequencies below 100 kHz.

C. Bubble sounds

1. Frequency

As Fig. 15 shows, the sound of an oscillating bubble is an exponentially damped sinewave, i.e. the acoustic pressure is given by:

$$p = p_i e^{-\beta t} \cos(\omega t + \phi), \tag{10}$$

where p_i is the initial pressure amplitude.

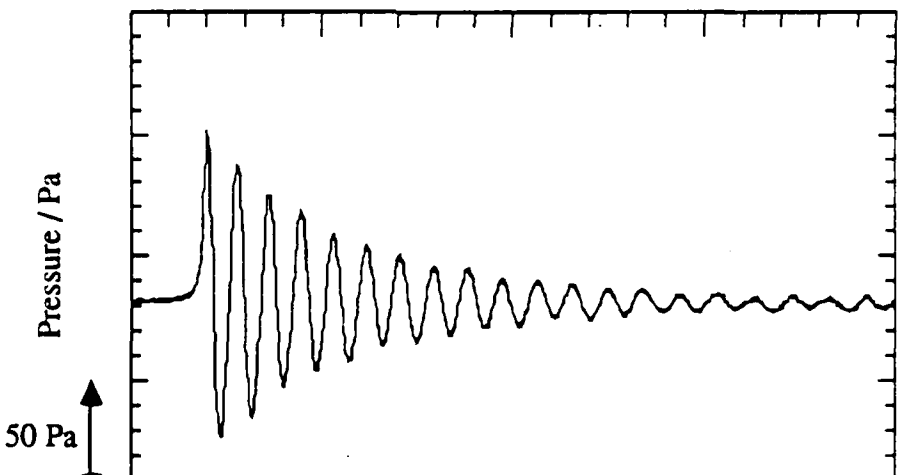

Fig. 15. Sound of a regularly entrained bubble. This one has a frequency of 11.5 kHz and a Q factor of 15. It was entrained by a drop of 3.4 mm diameter impacting at a velocity of 1.7 m/s as in Fig. 6.

We can measure ω, β and p_i and compare them with the theory of chapter I. Minnaert's [27] formula (Eq. 4) shows that ω is inversely proportional to the bubble radius or diameter. In Fig. 16, the inverse frequency $1 / f = 2\pi / \omega$ is plotted against bubble diameter; the agreement with theory is quite good when the error bars are taken into account. This data was all taken from high speed movie films; the main sources of error are blurring of images and the fact that many of the larger bubbles were non-spherical, making it difficult to estimate an effective diameter. The effect of the free surface has not been taken into account because Strasberg's theory suggests that it is usually much smaller than the experimental errors.

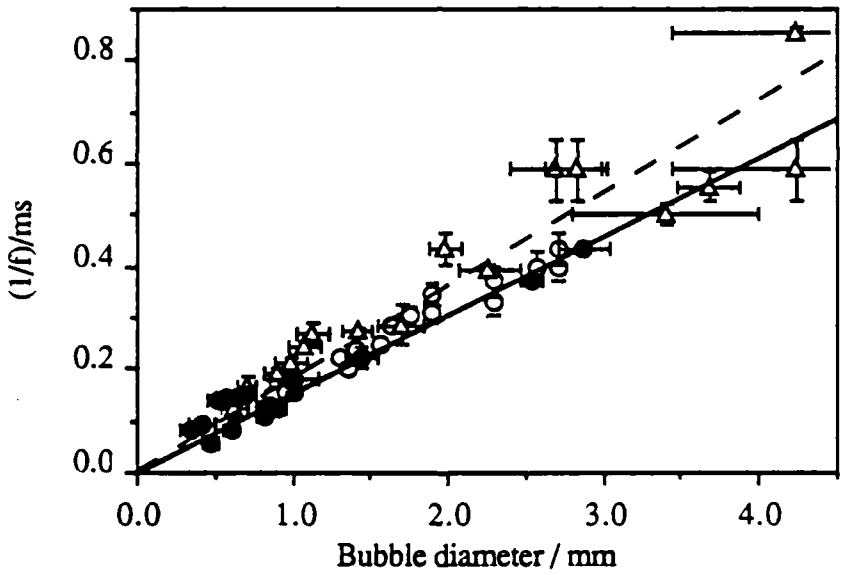

Fig. 16. Experimental confirmation of Minnaert's equation. The lines are the theoretical results for isothermal (dashed) and adiabatic (solid) oscillations. Bubbles in this size range should be nearly adiabatic. The experimental points represent bubbles entrained by various mechanisms: drop impacts (filled circles), breaking wave (triangles) and air forced through a hypodermic needle (open circles)

2. *Damping*

The damping was obtained by the following procedure. It is easiest to measure the amplitude, $p_i e^{-\beta t}$ at the maxima and minima, when $\cos(2\pi ft+\phi) = \pm 1$, that is, when $2\pi ft+\phi = 2n\pi$, the number of cycles, n, being an integer or half-integer. We therefore measure t from a maximum of p, so that $\phi = 0$ and plot the pressure p_n at each half cycle, where $t = n/f$. Substituting for t in Eq. (16) gives:

$$p_n = p_i e^{\frac{-n\beta}{f}} . \qquad (11)$$

We plot ln p_n against n to obtain a straight line of slope $-\beta/f = 2\pi\beta/\omega = \pi/Q$. The intercept of the straight line with the ln p_n axis at $t = 0$ is the initial amplitude, p_i. Figure 17 shows a typical example.

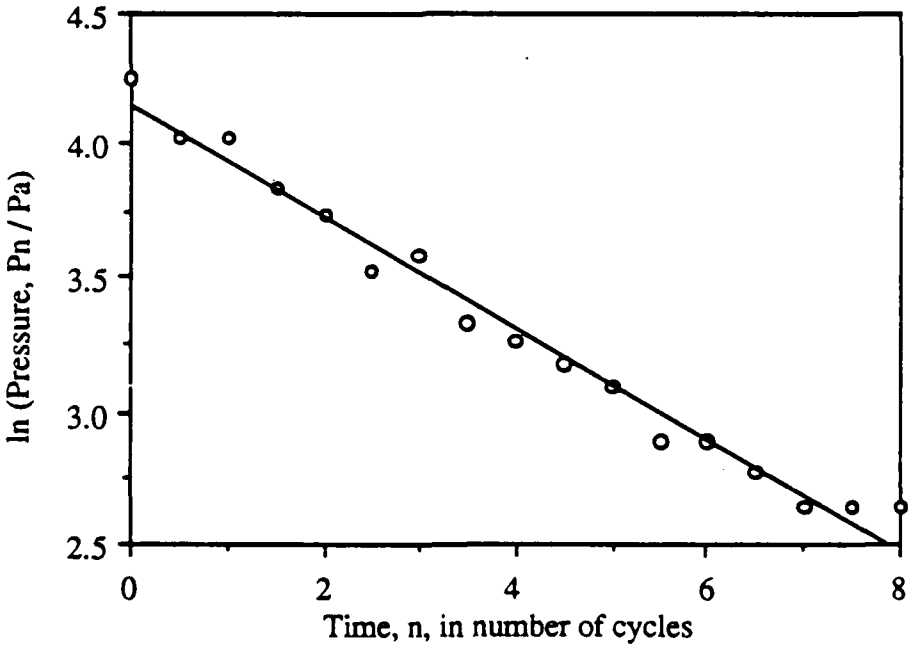

Fig. 17. Graph used to find the damping of Fig. 15. The natural log of the amplitude at each half-cycle is plotted against time in units of cycles to give a straight line of slope $-\beta/f = -2\pi\beta/\omega = -\pi/Q$. In this case, the slope is -0.209, giving a Q of about 15.

Initial plots of Q against f showed a large scatter, so the data taking process was automated, the computer carrying out the process outlined above and averaging the results over each of several frequency bands. The results are shown in Fig. 18 along with several theoretical curves.

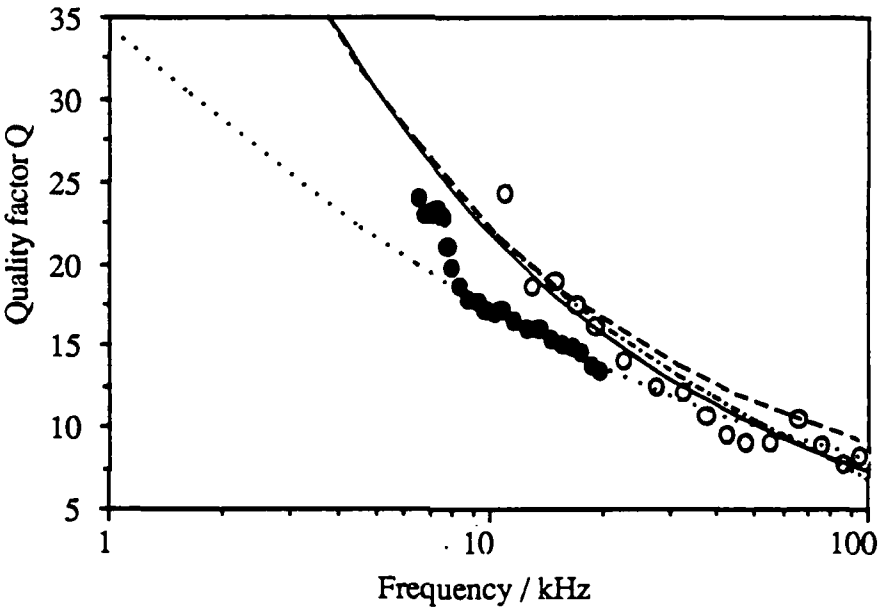

Fig. 18. Q factor as a function of frequency. The open circles are from bubbles entrained by spray #2, the filled circles represent bubbles regularly entrained by larger, slower drops. Note that there is a large range of bubble sizes in both cases, but in general the larger drops produce larger bubbles. The dotted line is Prosperetti's theory, while the dashed line is the same theory with the acoustic damping δ_{ac} reduced to zero. The dot-dash line includes all three damping mechanisms, but with δ_{ac} reduced by Eq. (5) with $l = 5$ mm. Finally, the solid line is a best-fit to the data from spray #2; it seems to agree best with the dot-dash line. This best fit is used for calculations in a subsequent chapter. The random errors in the data are fairly small, approximately ±1, and the various peaks are quite reproducible so they must be either systematic errors or a real physical effect.

As the figure shows, spray-entrained bubbles seem to obey Prosperetti's [31] theory quite well provided that the acoustic damping is modified by Eq. (5). The bubbles from single drops are rather more damped. The results for both frequency and damping agree with those of Leighton and Walton [39].

3. Radiation Pattern

Having dealt with the frequency ω and the damping β, we now look at the initial pressure p_i. We expect from Eq. (8) that $p_i = (D \cos\theta)/r$, i.e. that the acoustic pressure due to a bubble near the surface will vary inversely with distance and as the cosine of the polar angle. Figures 19 and 20 show that this is the case.

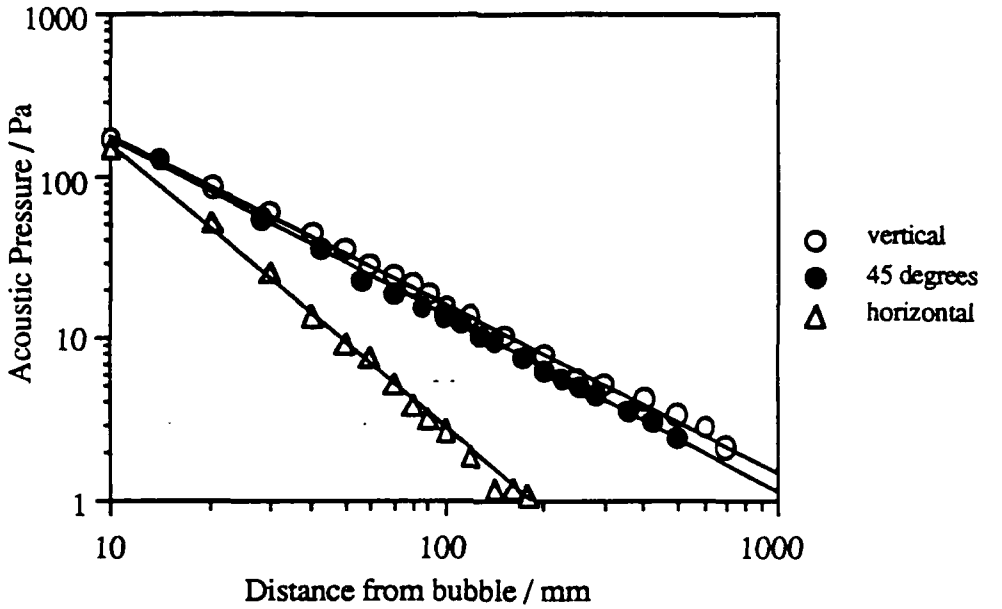

Fig. 19. This is a graph of the acoustic pressure from a bubble in three directions: vertically, horizontally, and at 45 degrees. It shows that p is inversely proportional to distance except in a horizontal direction. The bubbles used were produced by regular entrainment and had resonance frequencies of about 7-8 kHz.

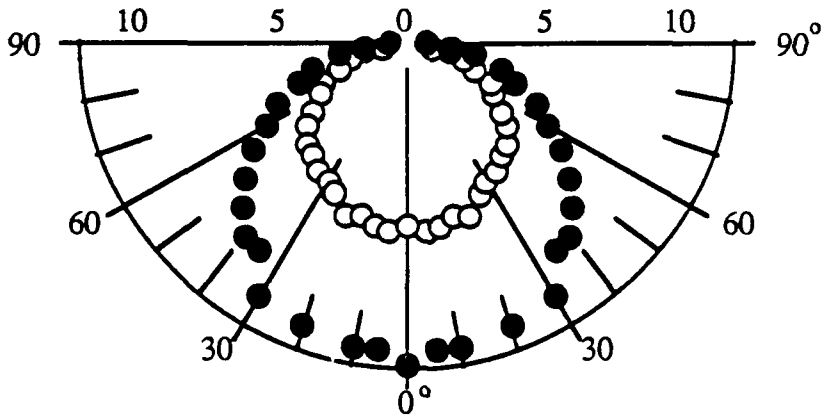

Fig. 20. Radiation pattern of a near-surface bubble. This polar plot shows how acoustic pressure (plotted in units of Pascals in the radial direction) varies with angle at two different distances. Bubble were similar to those used in Fig. 19.

4. Dipole source strength

We now have only the initial dipole strength D to examine. Experimentally, we measure D by measuring p_i and knowing θ and r, but first we will try to predict it

theoretically. Figure 21 shows a bubble before and after it is entrained (rather like frames l and m in Fig. 8).

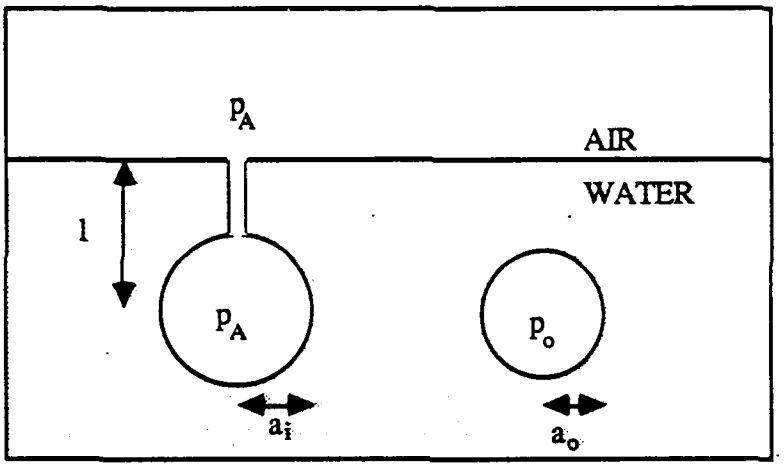

Fig. 21. Sketch showing bubble before and after entrainment.

The pressure inside the bubble after it is entrained is increased for two reasons: the Laplace pressure due to the surface tension and the hydrostatic pressure due to the bubble's depth below the surface. The Laplace pressure is given by $p_L = 2\sigma / a_o$, where σ is the surface tension, while the hydrostatic pressure is given by $p_H = \rho g l$. The interior pressure is therefore given by:

$$p_o = p_A + p_L + p_H = p_A + 2\sigma/a_o + \rho g l \,. \tag{12}$$

We assume that the gas is compressed adiabatically so that:

$$p_A V_A^{\gamma} = p_o V_o^{\gamma} \,, \tag{13}$$

and, assuming a spherical shape,

$$p_A a_i^{3\gamma} = p_o a_o^{3\gamma} \tag{14}$$

We substitute in for p_o from Eq. (12) to give:

$$p_A a_i^{3\gamma} = \left(p_A + 2\sigma/a_o + \rho g l\right) a_o^{3\gamma}, \tag{15}$$

and hence

$$a_i = a_o\left(1 + \frac{2\sigma}{p_A a_o} + \frac{\rho g l}{p_A}\right)^{\frac{1}{3\gamma}}. \tag{16}$$

We expand the bracket using the first term of the binomial expansion to give:

$$a_i = a_o\left(1 + \frac{2\sigma}{3\gamma p_A a_o} + \frac{\rho g l}{3\gamma p_A}\right), \tag{17}$$

and therefore:

$$a_i - a_o = \frac{2\sigma}{3\gamma p_A} + \frac{\rho g l\, a_o}{3\gamma p_A} \tag{18}$$

We have now obtained the initial amplitude of oscillation $x_i = a_i - a_o$. To find how much sound this will produce we go to equations (7) and (8) which tell us that the initial dipole strength D is given by :

$$D = 2\rho c U_i k^2 a_o^2 d = 2\rho x_i \omega^3 a_o^2 d/c. \tag{19}$$

We would like to know D as a function of frequency so we use Minnaert's formula (Eq. (4)) to substitute for a_o and Eq. (18) for x_i. This gives us:

$$D = \frac{2\rho}{c}\left(\frac{2\sigma}{3\gamma p_A} + \frac{\rho g l\left(\frac{3\gamma p_o}{\rho}\right)^{\frac{1}{2}}}{3\gamma p_A}\right)\left(\frac{3\gamma p_o}{\rho}\right)\omega l \tag{20}$$

which, if we make the small amplitude approximation that $p_A \sim p_o$, simplifies to

$$D = \frac{2}{c} g l^2 \left(3\gamma p_A \rho\right)^{\frac{1}{2}} + \frac{8\pi f l \sigma}{c}. \tag{21}$$

We set $p_A = 101300$ Pa, $g = 9.81$ m/s^2, $\rho = 1000$ kg/m^3, $\sigma = 72$ mN/m and $c = 1480$ m/s; this leaves us to guess l. We shall try 10 mm on the basis that this is

approximately the bubble depth in Fig. 8; we might expect a smaller l for bubbles entrained by smaller drops. The numerical result is then:

$$D = 0.0273 + 1.22 \times 10^{-5} f. \qquad (22)$$

The first (hydrostatic) term is small for frequencies above 10 kHz, so we ignore it and plot the second term for comparison with experimental data. The result is shown in Fig. 22.

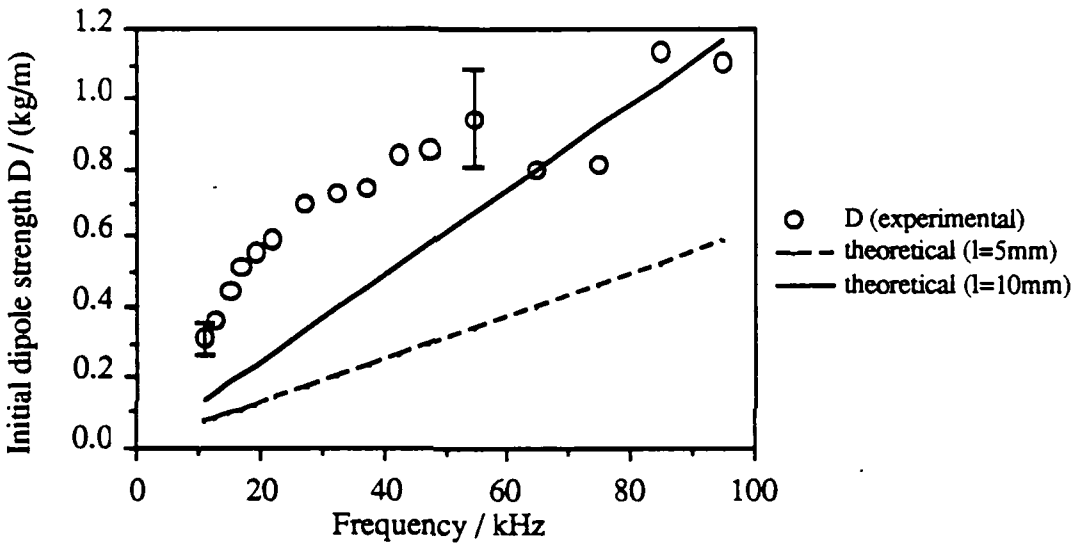

Fig. 22. Initial dipole strength D of drop-entrained bubbles as a function of frequency. Theoretical curves are shown for l = 10 mm (Eq. 22) and also for l = 5 mm. The error bars show experimental random error; there is also some systematic error introduced by the hydrophone response. This was not corrected for and has probably made the measured values of D smaller than they really were.

The experimental results are of the right order of magnitude so we can conclude that the Laplace pressure provides a large part of the energy which the bubble radiates as sound. They are, however, rather high and are not a straight line as predicted; there are several possible reasons for this. One is that the sound reflected from the surface not only interferes with the directly radiated wave to give a dipole field, but is also scattered by the bubble itself. It has been shown [33] that this assumption leads to higher amplitudes for the sound field than does the simpe dipole assumtion we have used so far.

Another possible reason for the failure of the theory described above is that some other mechanism is exciting the bubble; surface waves might be one such mechanism. So far, we have assumed that the bubble remains a sphere but inspection of high speed films shows that this is far from being the case. Strasberg [40] has shown that surface waves themselves do not radiate significant amounts of sound but recent work by Longuet-Higgins [41] suggests that surface waves of large amplitude will couple to the volume mode and hence cause it to radiate. This effect is largest at certain frequencies where a surface wave mode has twice the frequency of the volume mode. The frequency of the volume mode, ω_0, is given by Minnaert's equation, while the frequency Ω_j of the jth surface mode is given by:

$$\Omega_j^2 = (j-1)(j+1)(j+2)\frac{\sigma}{\rho a_o^3} \qquad (23)$$

We set $2\Omega_j$ equal to ω_0 to give a sequence of frequencies ω_j at which we expect the surface modes to interact most with the volume mode. These frequencies are listed in table (1).

TABLE 1: Bubble radii and resonance frequencies at which $2\Omega_j = \omega_0$.

j	a_0 / mm	f / kHz	j	a_0 / mm	f / kHz
2	0.0074	472	9	0.627	5.20
3	0.0274	121	10	0.847	3.85
4	0.0631	57.1	11	1.11	2.93
5	0.119	27.6	12	1.43	2.28
6	0.199	16.5	13	1.80	1.81
7	0.307	10.6	14	2.23	1.46
8	0.450	7.28	15	2.72	1.20

In Fig. 23, these frequencies are marked on a graph of Q factor as a function of frequency; they seem to coincide with the various peaks which we noted but did not explain in Fig. 18. It is not clear why surface waves should affect the damping constant in this way; a plausible argument is that near the frequencies ω_n the damping seems to be less because as energy leaves the volume mode via the three usual damping mechanisms, energy is also being pumped into the volume mode from a surface mode.

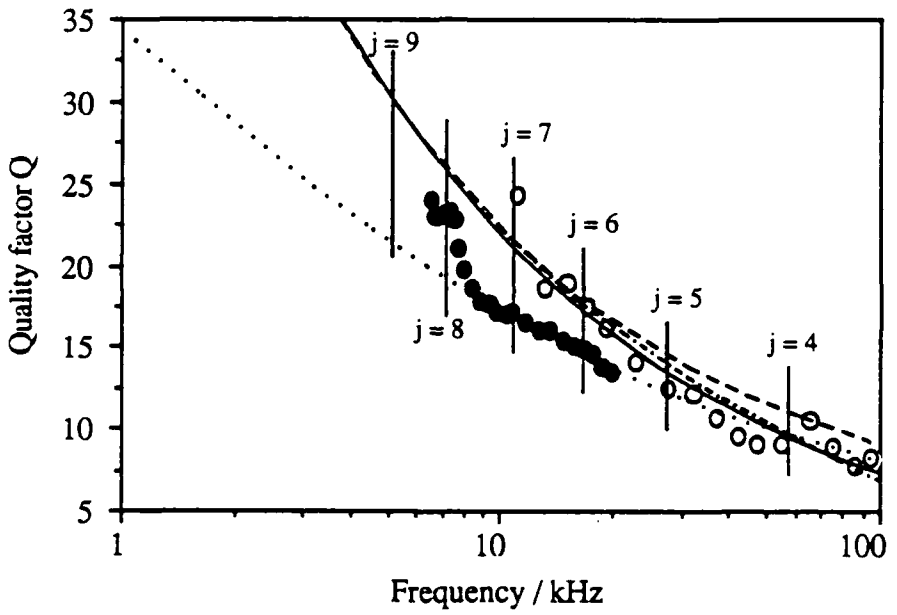

Fig. 23. This shows Q as a function of frequency like Fig. 19, but also shows the Longuet Higgins frequencies, which seem to coincide with various peaks in the experimental data, especially for j = 4 and j = 8.

The results presented in this chapter may be summarized by the following points:

1) There are two ways that a drop impact can produce sound: the impact of the drop itself and the entrainment of a bubble.

2) The initial impact pulse consists of two parts: a near-field hydrodynamic pressure which is not radiated (and therefore not important for ambient noise purposes) and a sharp initial spike.

3) Bubbles may be entrained by two mechanisms: the unpredictable process described by Franz, which I have dubbed irregular entrainment and a repeatable process which I have named regular entrainment. Which, if any of these processes occurs depends on the drop diameter and impact velocity.

Before applying these findings to make predictions, we will digress a little to discuss the hydrodynamics of a drop impact in order to understand how the regular entrainment process works.

CHAPTER IV: HYDRODYNAMICS OF A DROP IMPACT

A. Regular entrainment: when it occurs.

It was mentioned in the previous chapter that within a certain range of drop sizes and impact velocities, a drop impact would always entrain a bubble. In this chapter we present results which show when this happens and try to discuss why.

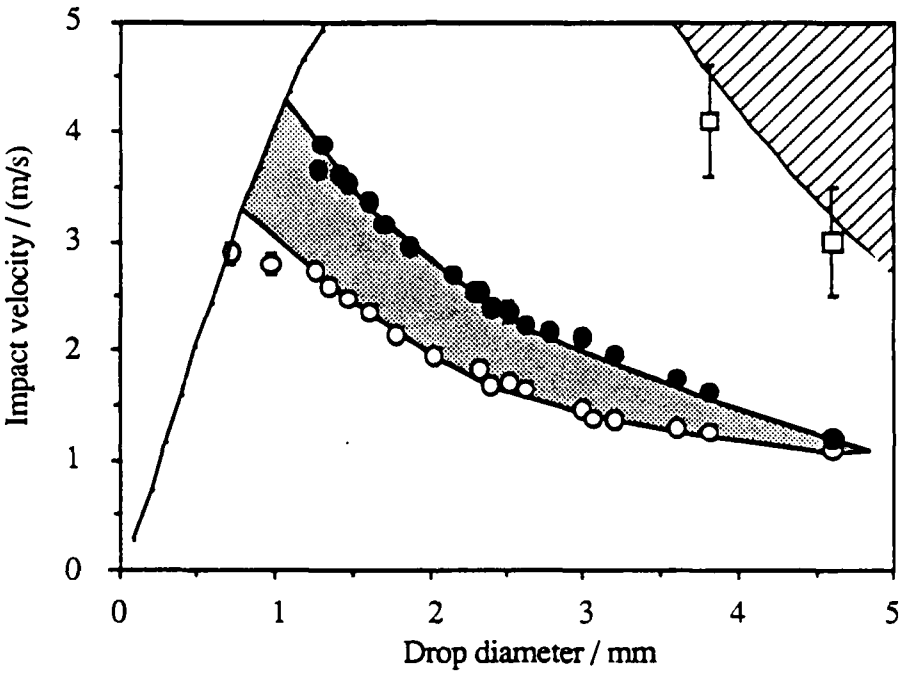

Fig. 24. This graph shows when regular entrainment occurs; see text for details.

Figure 24 is a plot of drop diameter against impact velocity; any drop impact can be represented by a point in this plane. Those impacts which entrain a bubble every time are represented by the shaded area in the center of the plot. The area above this represents impacts in which the drop travels too fast to entrain a bubble, the area below represents impacts where the drop travels too slowly. Most of the data points were taken by

producing drops of various sizes one at a time and finding the heights of fall for which they started and stopped producing bubbles. The two exceptions are the leftmost two of the open circles, which were inferred from high speed movies; they are less accurate than the other data. The striped area in the upper right-hand corner shows approximately where irregular entrainment as described by Franz [20] occurs; all but two of the data points used to draw this area are off the edge of the figure. The curve at the left-hand side of the figure is the terminal velocity curve for raindrops; all raindrop impacts will lie on this line. The line passes through the shaded region so we should expect raindrops within a certain range of sizes to cause regular entrainment. The implications of this to the sound produced by rainfall are discussed in the next chapter.

B. Simple hydrodynamics: no surface tension.

We now turn to the hydrodynamics of a drop impact to find if there is any simple way in which we can make theoretical progress in understanding how the entrainment process works. We begin by investigating the depth of the cavity formed by the drop impact. Figure 8 suggests that at impact energies which are too high for regular entrainment, the cavity in the water surface is hemispherical, as sketched in Fig. 25. Note that in this regime, surface tension is not very important.

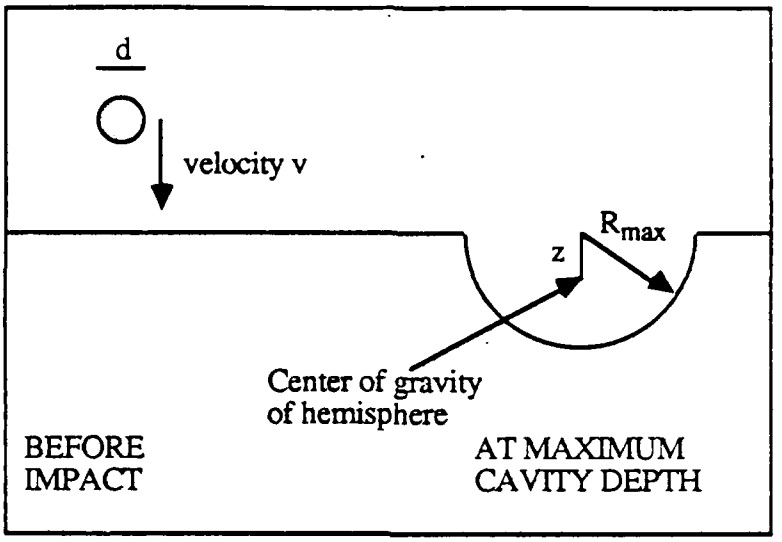

Fig. 25. Sketch showing how drop impact produces a cavity at the water surface. The cavity is shown at the point when its depth R is at its maximum value $R = R_{max}$.

We can calculate what the maximum cavity depth R_{max} should be by equating the kinetic energy E_k of the drop to the gravitational potential energy E_p of the cavity. We assume that the cavity has no kinetic energy when at its maximum depth because the water has stopped flowing outwards and is about to start flowing in. E_k is given by

$$E_k = \frac{1}{2} mv^2 = \frac{1}{12} \pi \rho d^3 v^2 \tag{24}$$

where m is the drop's mass and v is its impact velocity; we shall drop the subscript I from the impact velocity throught this chapter. E_p is given by $E_p = Mgz$ where M is the mass of the displaced hemisphere of water, z is the depth of its center of gravity and g is the acceleration due to gravity. Since z is given by $z = \frac{3}{8} R_{max}$, and M is given by $M = \frac{2}{3} \pi \rho R_{max}^3$ we can show that:

$$E_p = \frac{1}{4} \pi R_{max}^4 \rho g. \tag{25}$$

Equating equations (24) and (25) gives

$$\frac{1}{3} d^3 v^2 = g R_{max}^4 , \tag{26}$$

and hence

$$R_{max} = \left(\frac{1}{3} g\right)^{1/4} d^{3/4} v^{1/2} . \tag{27}$$

If we plot R_{max} against $d^{3/4}v^{1/2}$ we should get a straight line of slope $(1 / 3g)^{1/4}$.

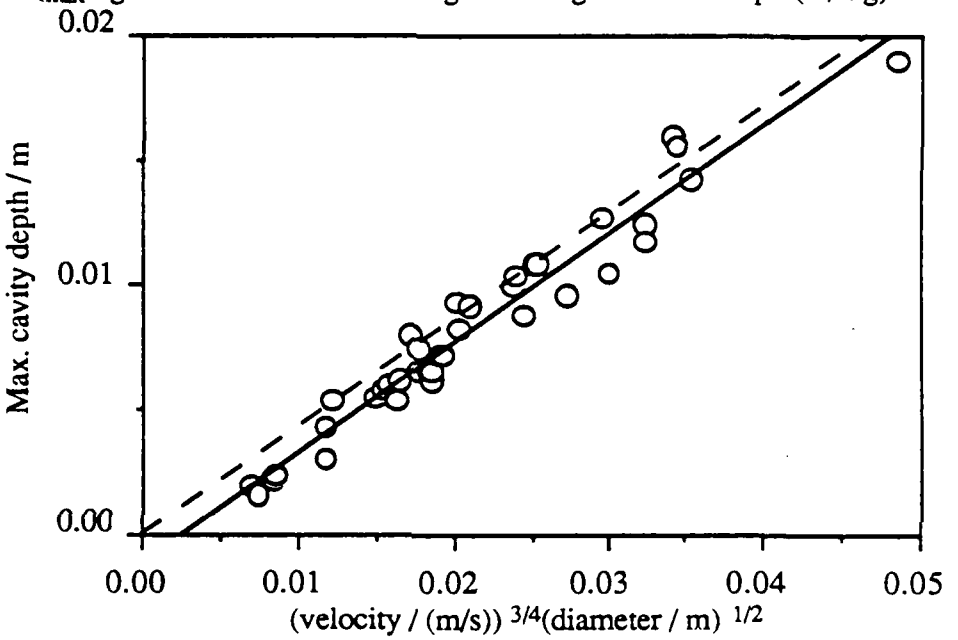

Fig. 26. This graph shows how the maximum cavity depth varies with drop diameter and impact velocity. The dashed line is the theoretical result described in the text while the solid line is a best fit straight line to the data points. Their slopes are 0.44 (experimental) and 0.4293 (theoretical). The data were taken from high-speed movies; the experimental error is about ±1 mm.

As Fig. 26 shows, the agreement with theory is remarkably good, even for small drop energies and cavity depths, where surface tension distorts the cavity from its hemispherical shape. Note that this is a simpler version of theory developed by Engel [42] for impacts of much higher energy.

We now consider the time which the cavity takes to grow to its maximum depth. As before, we will equate the kinetic energy of the impacting drop with the energy of the

cavity. Now, however, the cavity has both potential and kinetic energy. We assume that the water is moving radially away from the cavity in all directions from vertically downwards to horizontal.

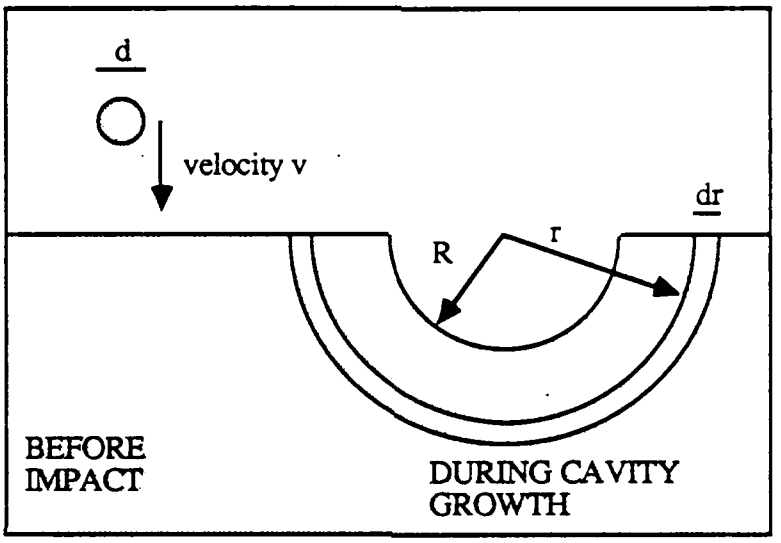

Fig. 27. Sketch showing hemispherical cavity as it grows.

We consider a hemispherical shell as shown in Fig. 27. The cavity is expanding at a rate $dR/dt = U(t)$ which is much less than the speed of sound, so we can assume that the water is incompressible. This means that the velocity $u(r,t)$ at a distance r from the cavity center is given by $u = U R^2 / r^2$. The kinetic energy dK of the shell is given by

$$dK = \frac{1}{2} 2\pi r^2 dr\, \rho(u(r))^2 = \pi\rho \frac{R^4 U^2}{r^2} dr \qquad (28)$$

and hence the total kinetic energy K(R) is

$$K(R) = \pi\rho R^4 U^2 \int_R^{\infty} \frac{1}{r^2} dr = \pi\rho R^3 U^2 \quad . \tag{29}$$

The potential energy P of the cavity is found by replacing R_{max} with R in Eq. (25); we can then get an equation of motion for the cavity by setting E_k equal to K + P; the result is:

$$R^3 U^2 + \frac{1}{4} g R^4 = \frac{1}{12} d^3 v^2 \quad . \tag{30}$$

This equation may be reduced to a dimensionless form by letting $X = R / R_{max}$, where X is a dimensionless cavity depth. Recalling that U = dR / dt, we get:

$$\left(\frac{dX}{dt}\right)^2 = \frac{g}{4R_{max}} \left(\frac{1-X^4}{X^3}\right) \quad . \tag{31}$$

We now introduce a dimensionless time T which is given by

$$T = \frac{t}{2} \sqrt[8]{\frac{3g^5}{d^3 v^2}} \tag{32}$$

which reduces the equation of motion to

$$\left(\frac{dX}{dT}\right)^2 = \left(\frac{1-X^4}{X^3}\right) \quad . \tag{33}$$

This equation is of the "variables separable" type and we can therefore write it as:

$$\int_0^X \left(\frac{X^3}{1-X^4}\right)^{1/2} dX = \int_0^T dT \quad , \tag{34}$$

if we let T = 0 when X = 0. This has to be integrated numerically to find X as a function of T, but we can find T_{max}, the dimensionless time at maximum cavity depth by integrating the left hand side from 0 to 1, that is up to the maximum depth. We make the substitution $X^2 = \sin\theta$, which gives us:

$$T_{max} = \int_0^1 \left(\frac{X^3}{1-X^4}\right)^{\frac{1}{2}} dX = \frac{1}{2}\int_0^{\pi/2} (\sin\theta)^{1/4} d\theta \quad , \tag{35}$$

$$= (2)^{-3/4} B\left(\frac{5}{8},\frac{5}{8}\right) \tag{36}$$

where B is the beta function. We have used the standard integration formula:

$$\int_0^{\pi/2} (\sin\theta)^{\mu-1} d\theta = (2)^{\mu-2} B\left(\frac{\mu}{2},\frac{\mu}{2}\right) \quad . \tag{37}$$

The numerical result is that $T_{max} \sim 0.67498$. The time t_{max} for a particular cavity to reach its maximum depth R_{max} is obtained by substituting this value for T_{max} into Eq. (32), *giving*

$$t_{max} = 2\ (0.67498) \sqrt[8]{\frac{d^3v^2}{3g^5}} = 0.28241 \sqrt[8]{d^3v^2} \quad . \tag{38}$$

Figure 29 shows experimental values of t_{max} plotted as a function of $d^{3/8}v^{1/4}$ together with the above theoretical result.

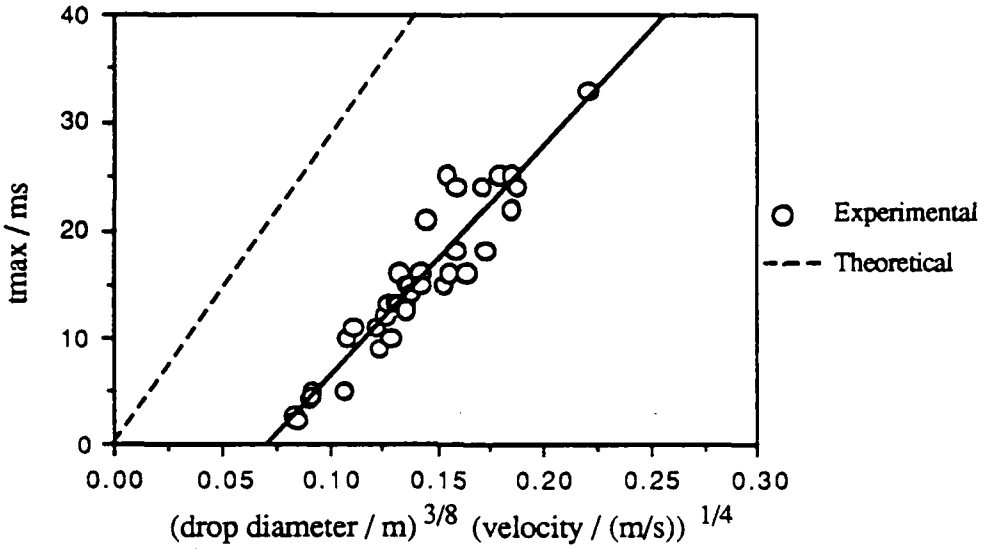

Fig. 28. Shows how the time t_{max} which a cavity takes to reach its maximum depth varies with drop diameter and impact velocity. The theoretical result does not agree very well with the experimental data for reasons discussed in the text.

It is evident from Fig. 28 that the theory is somehow flawed and that a given cavity will reach its maximum depth in a much shorter time than predicted. This is also obvious from Fig. 29, which shows a numerical solution of Eq. (34) and also some experimental curves for X as a function of T.

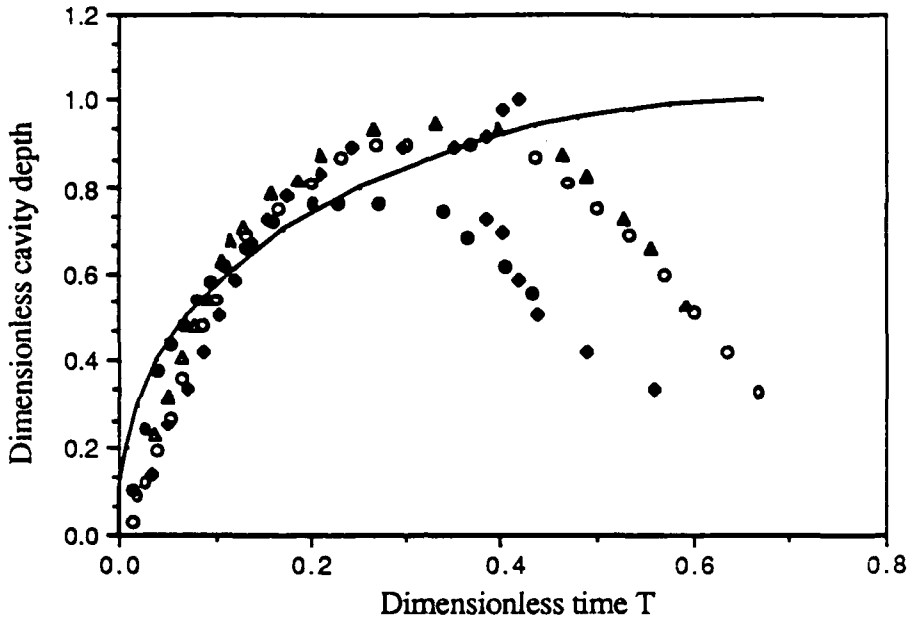

Fig. 29. Shows dimensionless cavity depth X as a function of dimensionless time T. The line is a numerical solution to Eq. (33), while the various sets of points are experimental data. The measured values of R and t were made dimensionless by using equations (36) and (41) and the experimental values of d and v.

The main reason for the failure to predict T_{max} or describe how X varies as a function of T is that in real life, the flow is not anything like hemispherically symmetrical. This means that the effective mass of water which is moving is smaller and therefore easier to accelerate. The end result is that the cavity can grow faster than predicted. Just after the drop strikes, the cavity actually grows slower than predicted; this is probably connected with the fact that the drop has a finite size and that we cannot expect the cavity to have an infinite initial growth rate. Note that our prediction of R_{max} was good because that required only that the final cavity should be hemispherical and that the flow should stop at that point; we did not require the *flow pattern* to be hemispherical. It is also important for

the ideas in the next section that the values of R_{max} were good even when the cavity was small enough to be distorted considerably from a hemispherical shape.

C. Effect of surface tension

So far, we have ignored surface tension and have yet to explain how the bubble is entrained. In one experiment a surfactant was added to the water in the tank and it was noticed that this prevented regular entrainment from occurring; Fig. 30 shows frames from a high speed movie of this process. It is therefore clear that surface tension has something to do with the entrainment process.

Fig. 30 (over page). Frames from a high speed movie showing a drop of 3.8 mm diameter impacting at 1.5 m/s. These parameters fall inside the regular entrainment region so we should expect the drop to entrain a bubble. The reason it does not is that a surfactant (Kodak Photoflo) has been added to the water, reducing the measured surface tension from 72 mN/m (= 72 dyn / cm) to about 30 mN/m. Note that the cavity is much more rounded than the one in Fig. 8; it *is the surface tension* which causes the sharp edge at the bottom of the cavity in frames i and j of that figure.

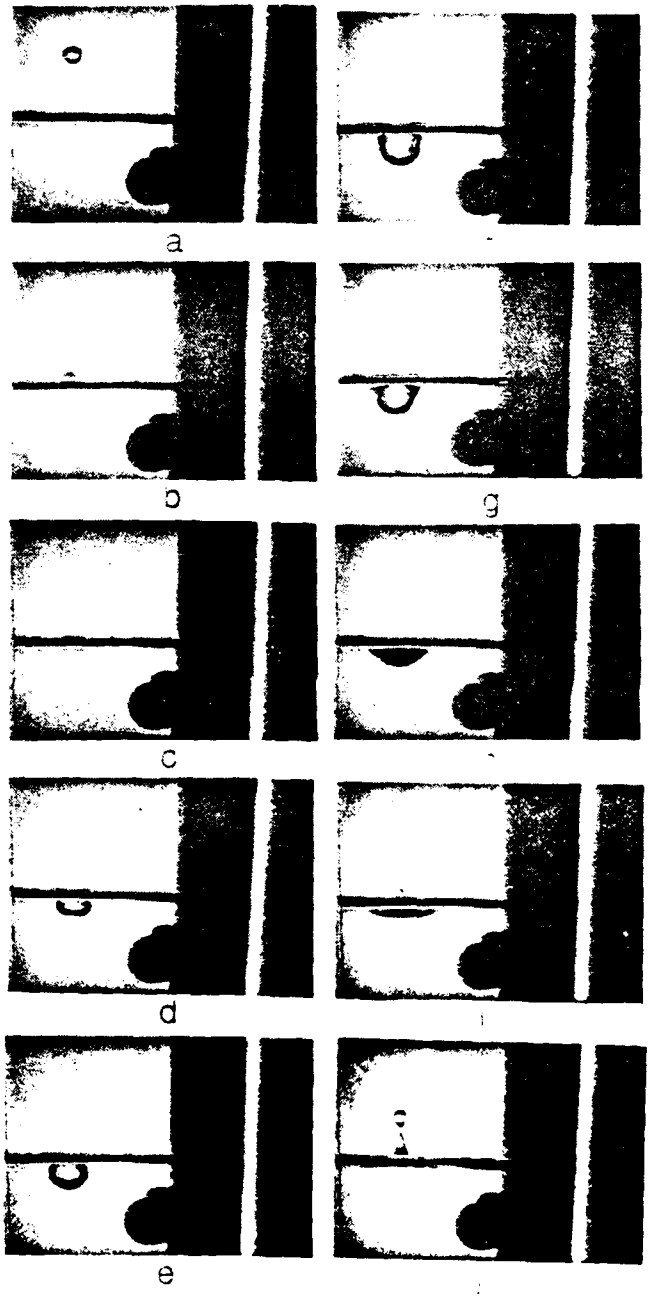

Figure 31.

It is also clear that surface tension is the force which distorts the cavity from the hemispherical shape seen at large drop impact energies. Some films suggest that what is happening is that a capillary wave is starting at the open end of the cavity and travelling down to the bottom, where it increases in amplitude due to the focussing effect caused by the narrowing of the cavity.

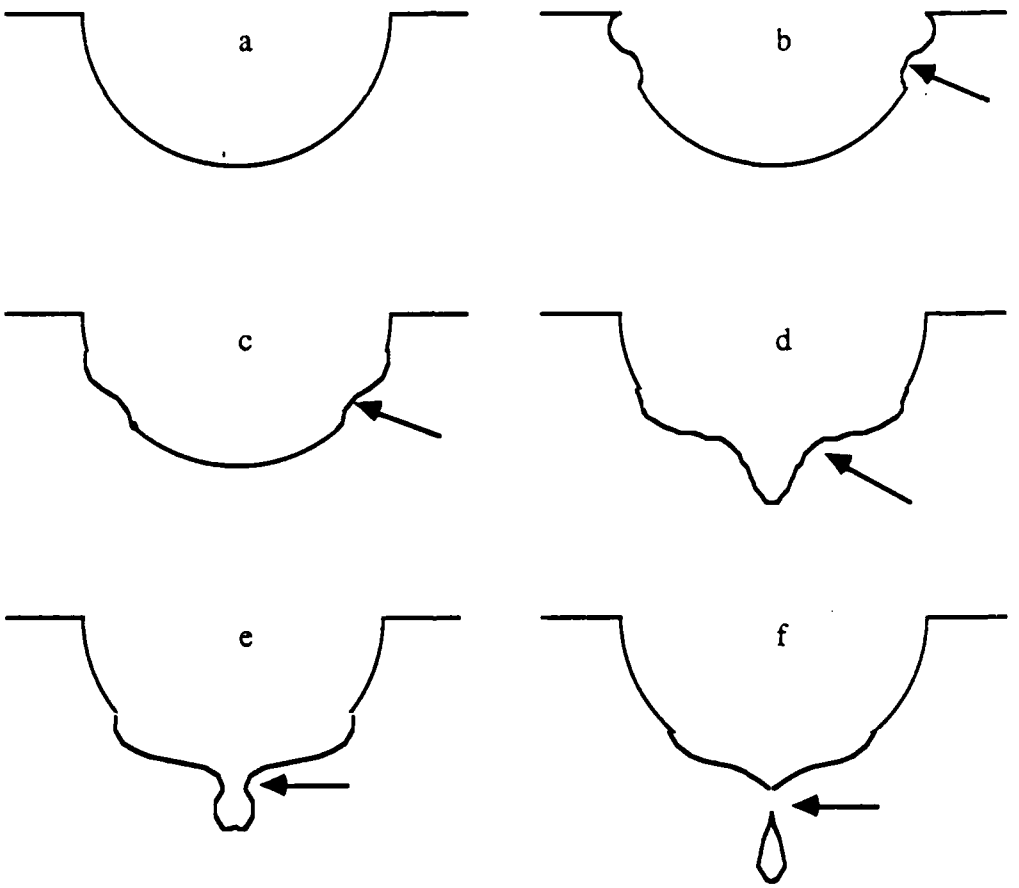

Fig. 31. This series of sketches shows how a surface tension wave is formed (b), begins to move down the cavity (c-d), how the crests on either side of the cavity approach each other (e) and meet, causing a bubble to pinch off (f). The arrow indicates the crest of the wave. Part (a) shows a cavity with no surface wave. These sketches are not intended to be accurate representations of the surface shape; they are all based on a hemispherical cavity (as in (a)) whose size remains constant.

The crest of the wave on one side of the cavity then meets the crest on the other side, thus entraining a bubble. Figure 31 shows a schematic of this process; note that this bears a slight similarity to the behavior of linear surface tension waves of finite amplitude [43].

The question of whether a bubble is entrained or not is determined by whether the capillary wave reaches the bottom of the cavity at the right time, which must be some fraction of t_{max}, or rather some range of fractions of t_{max}. For the sake of argument, let us assume that the time τ which the wave takes to travel a distance R_{max} must be between 0.9 t_{max} and 1.1 t_{max}. The velocity v_σ of a capillary wave of wavelength λ is given by $v_\sigma^2 = 2\pi\sigma / \rho\lambda$, where ρ is the liquid density and σ is the surface tension, and hence τ is given by:

$$\tau = \frac{R_{max}}{v_\sigma} = R_{max}\sqrt{\frac{\rho\lambda}{2\pi\sigma}}. \qquad (39)$$

We now assume that λ is some fraction α of R_{max} i.e. $\lambda = \alpha R_{max}$, which gives us:

$$\tau = \sqrt{\alpha} R_{max}^{3/2}\sqrt{\frac{\rho}{2\pi\sigma}}, \qquad (40)$$

we can now set this to be between 0.9 t_{max} and 1.1 t_{max}. Equation 38 does not give us a very good answer for t_{max} so we shall half the answer in a rather arbitrary fashion; note that in Fig. 28 the experimental values are often about half of the theoretical ones. We get the following inequality for d and v to be inside the regular entrainment region:

$$(0.9)\tfrac{1}{2}(0.28241)\sqrt[8]{d^3v^2} < \sqrt{\alpha}\left(\frac{d^3v^2}{3g}\right)^{3/8}\sqrt{\frac{\rho}{2\pi\sigma}} < (1.1)\tfrac{1}{2}(0.28241)\sqrt[8]{d^3v^2}. \qquad (41)$$

If we let $\alpha = 0.5$ and use the standard values for ρ,σ and g we get the following two equations for the boundaries of the regular entrainment region:

$$v = {}^{1}\!/\!\left(5416.1\, d^{3/2}\right) \tag{42}$$

and

$$v = {}^{1}\!/\!\left(3625.6\, d^{3/2}\right). \tag{43}$$

These equations are plotted in Fig. 32 with the data of Fig. 24 and it is obvious that the functional relationship between v and d is not correctly predicted. This is hardly surprising when one considers the approximations which we have had to make. On the other hand, we have managed to predict approximately the correct numerical values of v over the range of values of d in which we are interested.

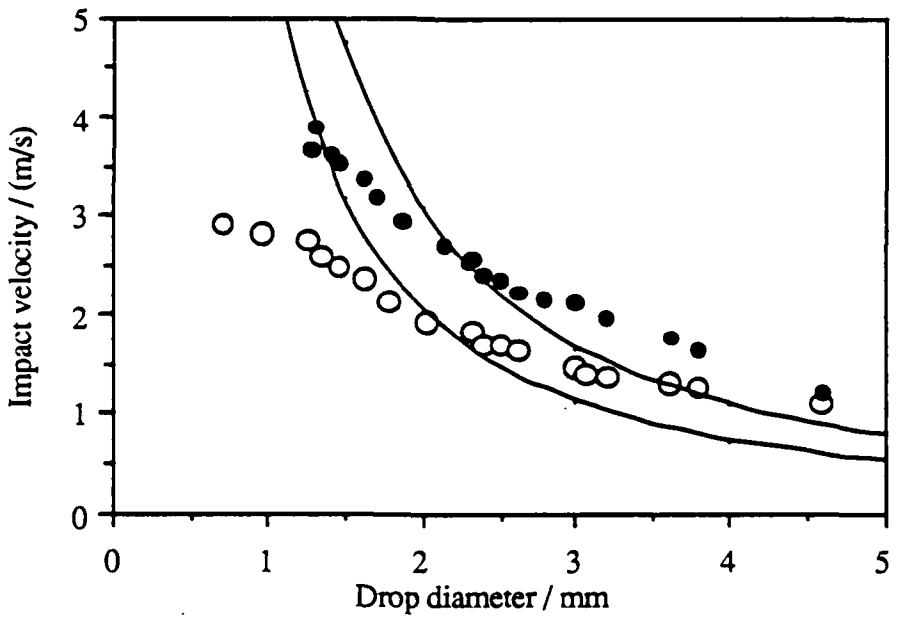

Fig. 32. A comparison of the theory of equations 42 and 43 (solid lines) and the data of Fig. 24.

This section has taught us two things: firstly, that surface tension waves travel at about the right speed to account for the effects we observe and, secondly, that the above explanation

is far from complete. Prosperetti has suggested (in a private communication) an alternative explanation in which the bubble is trapped because the outward flow of water from the cavity reverses and becomes an inward flow at the sides of the cavity before it does so at its base. This explanation makes no mention of surface tension, which we know to be important from the experiment described in Fig. 30, so it cannot be the whole story either. It seems that this problem is too complicated for the kind of simple analysis I have attempted and that in order to make further progress some computer flow simulation would be necessary. Prosperetti's group at JHU is currently making progress in this direction and some of their (as yet unpublished) results are included in appendix B.

So far in this chapter, we have applied simple theory to learn about the dynamics of a drop impact cavity and to explain why a bubble is sometimes entrained. We shall now proceed to look at a major application of the previous chapters: the underwater noise produced by rain.

CHAPTER V: THE UNDERWATER SOUND OF RAIN

A. Experimental observations

There have been a few reports of the underwater noise of rain available since the Second World War [44], but they were all of poor quality or covered only a small frequency range. In 1985 two independent groups [22, 23] discovered that the spectrum of rain noise showed a peak at about 14 kHz with a sharp cutoff on the low frequency side and a shallower slope on the high frequency side. This result has since been duplicated by several groups [24, 37] and seems to be a universal property of rain noise.

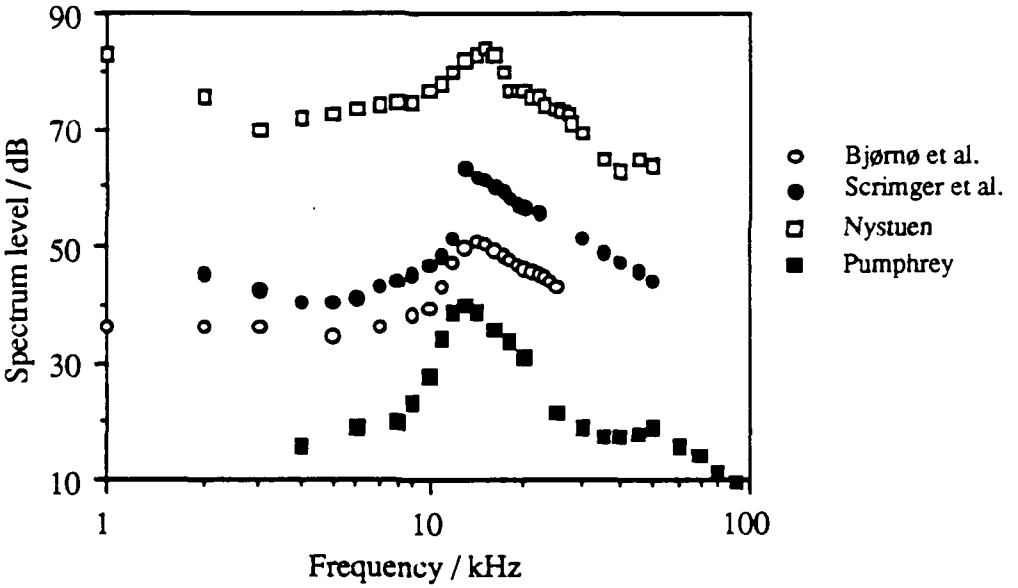

Fig. 33. Rain spectra from around the world. Nystuen's data is from Clinton lake, IL and was taken in heavy rain. The others are all caused by light rain: Scrimger's is from Cowichan lake on Vancouver Island, BC, Bjørnø's is from a large tank in a parking lot at the Technical University of Denmark, Lyngby, Denmark. The remaining data set was recorded by the author in a container placed on the roof of the old Chemistry building at the University of Mississippi. Scrimger's and Nystuen's data are in decibels referenced to a level of 1 μ Pa^2 / Hz; the other data sets have arbitrary reference levels.

The 14 kHz peak is not just a feature of real rain, it is also easy to duplicate in the laboratory, provided that one uses a spray of drops of small enough size and large enough height of fall to resemble real rain. Figure 34 shows some examples.

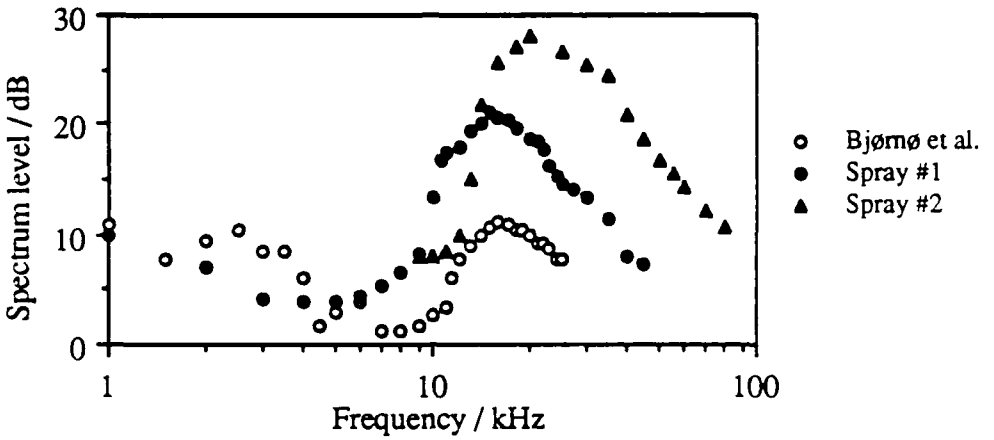

Fig. 34. Artificial rain noise spectra. Note that all show the 14 kHz peak but that its shape and its height above the rest of the spectrum vary a little. (Absolute height is not meaningful as all decibel reference levels are arbitrary.) Spray #1 contained a range of drop sizes from 0.7 to 1.5 mm in diameter, with a few drops as large as 1.8 mm; Bjørnø's data was produced with a spray similar to spray #1. Spray #2 was largely made of smaller drops in the range 0.6 to 1.2 mm, falling onto a very small area.

The mechanism by which the 14 kHz peak is produced has been discussed by Nystuen, who claims that it is caused entirely by the initial impacts of the drops. His computer simulations suggest that the initial impact spike should have a width of about 60 μs and should therefore contain a large frequency component at 1 / 60 μs ~ 16 kHz. This explanation seems rather unlikely because the experimental results of Chapter III suggest that the spike is much narrower than 60 μs; the results described below show that this suspicion is confirmed.

To investigate the source of the 14 kHz peak, we begin by examining oscilloscope traces of the sound. Figure 35 shows a typical example; Fig. 36 shows an averaged FFT of many such traces.

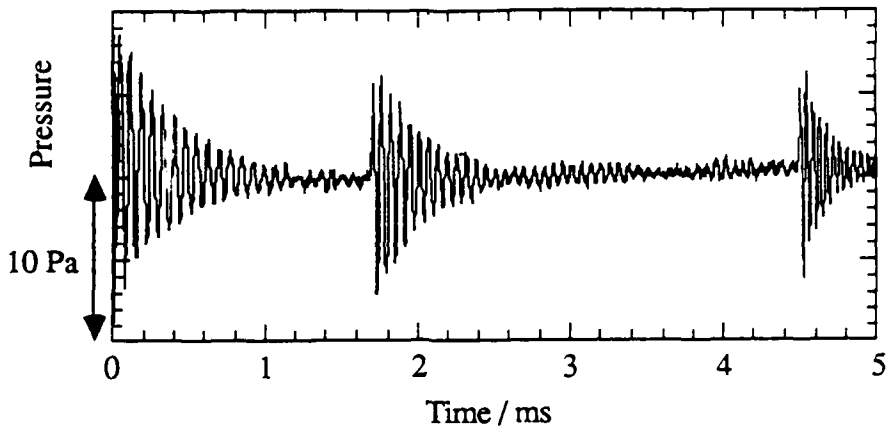

Fig. 35. Oscilloscope trace showing sounds of artificial rain. Note that the trace consists of a series of bubble-like oscillations.

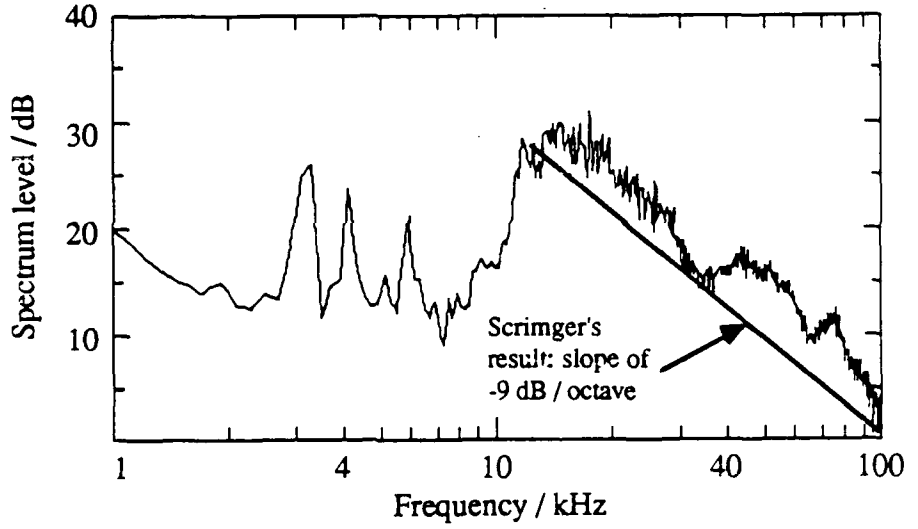

Fig. 36. Spectrum of artificial rain (spray #2). Note the 14 kHz peak and the -9 dB / octave slope on the high frequency side. The three large spikes between 2 kHz and 7 kHz are probably caused by large bubbles irregularly entrained by large drops; these can produce very large spectral peaks, especially if their frequencies are close to one or other of the tank resonances.

The FFT is a spectrum like those in Fig. 33, while the pressure trace is made up of a series of damped sinewaves. These seem to be produced by bubbles as they have the correct damping constants, in fact the sounds from a spray like this were used to obtain some of the damping data in Fig. 18.

Further proof that bubbles are the cause of the peak is provided by the sensitivity of the 14 kHz peak to surface contamination; Fig. 37 shows how the spectrum varies with concentration of a detergent.

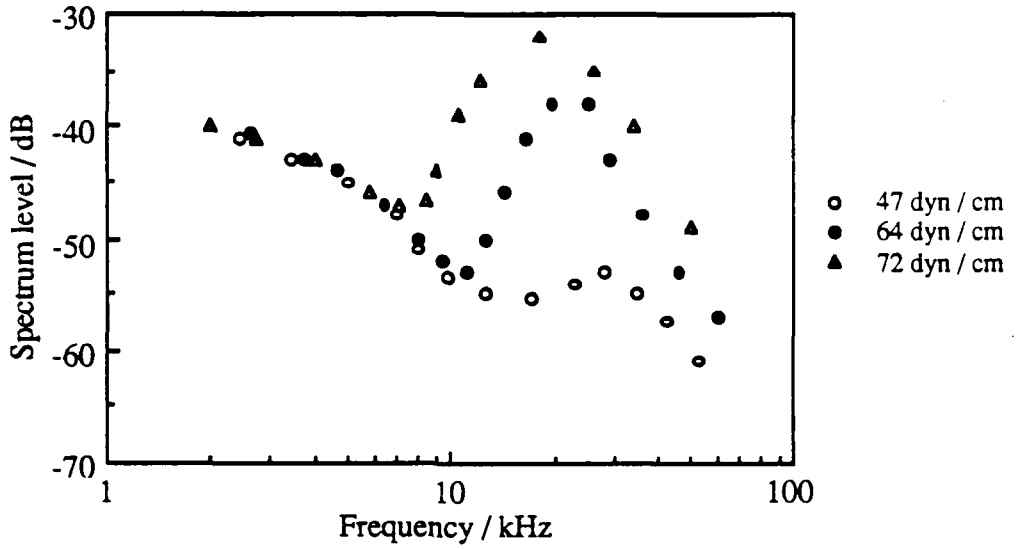

Fig. 37. Dependence on surfactant concentration of the 14 kHz peak. The surfactant used was Kodak Photoflo, which was added in various concentrations, lowering the measured surface tension from the clean-water value of 72 dyn / cm.

It is plain that the surfactant prevents the peak from being produced and it seems likely that it does so by preventing regular entrainment from occurring. We already know from Fig. 30 that a surfactant can have exactly this effect; we also know that it has little effect on the initial impact. It is therefore probable that the peak is caused by regular entrainment of bubbles; we must check to see if raindrops have suitable sizes and velocities.

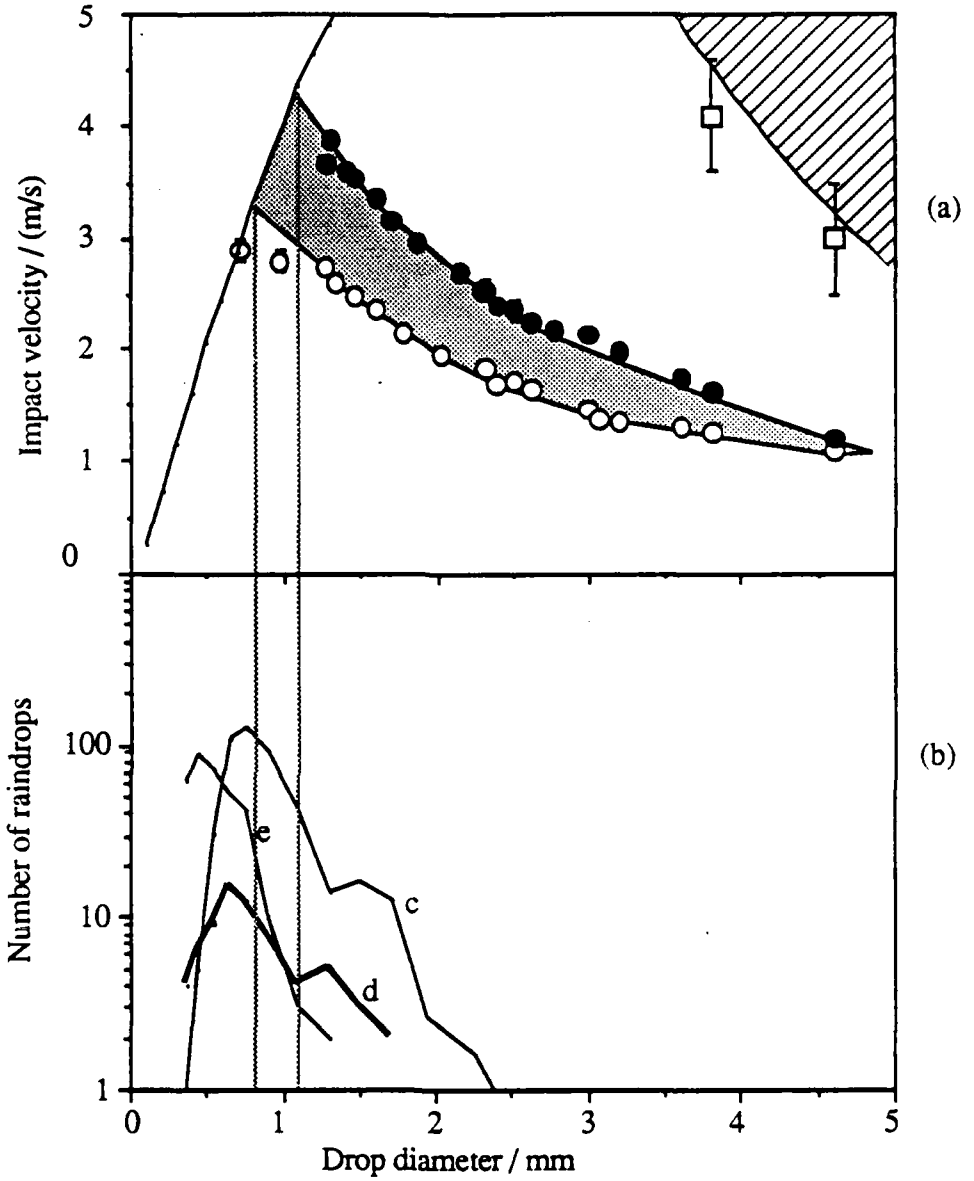

Fig. 38. Part (a) is the same as Fig. 24 and shows the range of drop diameters and velocities for which regular entrainment occurs. The curve at the left hand side is the terminal velocity curve for raindrops; it lies within the regular entrainment region for drop diameters between 0.8 and 1.1 mm. The two vertical dotted lines are drawn at these values of the drop diameter.

Part (b) shows drop size distributions for three rain showers [24]. The units on the ordinate are: number of drops in a 0.1 mm size range striking an area of 50 cm^2 in a time of 90 s. Note that all three showers have a large number of drops between the lines and hence in the regular entrainment region.

Figure 38 shows that some typical rain showers have many drops of the correct sizes to cause regular entrainment. The next question is what sizes of bubbles are entrained and how many of each size.

We begin with a brief qualitative description of the sizes of the entrained bubbles at the different points of the shaded region of Fig. 38. For impacts which are well inside the regular entrainment region, smaller drops give rise to smaller bubbles, although the decrease is less than proportional. For example, with a drop diameter of 4.3 mm and an impact velocity of 1.2 m/s, the entrained bubble has a radius of about 0.5 mm and a resonance frequency of about 6.5 kHz while a drop diameter of 2.25 mm and an impact velocity of 2.2 m/s produce a bubble of around 0.38 mm in radius with a resonance frequency of about 8.5 kHz. For a fixed drop size, as the impact velocity is increased so as to traverse the shaded region in the vertical direction, the bubble starts at a relatively small size, rapidly gets bigger, and decreases in size again near the upper boundary. This variation of the entrained bubble radius with impact velocity can be large, but is very rapid near the boundaries of the shaded region. Therefore, most of the bubbles produced by drops of a given diameter impacting at different velocities have more or less the same size.

This behavior is complicated and difficult to measure, so it was not possible to infer from it how many bubbles of a given size would be entrained by a spray of drops. Instead, this was measured by a computer which read data from the digital oscilloscope; it examined the sequence of damped sinuosoids (like in Fig. 35) and counted how many there were in each frequency band. Figure 39 shows typical results for artificial and real rain; in both cases we see that the number of bubbles entrained as a function of resonance frequency, f, is given by $n(f) = N / f^{\alpha}$, where α is approximately equal to 3.

Furthermore, both distributions show a peak between 11 and 15 kHz with a steep slope on the low frequency side. This is presumably because there is an upper limit on the size of bubbles which can be entrained by drops of a particular size; we know that only drops in the size range 0.8 - 1.1 mm are entraining bubbles here.

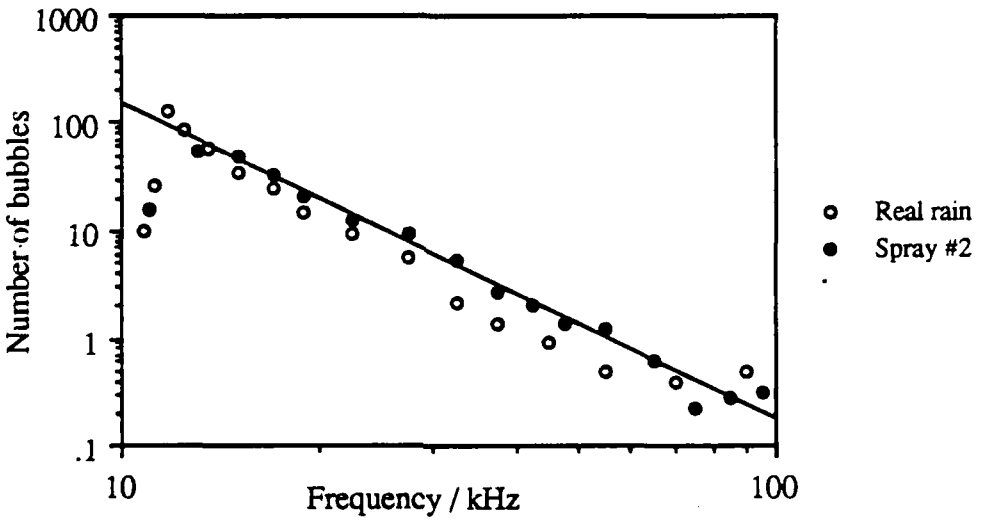

Fig. 39. This graph shows how the number of bubbles entrained in a certain time varies as a function of their resonance frequency. The two data sets are superimposed because the computer was programmed to take data until the total number of bubbles reached a pre-set value. Although this graph gives the form of n(f), it does not tell us the absolute value as a function of rain rate.

B. Theoretical prediction of rain spectrum

We now use this result to predict the spectrum intensity level of rainfall. If rainfall noise is bubble-related, it will be caused by a distribution of many bubbles over the ocean surface. It was mentioned in the introduction that the acoustic pressure of a near-surface bubble is given by:

$$p = \frac{D}{r} e^{-\beta(t-r/c)} \cos\theta \, e^{i(\omega t - kr)} \qquad (44)$$

The instantaneous intensity due to one bubble is given by

$$I(r,\theta,t) = \frac{p^2}{\rho c} = \frac{D^2 e^{-2\beta(t-r/c)}}{\rho c r^2} \cos^2\theta \cos^2(\omega t - kr) \quad (45)$$

We now integrate this over time from the moment that the bubble begins to oscillate to find E, the total energy flowing out through unit area:

$$E = \frac{D^2 \cos^2\theta}{\rho c r^2} \int_0^{\infty} e^{-2\beta\tau} \cos^2\omega\tau \, d\tau \quad , \quad (46)$$

where we have made the substitution $\tau = t - r/c$. This integration can be done by standard analytical techniques; the result is:

$$E = \frac{D^2 \cos^2\theta}{2\rho c r^2} \left(\frac{1}{2\beta} + \frac{\beta}{2(\beta^2 + \omega^2)} \right) . \quad (47)$$

For bubbles, where Q>6, it turns out that the second term is less than 0.6% of the first and may be ignored, leaving the result:

$$E = \frac{D^2 \cos^2\theta}{4\beta\rho c r^2} . \quad (48)$$

The spectrum level is defined to be the intensity due to sound in a 1 Hz bandwidth. To calculate this, we will assume that n(f) bubbles per second with resonance frequencies in that 1Hz bandwidth are entrained and begin to oscillate over a unit area of the water surface. The intensity dI_T at a hydrophone, which is caused by bubbles entrained over an infinitesimal area dA is given by

$$dI_T = n(f)\, E\, dA = \frac{n(f)\, D^2 \cos^2\theta}{4\beta\rho c r^2} dA . \quad (49)$$

We find the total intensity I_T at the hydrophone by integrating dI_T over the whole surface.

The setup is shown in Fig. 40, our infinitesimal area dA is a circular ring of radius R on the water surface; $dA = 2\pi R dR$.

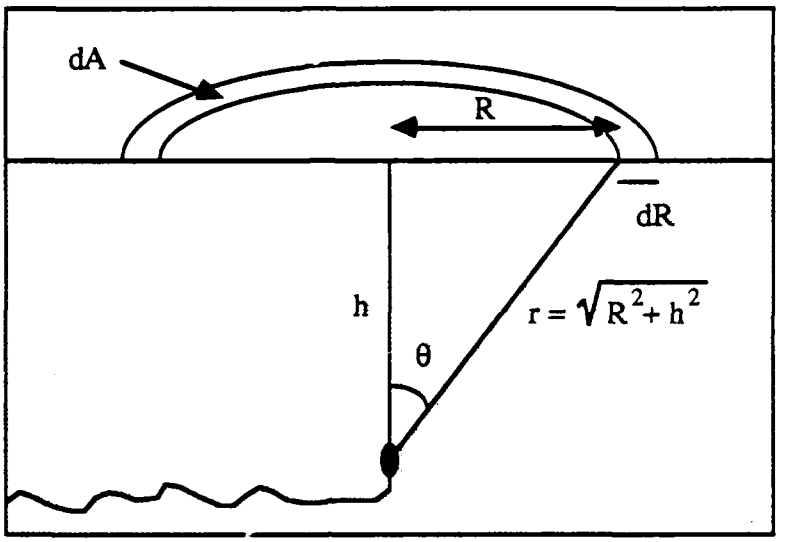

Fig. 40. Sketch to show how integration is done to find intensity at the hydrophone due to bubbles oscillating over the whole ocean surface.

Substituting for cos θ leads to the integral

$$I_T = \frac{n(f)\, D^2}{4\beta\rho c} \int_0^{\infty} \frac{h^2}{(R^2+h^2)^2} 2\pi R\, dR \,, \tag{50}$$

which gives us

$$I_T = \frac{\pi n(f)\, D^2}{4\beta\rho c} \,. \tag{51}$$

The intensity spectrum level (ISL) is defined as

$$ISL = 10 \log_{10} \frac{I_T}{I_{ref}/1\ Hz}, \tag{52}$$

where I_{ref} is a reference intensity, we shall take I_{ref} to be an intensity such that the acoustic pressure is 1 μPa. Inserting I_T from Eq. (51) gives the final result:

$$ISL = 10 \log \frac{\pi n(f)\, D^2/4\beta}{1\mu Pa^2/Hz}. \tag{53}$$

C. Comparison with experiment

In order to calculate ISL we need three pieces of information. We cannot obtain all of these theoretically, but we have measured all of them and will use the measured values. The spectra thus obtained are not truly theoretical, but are simply the result of taking the process to pieces, measuring each of the contributing parts, and using Eq. (53) to put them back together. The three things we need are:

1). The initial dipole strength of a bubble as a function of frequency. We obtain this from a fit to the data of Fig. 23; a fit of the form D = A + B log (f) was used.

2). The damping constant β as a function of frequency. We use the best fit to the data from spray #2 shown in Fig. 18; this agrees closely with theory and is easier to calculate.

3). The number of bubbles, n(f), entrained per second in a 1 Hz frequency band over a unit area of the surface. The form of n(f) is shown in Fig. 39, but the actual value is different for every rain shower. We therefore need simultaneous measurements of n(f) and spectrum level. These can be obtained from the data of Scrimger et al. [24], who give drop size distributions in units of "number of drops in a 0.1 mm size range striking an area of 50 cm^2 in a time of 90 s" (The 50 cm^2 is the area of their disdrometer, 90 seconds is the time over which they averaged the data, this was actually presented in three 30 s lots which I

added together). We select from this data the number of drops with diameters between 0.8 and 1.2 mm and divide this figure by 90 s and by 0.005 m^2 to give n_T, the total number of drops in the active size range impacting unit area in one second and hence also the total number of bubbles entrained over the same area per second. Note that we are forced to use the range 0.8-1.2 rather than 0.8-1.1 because of the way Scrimger's data was taken and presented. Now, n_T is the integral of n(f) over all frequencies, and if we assume, on the basis of Fig. 39, that no bubbles have resonance frequencies below a cutoff frequency f_p and that above f_p, n(f) is given by $n(f) = N / f^3$, we can write

$$n_T = \int_{f_p}^{\infty} n(f)\, df = \int_{f_p}^{\infty} \frac{N}{f^3}\, df = \frac{N}{2f_p^2} \tag{54}$$

and hence

$$n(f) = \frac{2n_T f_p}{f^3} \tag{55}$$

This result was substituted into Eq. (53) to give

$$ISL = 10 \log \frac{\pi n_T f_p^2 D^2 / 2\beta f^3}{1\mu Pa^2/Hz}, \tag{56}$$

which is plotted in Fig. 42 for two values of n_T. Scrimger et al. present spectra taken at the same time as the drop size distributions; these are plotted for comparison.

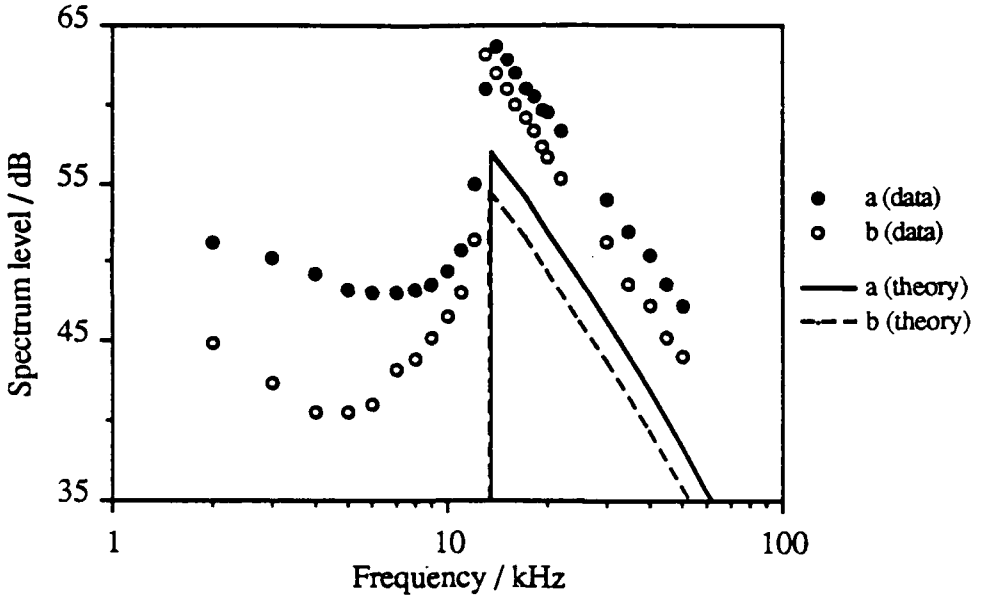

Fig. 41. This graph shows spectra a and b from Scrimger et al. [24] and the theoretical predictions, given their drop size distributions, of Eq. (56). The dB reference level is 1 μPa^2 / Hz.

It is clear that the theory predicts the shape of the spectrum well and also the amount by which it gets louder as n_T increases. The big problem is that the predictions are all about 7 dB too low; this is probably due to reverberations in the lake. There is some evidence for this explanation to be found in the wind noise curves which Scrimger et al. present for the same location as their rain noise spectra. They compare these with the Knudsen [3] curves and find a good agreement, hence we conclude that the acoustic environment in the lake is similar to that in the parts of the sea where Knudsen's measurements were made. Now, Knudsen's data were all taken in shallow seas and if they are compared with data from deep oceans it is found that, in general, ambient noise in shallow water is about 5 dB louder than that in deep water . The calculation of rain noise spectra which we have made in this paper assumes that the water is infinitely deep; we might make a crude attempt to adapt it to shallow water by adding 5 dB to the result. This would bring the calculated results to within 2 dB of Scrimger's naturally measured ones. A more accurate calculation

requires detailed knowledge of the acoustic properties of the lake, particularly the reflection coefficient of the lake bottom. In addition, recent work [45, 46] reports that differences in acoustic properties of the site can cause the ambient noise in comparable weather conditions to vary by as much as 10 dB. There are other possible sources of the discrepancy; some of it is probably due to inaccuracy in the measurement of D, shown in Fig. 22, but this could not account for all 7 dB. We also know nothing about the accuracy of Scrimger's values of $\dot{n}_T$.

Spectra a and b were taken in calm conditions; Fig. 42 shows a similar comparison for spectra c and d which were taken with a wind blowing, note that the peaks are more rounded. Note also that for spectrum d the prediction is about 7 dB too low, except near the peak. Spectrum c was taken in heavier rain and wind; it does not have the same slope as the other spectra, nor does it show the same 7 dB discrepancy with the theory. This is in agreement with other measurements [25, 47] which show quite clearly that the 14 kHz peak is sensitive to wind speed and may be reduced by 5 dB by a wind of 5 m/s.

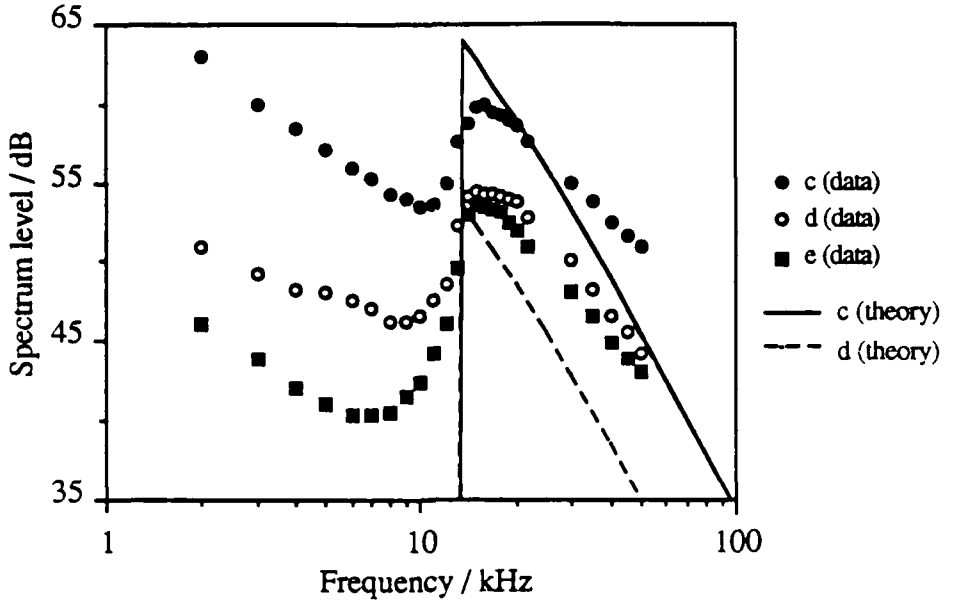

Fig. 42. This graph shows spectra c, d and e from Scrimger et al. [24] and the theoretical predictions for c and d, given their drop size distributions, of Eq. (56). The dB reference level is 1 μPa^2 / Hz.

Why does wind have these effects? Wind does two things, it blows the drops sideways and it creates waves on the surface; the end result being that the drops do not strike the surface at right angles. It is difficult to study this effect systematically in the laboratory, but high speed movies of the process seem to suggest that oblique incidence will partly eliminate the regular entrainment process. If this is so, it would explain the fact that wind reduces the 14 kHz peak.

So far, we have shown that the 14 kHz peak is caused by regular entrainment of bubbles by drops in a certain range of sizes. Rain produces quite a large amount of sound at lower frequencies which is presumably caused by some other mechanism. Published data seems to indicate that this sound is correlated with the presence of large raindrops while the peak is correlated with drops in the 0.8-1.1 mm size range. A typical example is provided by Scrimger's spectra c, d and e shown in Fig. 42 and the corresponding drop size distributions shown in Fig. 38b. At a frequency of 15 kHz, d and e have the same

spectral level, whereas at 5 kHz d is much louder. This suggests that they should have similar numbers of drops in the 0.8-1.1 mm range of sizes and that d should have more large drops. Figure 38b shows that this is indeed the case. Shower c has more drops than d or e for all drop diameters above 0.6 mm and its spectrum is therefore louder than d or e at all frequencies. Shower e has the most drops with diameters less than 0.6 mm and yet has the quietest spectrum. It therefore seems likely that these very small drops have little effect on the sound produced. The larger drops could produce sound by two mechanisms: the initial impact sound and irregular (Franz) entrainment of bubbles; it seems likely that both contribute to some extent and possibly in different ways. Irregularly entrained bubbles are usually quite large and would contribute most at frequencies below the peak, as described above. The initial impacts are very narrow spikes and therefore will give a very broad spectrum, almost like white noise, which would tend to swamp out the peak.

We have succeeded in describing in a fair amount of detail how rain makes the sound that it makes, but this sound is very unlike the Knudsen spectrum which we would like to explain. It was clear that some further experiments were necessary; these are described in the next chapter.

CHAPTER VI: SOUNDS FROM OTHER PROCESSES

A. Experimental results

1. Breaking Waves

So far, we have studied the sound made by drop impacts and have used the results to explain the sound made by rainfall on the ocean. We now turn to the Knudsen spectrum, i.e. the sound made by wind and waves at the ocean surface. To a certain extent, this must be due to drop impacts because a strong wind can lift spray from the crest of a breaking wave; the spray can then fall onto the surface. It is clear, however, that this is not the only mechanism which takes place because the Knudsen spectrum persists at wind speeds which are too low to cause spray. As mentioned in the introduction, breaking waves are the most likely candidates, so it seemed logical to try to make one in the laboratory. Real breaking waves are travelling waves, which makes them difficult to duplicate, so a standing wave was used, i.e. the water was allowed to flow, while the wave stayed still. The wave was in a small plexiglass trough 37 mm wide and 0.4 m long and was caused by water passing over an obstruction in the trough. The whole wave channel was placed in the large water tank in order to provide a large body of water in which to detect the sound. Figure 43 shows a typical pressure trace; it is made up of many bubble-like oscillations.

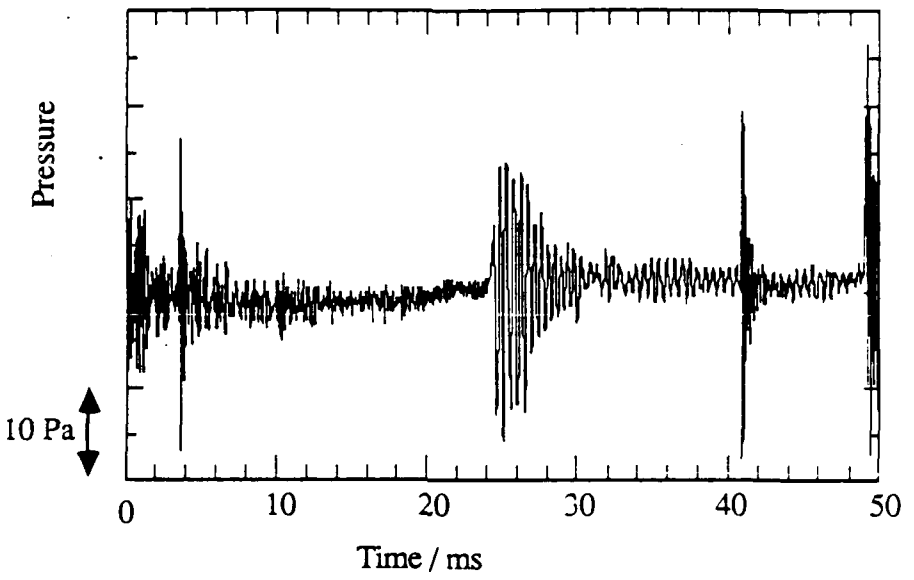

Fig. 43. Typical sound traces produced by an imitation laboratory breaking wave.

In order to confirm that the sound of the breaking wave is in fact due to bubbles, a high-speed movie was made of it; Fig. 44 shows two sequences of bubbles being entrained, taken from this film. It can be seen that the sound is produced at the moment when a bubble is formed, just as in drop impacts. Once this has happened, the bubble is silent thereafter, as found by Banner and Cato [48]. The wave is certainly a good model of the processes which make the sound of a babbling brook or creek; the result that the sound is due to bubbles agrees with the work of Leighton and Walton [39] and the observations of Bragg [49]. If this wave were a good model of real ocean surface processes, we could conclude that the Knudsen spectrum was mainly due to free oscillations of newly entrained bubbles. To see whether this was a good assumption, an averaged spectrum of the wave sound was taken for comparison with the Knudsen spectrum; it is shown in Fig. 45.

Fig. 44 (over page). Frames from a high speed movie of a laboratory breaking wave. A shallow stream of water is flowing from right to left over a horizontal cylindrical obstacle into deeper water. Frames a to e are a consecutive series at intervals of 1 ms, as are frames f to j. In both cases the trace is a straight line until a bubble is formed, at which point oscillations begin to occur. Unfortunately, the trace on the original film was rather faint and it was necessary to touch it up to ensure good reproduction; in frame g it was completely invisible so even this was not possible. Frequencies of bubbles from this film are plotted as a function of their diameters in Fig. 16.

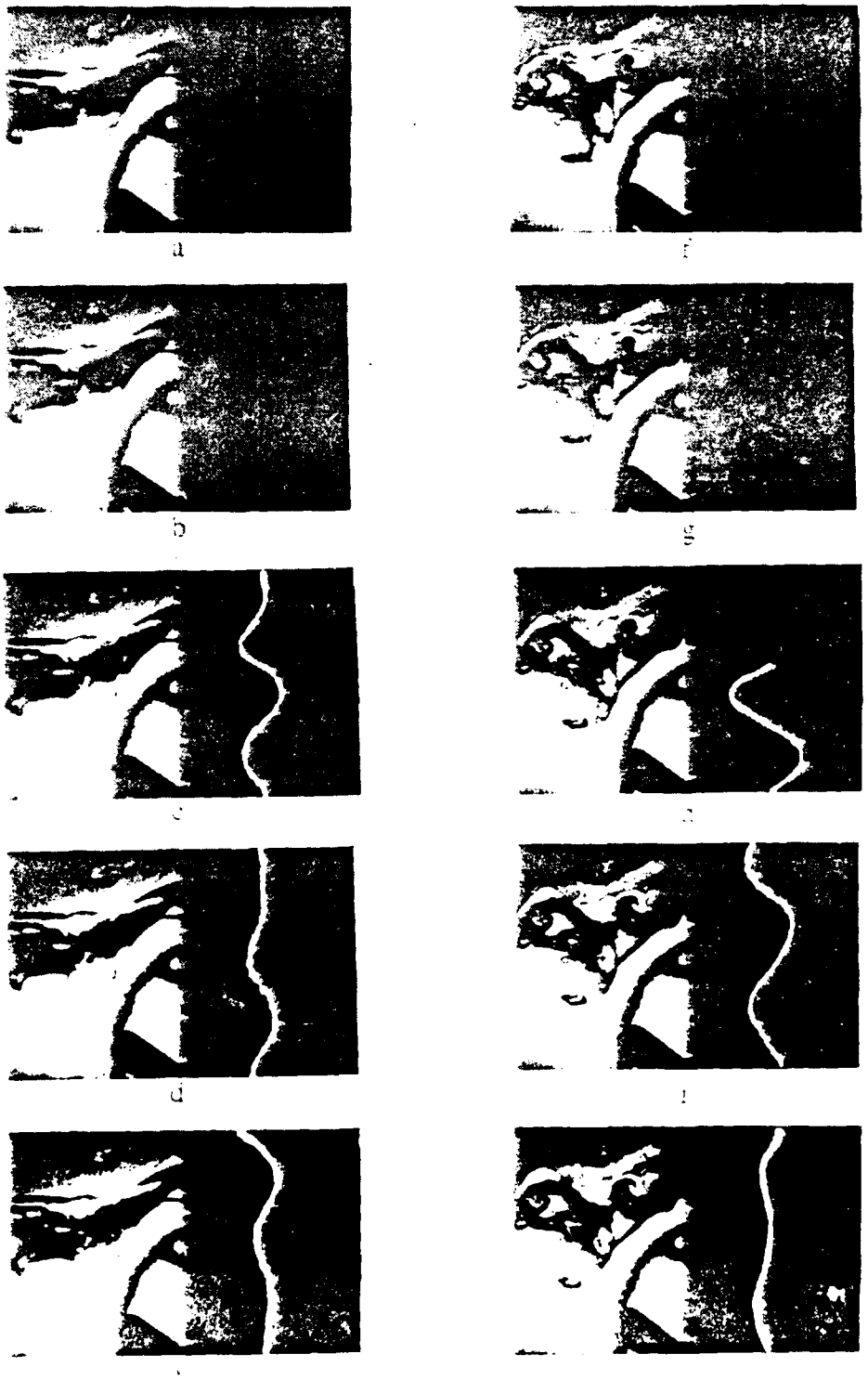

Figure 44.

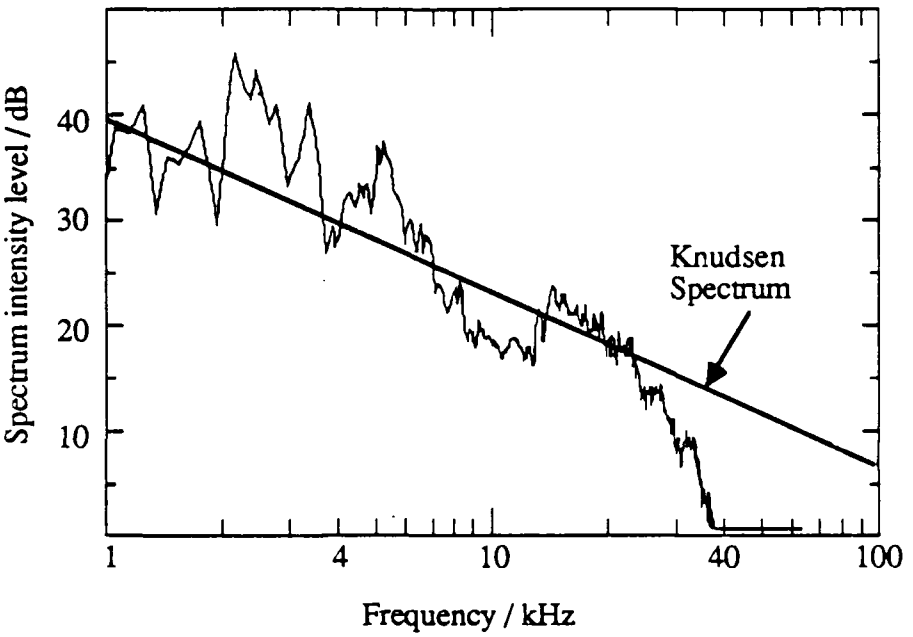

Fig. 45. Spectrum from a lab. breaking wave.

The result is not really conclusive, at higher frequencies it seems to have too great a slope, while at low frequencies the spectrum is confused by resonances of the tank.

One large difference between this wave and a real one is that in this wave the bubbles are formed, radiate, and are then carried away rather rapidly; in a real wave it seems likely that they might remain in the active part of the wave for a longer time and perhaps be made to oscillate again.

2. Interaction of bubbles and turbulence.

In order to study ways in which an already entrained bubble might produce sound, some experiments were done in which bubbles were allowed to rise from a hypodermic

needle into a submerged jet of water. If the water was flowing fast enough, the bubbles broke up as they entered the jet and radiated a lot of noise in the process; Fig. 46 shows a pressure trace of this process.

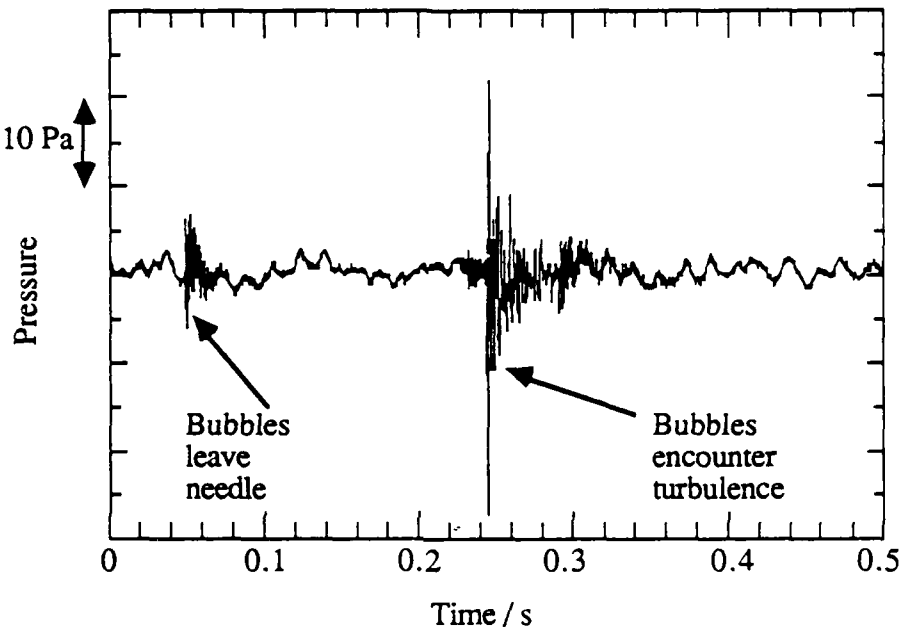

Fig. 46. Sounds of bubbles leaving a hypodermic needle, floating up for a while, then encountering a turbulent jet.

Fig. 47 shows frames from a high-speed movie of this process. Note that the bubbles produce a typical damped sinewave as they leave the needle, and that the sound that they make upon breaking up has many higher frequency components.

Fig. 47 (over page). High speed pictures of bubbles being formed at a nozzle and broken up by a submerged jet of water. Frames a to g show the bubbles being formed; in frame a one bubble is detached and floating upwards while the other is still attached to the needle. In frame b, a small fragment breaks off the upper bubble; the fragment was too small to reproduce onto the figure and could only just be seen on the original film. The oscilloscope trace shows an oscillation of about 25 kHz from which we calculate the diameter of the fragment to be 0.3 mm. This process is not common, but we might expect it to occur occasionally in nature when large bubbles are formed in non spherical shapes. In frames c through g, the lower bubble detaches itself from the needle; it seems to do this in two stages as an oscillation begins in frame c while a new and louder one of a similar frequency begins in frame f. In frames d and e one can see what looks like a small bubble emerging from the nozzle below the main one; this appears to join on to the main bubble before frame f. The measured diameter of the lower bubble is 2.0±.2 mm and the measured oscillation frequency is 2.0±.1 kHz; Minnaert's equation gives a frequency of 3.2±.2 kHz. (The bad agreement is probably systematic error in measuring the bubble size; there was no object of known size at the same distance from the lens as the bubble so the scale on the tank wall was used. The bubble is further away than this and therefore appears smaller than it really is.)

Frames h-n show the bubbles encountering the turbulent jet, which is flowing horizontally from left to right. In frame h, the upper bubble is feeling the influence of the jet but is not emitting any sound yet. In frame h, it begins to emit a sound which is composed of two sinusoidal oscillations, one of 2 kHz and one of 12 kHz; presumably a small bubble has been broken off the original one and both fragments are oscillating at their resonance frequencies. The small bubble can not be seen, presumably it is behind the large one. This process is repeated somewhat more clearly in frames j to n. In frames j and k the jet pulls a thin filament of air from the second bubble from the left, in frame l this has snapped off to form a small fragment. The fragment is just visible on the original film, but has not reproduced well onto the figure. As in frame j we see oscillations at two frequencies, one from the small fragment and one from the large; the frequencies are approximately 2.5 kHz and 12 kHz.

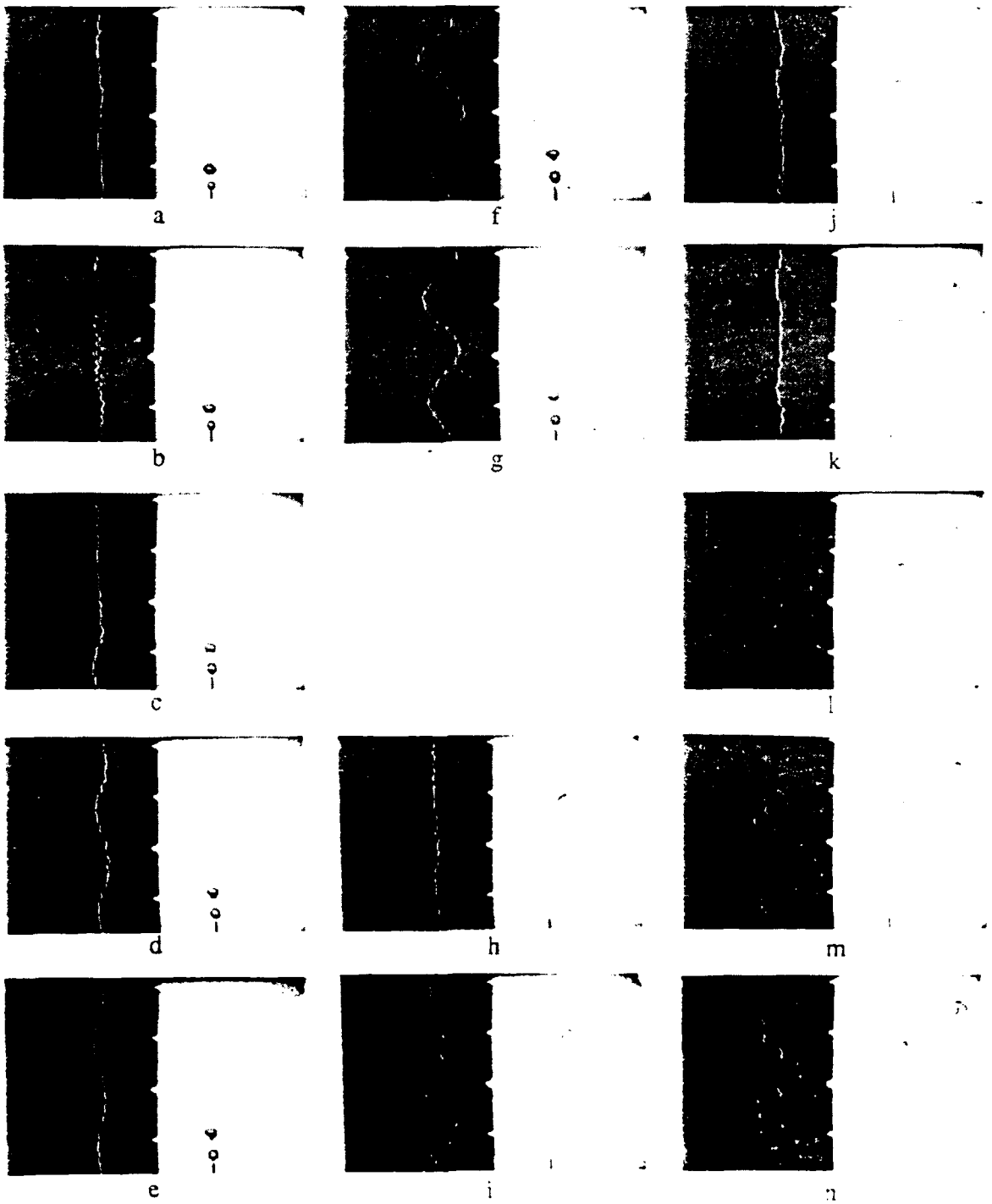

Figure 47.

This is also clear from the spectra of Fig. 48, note that when breaking up, the bubbles can emit any frequency which is higher than their original resonance frequency, but that they produce little sound below this frequency.

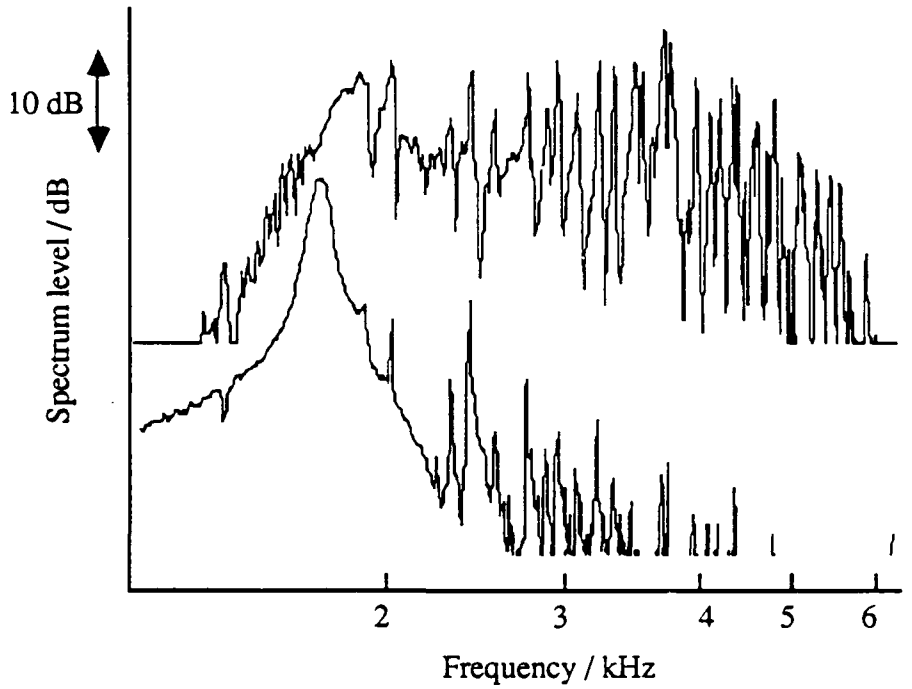

Fig. 48. Spectra of bubbles leaving a needle (below) and breaking up in turbulence (above). The spectra had about the same peak level and have been separated vertically for clarity. The large number of sharp spikes between 2 and 6 kHz are resonance frequencies of the tank.

What presumably is happening here is that the bubbles are breaking into fragments each of which must be smaller than the original bubble and must therefore oscillate at a higher resonance frequency. In Fig. 49 the bubble breaking spectrum of Fig. 48 is shown over a larger frequency range; it has a slope of about 10 dB per octave.

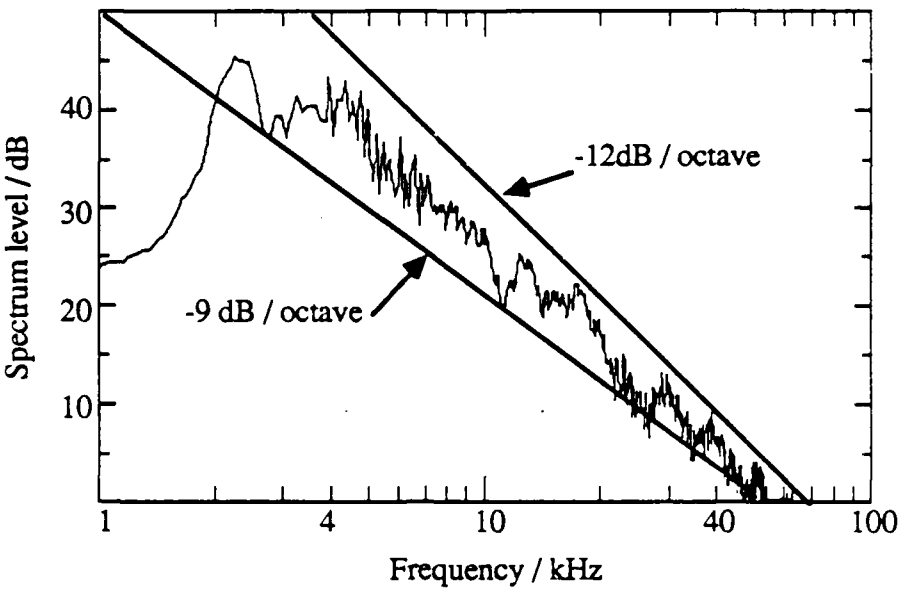

Fig. 49. Spectrum of bubbles being broken up by turbulence.

Another question is: is it necessary for the bubbles to be broken up for them to be excited by the turbulent jet? In order to find out, the jet was slowed down so that it was just too slow to cause breakup. The result, shown in Fig. 50, is that the bubbles emit a small amount of sound at their resonance frequency, this sound is about 20 dB quieter than the sounds they make upon leaving the needle or breaking up.

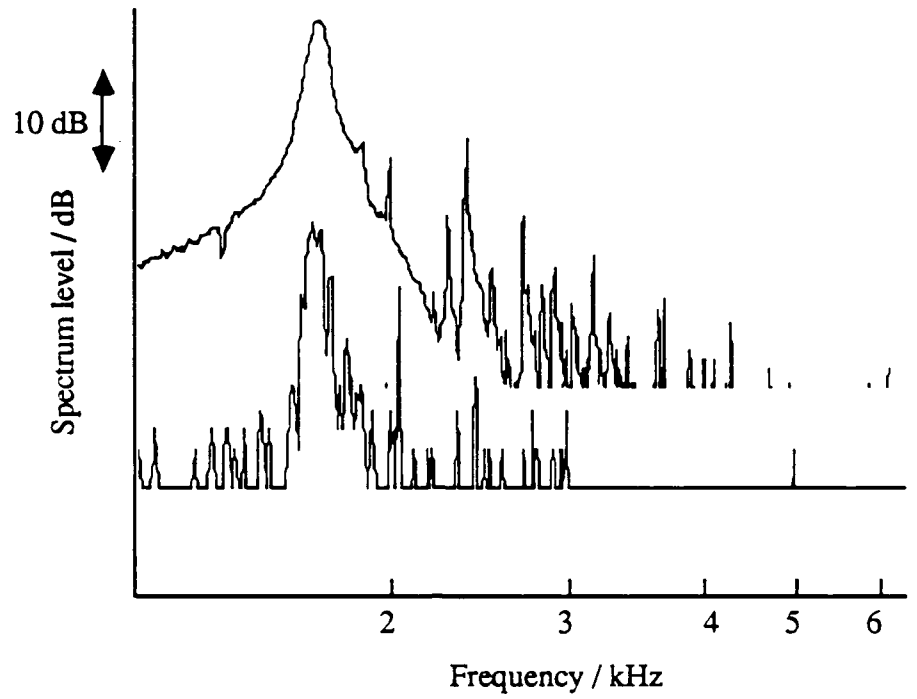

Fig. 50. Spectra of bubbles leaving needle (above) and passing through turbulence but NOT breaking up (below). The 20 dB difference between the two spectra is real.

The conclusion we draw from this is that in an environment where the turbulence is sufficiently violent to excite the bubbles noticeably, it is also violent enough to break them up; a process which produces far more sound than the direct excitations.

B. Discussion

What can we infer from these results? The most obvious thing is that more work needs to be done; this will be discussed further in the final chapter. The above results enable us to draw some conclusions, however, the most important being that a large part of the Knudsen spectrum is produced by bubble oscillations and that the important mechanisms for exciting the bubbles are their entrainment and breakup, with entrainment

being the most important, especially at low wind speeds and sea states. This hypothesis is at variance with many others, so we now proceed to look in detail at the various hypotheses and how well they agree with the data.

Ffowcs Williams and Guo [15,16] have argued that bubbles are not important and that splashing of sprays is the dominant mechanism; this theory seems rather unlikely for two reasons. Firstly, as has already been pointed out, their reason for dismissing bubbles is not valid; reflections from the free surface do reduce the radiated sound but do not eliminate it completely. Secondly, the Knudsen spectrum persists at sea states as low as force 1 on the Beaufort scale (wind speed approximately 1.5 m/s), while spray is not produced in large amounts by winds of force 5 (8-10 m/s) or below. We shall therefore assume that bubbles are important and look at various excitation mechanisms.

The first thing we note about most writings on this subject is that most theories tend to note a difference between high and low wind speeds, low meaning force 0-3 on the Beaufort scale i.e. a wind speed below about 5-6 m/s. This is approximately the speed above which extensive whitecapping occurs [50]. Shang and Anderson [13] propose two mechanisms for sound production at low wind speeds: bubbles cavitating and bubbles popping at the surface. The latter idea is a tentative suggestion and is not borne out by experiment. The popping process is very quiet and most of the sound is emitted into the air; the part going into the water is so faint that it is almost impossible to detect. Cavitation has frequently been suggested as an ambient noise source, but there is no experimental evidence for it, and Prosperetti and Lu [17] have shown theoretically that it cannot occur in the ocean because the turbulent pressure variations are not large enough.

For high wind speeds, high enough to cause whitecaps, Kerman [10] has developed a model which is based on what he calls weak cavitation; that is, bubble oscillations which

are large enough to be non-linear. He assumes these motions to be forced by the violent turbulence present in a whitecap. This mechanism is again at variance with Prosperetti's insistence that cavitation is impossible in an ocean environment and also with the experimental results described above. These suggest that if the turbulence was violent enough to force the radial oscillations of the bubbles to any noticable extent, it would be accompanied by shear forces strong enough to break the bubbles up. Prosperetti [18] himself has put forward an alternative theory which at high frequencies is based on free oscillations of newly-entrained bubbles, as observed in the breaking wave experiment described above. He is reluctant to extend this mechanism to the low-frequency end of the Knudsen region as the bubbles involved would be extremely large, proposing instead that what we are seeing here are collective oscillations, i.e. the coupled oscillations of a group of bubbles. This is plausible at higher wind speeds, when many bubbles are entrained very close to each other to form whitecaps. At low wind speeds, where whitecaps do not form, we must assume that the bubbles are entrained by waves which break very slightly, but not enough to form a whitecap. This process has been observed by Rohr et al. [51] and named microbreaking; their description of it suggests it to be a similar process to that observed in Fig. 45. The only problem is that the Knudsen spectrum tends to peak at 500 Hz and is probably significant down to 200 Hz. This would require many bubbles of 1.2 cm diameter and a few as large as 3.2 cm; we have to ask if this is impossibly large, if microbreaking entrains bubbles close enough together to make collective oscillations significant and if proximity to the surface will lower the frequency by very much. If the bubble center is less than a diameter away, the resonance frequency may be lowered by 15% or more, but this is not much and will be partly offset by the effects of non-sphericity. We are left with the two options of large bubbles or collective oscillations. The largest

bubbles seen in the film of Fig. 44 have diameters of 0.5 - 0.6 cm and therefore have resonance frequencies of 1.1 to 1.3 kHz; Monahan and Zeitlow [52] have observed similar though rather larger bubbles in a laboratory breaking wave. If free oscillations are the main source of the Knudsen spectrum we must assume that bubbles of twice this size and larger are entrained frequently in the sea. This may sound unlikely, but remember that the bubble only has to survive for 10 or 20 ms before breaking up and that even in calm conditions sea waves are larger than our lab wave. Experiments carried out in a swimming pool suggest that this last point is rather important and that waves which are not constrained to be 3 cm wide will entrain bubbles of several centimeters diameter.

It therefore seems most likely that the mechanism is the oscillation of entrained air bubbles as described in the above experiments. The low frequencies, around the peak of the Knudsen spectrum, are accounted for either by large bubbles being entrained, or by the lowering of resonance frequencies by the proximity of other bubbles, i.e. collective oscillations. The large bubble explanation seems to be the most likely of the two, especially at low wind speeds when few bubbles are entrained. The bubbles are mainly excited by their initial entrainment, especially at low sea states, but also by being broken up in high-shear turbulent flows such as occur in a whitecap. Direct forcing of the bubbles by turbulent oscillations probably also occurs, but is less important.

CHAPTER VII: CONCLUSIONS AND IDEAS FOR FUTURE WORK

This study has produced several interesting results and answered several questions, but it has also raised a number of new problems. The simple bubble dynamics described in chapter I have been largely confirmed: a near-surface bubble has the frequency and damping constant predicted by theory and it radiates as a dipole, much as we would expect. This in itself should prove useful to future workers in the field. The initial impact sound produced by a drop has proved less easy to understand; the present work does little other than to show that Franz's and Nystuen's theories are not adequate descriptions. It has, however been shown that the initial impact is not the cause of the now famous 14 kHz peak in the rain noise spectrum and that this feature is caused by bubble sounds. This has been studied in exhaustive detail and we may be sure that the conclusion is correct.

We have had less success in explaining the Knudsen spectrum, but several results point the way to a theory based on free oscillations of newly entrained or newly broken bubbles similar to that described by Prosperetti [18] or by Hollet and Heitmeyer [19]. The experiments tend to disagree with other theories, such as cavitation, spray impact or forced bubble oscillations. It is evident that there is more work to be done; we now proceed to discuss ideas for the future.

The drop impact process is now so well understood that there is little laboratory work to do on it. The only important thing which has not been studied is the effect of impact angle; the reason being that gravity is irritatingly effective at keeping water surfaces horizontal and making drops fall vertically. It would be nice to know how the regular entrainment region of Figs. 24 and 38 varied with impact angle and there are several possible ways of achieving this, such as blowing the drop sideways with a fan or making waves on the water. The difficulty is always that it becomes very difficult to measure the

impact velocity. High speed movies suggest that oblique incidence tends to prevent regular entrainment from occurring, which would explain Scrimger's observation that the 14 kHz peak is much reduced by wind; to go beyond this would probably take more time and effort than it was worth. Scrimger's real-rain data are fairly exhaustive; any further fieldwork would have to be done very carefully indeed to be worthwhile. In addition to measuring spectra, wind speed and drop size distributions, an experiment should have a hydrophone very close to the surface to study individual bubble traces and to measure D(f) and n(f) as described in chapters 4 and 6. It would also be necessary to make careful measurements of the amount of reverberation in the lake, so that theoretical predictions could be compared directly with experimental spectra. The data would have to be processed to look for correlations between the 14 kHz peak and drops in the 0.8-1.1 mm size range, and also for correlations between low frequency sounds and large drops; these would both be useful evidence for the bubble theory.

Much more work remains to be done on the Knudsen spectrum. The first priority is to set up a breaking wave in the laboratory which produces a better imitation of the sound of the real ocean than Fig. 45. It would then probably be possible to measure the average initial dipole strength D(f) and the number of bubbles n(f) as functions of frequency, just as was done for rain noise. The spectrum could then be calculated from Eq. (53) and compared with experiment. There are several reasons why this may be difficult to do, the most obvious being the size of tank required to work at the low frequencies required. If we need a depth of 0.75 m to work at 10 kHz, we need a depth of 15 m to work at 500 Hz; the depths are chosen to allow a bubble to oscillate 10 times before the reflected sound comes back from the bottom of the tank. The only alternative to a very deep tank is one which is anechoic; this is hard to achieve at low frequencies. A possible alternative is to do the

experiment at sea or in a lake; like the rain experiment suggested above one would use a hydrophone at a large depth to obtain averaged spectra and one near the surface to measure D(f) and n(f). The only disadvantage of this approach would be the reliance one would have to place on the weather.

To sum up, we have learned a great deal, but much remains to be done. I can only hope that the results described in this work will prove useful and interesting to both present and future workers in this field.

REFERENCES

1. R. J. Urick, *Principles of underwater sound*, (McGraw - Hill, 1983)

2. W. S. Burdic, *Underwater acoustic system analysis*, (Prentice - Hall, 1984)

3. V. O. Knudsen, R. S. Alford and J. W. Emling "Underwater ambient noise," Journal of Marine Research **7**, 410-429 (1948)

4. G. Wenz "Acoustic ambient noise in the ocean: spectra and sources," J. Acoust. Soc. Am. **34**, 1936-1956 (1962)

5. A. J. Perrone, "Deep ocean ambient noise spectra in the Northwest Atlantic," J. Acoust. Soc. Am. **46**, 762-770 (1969)

6. E. M. Arase and T. Arase, "Ambient noise in the deep and shallow ocean," J. Acoust. Soc. Am. **42**, 73-77 (1967)

7. M. S. Longuet - Higgins, Phil. Trans. Roy. Soc. (Lond.) **A243**, 1 (1950)

8. A. C. Kibblewhite, "Ocean noise spectrum below 10 Hz – Mechanisms and measurements," in *Sea Surface Sound*, edited by B.R. Kerman (Kluwer Academic Publishers, 1988), pp 337-360

9. H. W. Marsh, "Origin of the Knudsen spectra," J. Acoust. Soc. Am. **35**, 409-410 (1963)

10. B. R. Kerman, "Underwater sound generation by breaking wind waves," J. Acoust. Soc. Am. **75**, 149-165 (1984)

11. G. R. Fox, "Ambient-noise directivity measurements," J. Acoust. Soc. Am. **36**, 1537-1540 (1964)

12. E. M. Arase and T. Arase, "Ambient noise measurements in an insonified ocean," J. Acoust. Soc. Am. **56**, 703-705 (1974)

13. E. C. Shang and V. C. Anderson, "Surface-generated noise under low wind speeds at kilohertz frequencies," J. Acoust. Soc. Am. **79**, 964-971 (1986)

14. Y. P. Guo, "Sound generation in the ocean by breaking surface waves," J. Fluid. Mech. **181**, 329-347 (1987)

15. J. E. Ffowcs Williams and Y. P. Guo, "Mechanisms of sound generation at the ocean surface," in *Sea Surface Sound*, edited by B.R. Kerman (Kluwer Academic Publishers, 1988), pp. 309-324

16. J. E. Ffowcs Williams, "Sources of sound at the ocean surface; Bubbles and other noise," in *Sea Surface Sound*, edited by B.R. Kerman (Kluwer Academic Publishers, 1988), 617-620

17. A. Prosperetti and N. Q. Lu, "Cavitation and bubble bursting as sources of oceanic ambient noise," J. Acoust. Soc. Am. **84**, 1037-1041 (1988)

18. A. Prosperetti, "Bubble related ambient noise in the ocean," J. Acoust. Soc. Am. **84**, 1042-1054 (1988)

19. R. Hollet and R. W. Heitmeyer, "Noise generation by bubbles formed in breaking waves," in *Sea Surface Sound*, edited by B.R. Kerman (Kluwer Academic Publishers, 1988), pp. 449-461

20. G. J. Franz, "Splashes as sources of sound in liquids," J. Acoust. Soc. Am. **31**, 1080-1096 (1959)

21. N. Bom, " Effect of rain on underwater noise level," J. Acoust. Soc. Am. **45**, 150-156 (1969)

22. J. A. Scrimger "Underwater noise caused by precipitation, " Nature **318**, 647-649 (1985)

23. J. A. Nystuen "Rainfall measurements using underwater ambient noise," J. Acoust. Soc. Am. **79**, 972-982 (1986)

24. J. A. Scrimger, D. J. Evans, G. A. McBean, D. M. Farmer and B. R. Kerman, "Underwater noise due to rain, hail and snow," J. Acoust. Soc. Am., **81**, 79-86 (1987)

25. J. A. Scrimger, D. J. Evans and W. Yee, "Underwater noise due to rain - open ocean measurements," J. Acoust. Soc. Am. **85**, 726-731 (1989)

26. J. A. Nystuen and D. M. Farmer, "The sound generated by precipitation striking the ocean surface," in *Sea Surface Sound*, edited by B.R. Kerman (Kluwer Academic Publishers, 1988), pp. 485-500

27. M. Minnaert, "On musical air-bubbles and the sounds of running water," Phil. Mag. **16**, 235-248 (1933)

28. C. Devin, "Survey of thermal, radiation, and viscous damping of pulsating air bubbles in water," J. Acoust. Soc. Am. **31**, 1654-1667 (1959)

29. A. Prosperetti, "Bubble Phenomena in sound fields," Ultrasonics **22**, 69-77, 115-124 (1984)

30. A. Prosperetti, L.A. Crum and K. Commander, "Nonlinear bubble dynamics," J. Acoust. Soc. Am. **83**, 502-514 (1988)

31. A. Prosperetti, "Bubble dynamics in oceanic ambient noise," , in *Sea Surface Sound*, edited by B.R. Kerman (Kluwer Academic Publishers, 1988), pp. 151-172

32. M. Strasberg "The pulsation frequency of nonspherical gas bubbles," J. Acoust. Soc. Am. **25**, 536-537 (1953)

33. P. A. Crowther "Bubble noise creation mechanisms," in *Sea Surface Sound*, edited by B.R. Kerman (Kluwer Academic Publishers, 1988), pp. 131-150

34. L. E. Kinsler, A. R. Frey, A. B. Coppens, J. V. Sanders, *Fundamentals of Acoustics* (John Wiley & Sons, Inc., 1982)

35. J. E. Lane, "Microprocessor based rainfall distribution methods," (University of Mississippi internal report).

36. H. C. Pumphrey and L. A. Crum, "Acoustic emissions associated with drop impacts," in *Sea Surface Sound*, edited by B.R. Kerman (Kluwer Academic Publishers, 1988), pp. 463-484

37. H. C. Pumphrey, L. A. Crum and L. Bjørnø, "Underwater sound produced by individual drop impacts and rainfall," J. Acoust. Soc. Am. (Accepted for publication)

38. H. C. Pumphrey and L. A. Crum, "Free oscillations of near-surface bubbles as a source of underwater ambient noise," J. Acoust. Soc. Am. (Submitted for publication)

39. T. G. Leighton and A. J. Walton "An experimental study of the sound emitted from gas bubbles in a liquid," Eur. J. Phys. **8**, 98-104 (1987)

40. M. Strasberg, "Gas bubbles as sources of sound in liquids," J. Acoust. Soc. Am. **28**, 20-26 (1956)

41. M. S. Longuet-Higgins, "Monopole Emission of sound by asymmetric bubble oscillations," J. Fluid Mech., (in preparation)

42. O. G. Engel, " Crater depth in fluid impacts," J. Appl. Phys. **37**, 1798-1808 (1966)

43. G. D. Crapper, " An exact solution for progressive capillary waves of arbitrary amplitude," J. Fluid Mech. **2**, 532-540 (1957)

44. T. E. Heindsman, R. H. Smith and A. D. Arneson, "Effect of rain upon underwater noise levels," J. Acoust. Soc. Am. **27**, 378-379 (1955)

45. R. M. Hamson, "The effect of propagation conditions on wind-generated noise at real shallow water sites," in *Sea Surface Sound*, edited by B.R. Kerman (Kluwer Academic Publishers, 1988), pp. 281-293

46. F. Ingenito and S. N. Wolf, "Site dependence of wind-dominated ambient noise in shallow water," J. Acoust. Soc. Am. **85**, 141-145 (1989)

47. J. A. Nystuen and D. M. Farmer, "The influence of wind on the underwater sound generated by light rain," J. Acoust. Soc. Am. **82**, 270-274 (1987)

48. M. L. Banner and D. H. Cato, " Physical mechanisms of noise generation by breaking waves - a laboratory study," in *Sea Surface Sound*, edited by B.R. Kerman (Kluwer Academic Publishers, 1988), pp. 429-436

49. W. Bragg, *The World of Sound* (G.Bell and Sons, Ltd.,London, 1920)

50. E. C. Monahan, " Fresh water whitecaps," J. Atmos. Sci. **26**, 1026-1029 (1969)

51. J. Rohr, R. Glass and B. Castile, "Effect of monomolecular films on the underlying ocean ambient noise field", J. Acoust. Soc. Am. (Accepted for publication)

52. E. C. Monahan and C. R. Zeitlow, "Laboratory comparisons of fresh-water and salt-water whitecaps," J. Geophys. Res. **74**, 6961-6966 (1969)

53. Gunn, R. and G. D. Kinzer, "The terminal velocity of fall for water droplets in stagnant air," J. Met. **6**, 243-248 (1949)

54. Dingle, A. N. and Y. Lee, "Terminal fallspeeds of raindrops," J. Appl. Met **11**, 877-879 (1972)

55. F. H. Harlow and J. P. Shannon, "The splash of a liquid drop," J. Appl. Phys. **38**, 3855-3866 (1967)

APPENDIX A: THE VELOCITY OF A FALLING DROP

As a drop falls through the air, there are two forces on it: its weight and a drag force D which is a function of the velocity v. Applying Newton's 2nd law, we find that the drop's motion is governed by the equation:

$$m\frac{d^2z}{dt^2} = mg - D(v) \quad , \tag{1A}$$

in which m is the drop mass, z is the distance through which it has fallen and g is the acceleration due to gravity. We make the substitution dz/dt = v to get

$$mv\frac{dv}{dz} = mg - D(v) \quad , \tag{2A}$$

so that we can calculate v as a function of z. We begin by making the simplifying assumption that $D(v) = \alpha v^2$ from which we can find the terminal velocity v_T by setting the acceleration to zero, obtaining:

$$v_T = \sqrt{\frac{mg}{\alpha}} \quad . \tag{3A}$$

Substituting for D(v) in (2A) gives

$$mv\frac{dv}{dz} = mg - \alpha v^2 \tag{4A}$$

but it turns out more convenient to substitute for a because the mass then cancels, leaving

$$v\frac{dv}{dz} = g\left(1 - \frac{v^2}{v_T^2}\right) \quad . \tag{5A}$$

This is a differential equation of the "variables separable" type; separating the variables leads to:

$$\int_0^v \frac{vdv}{\left(1 - v^2/v_T^2\right)} = \int_0^z gdz \quad . \tag{6A}$$

Integrating both sides gives

$$\frac{-v_T^2}{2} \ln\left(1 - v^2/v_T^2\right) = gz \,, \tag{7A}$$

which can be solved for v, giving

$$v = v_T \sqrt{1 - \exp\left(-2gz / v_T^2\right)} \tag{8A}$$

which is the same as Eq. (9). In order to calculate v for a particular drop, we need to know v_T as a function of the drop diameter d. This could come from Eq. (3A) if we knew α, which we don't. Equation (3A) can be written as

$$mg = \tfrac{1}{8} \pi d^2 \rho_A C_d v_T^2 \,, \tag{9A}$$

where ρ_A is the density of air and C_d is the drag coefficient of a drop. Note that this means that our assumption is equivalent to assuming a constant drag coefficient, but this does not help us much if we don't know how big C_d is. Since most experimental measurements have measured v_T directly, the simplest approach seems to be to obtain v(z) by using experimental values of $v_T(d)$ in Eq. (8A) and this is what was done. The data used was that of Gunn and Kinzer [53], which agrees well with other measurements; v_T values were actually found from a polynomial fit to this data [54]. Some examples are shown in Fig. 1A together with some experimental data.

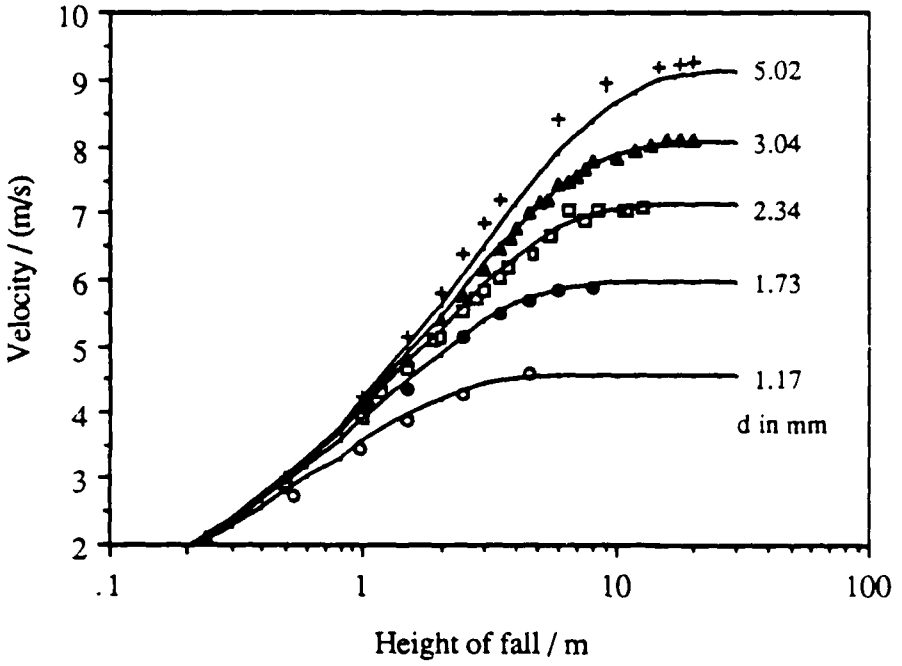

Fig. 1A. Shows plots of velocity v as a function of height of fall z for various values of drop diameter d. The data are those of Laws and are not very accurate; their terminal velocities differ slightly from Gunn and Kinzer's, especially at large values of d. They are, however, the only data available for v as a function of z, and the form of the approach to terminal velocity agrees very well with the theoretical curves.

APPENDIX B: COMPUTER SIMULATION OF DROP IMPACTS

There have been attempts in the past [23, 26, 55] to simulate drop impacts by using a computer to solve the equations of fluid mechanics with the relevant initial conditions, i.e. a liquid half-space with a sphere of liquid moving at some velocity in contact with it. These simulations had many features in common with real drop impacts but never showed bubbles being entrained, probably because the formulations used did not include the effects of surface tension. Recently, however, Prosperetti and Oguz have done some calculations for drop impacts within the regular entrainment region of Fig. 24 and have been able to show that regular entrainment does occur; this work had not been published when this dissertation was written. A typical set of their results are shown in Fig. 1B.

Fig. 1B (over page). This figure shows a numerical simulation of the behaviour of the water surface during the regular entrainment process. Each individual picture represents the shape of the surface at some time t which is shown (in arbitrary units) at the top of the picture. The pictures stop at the point when a bubble is created because the computer code cannot cope with multiple free surfaces.

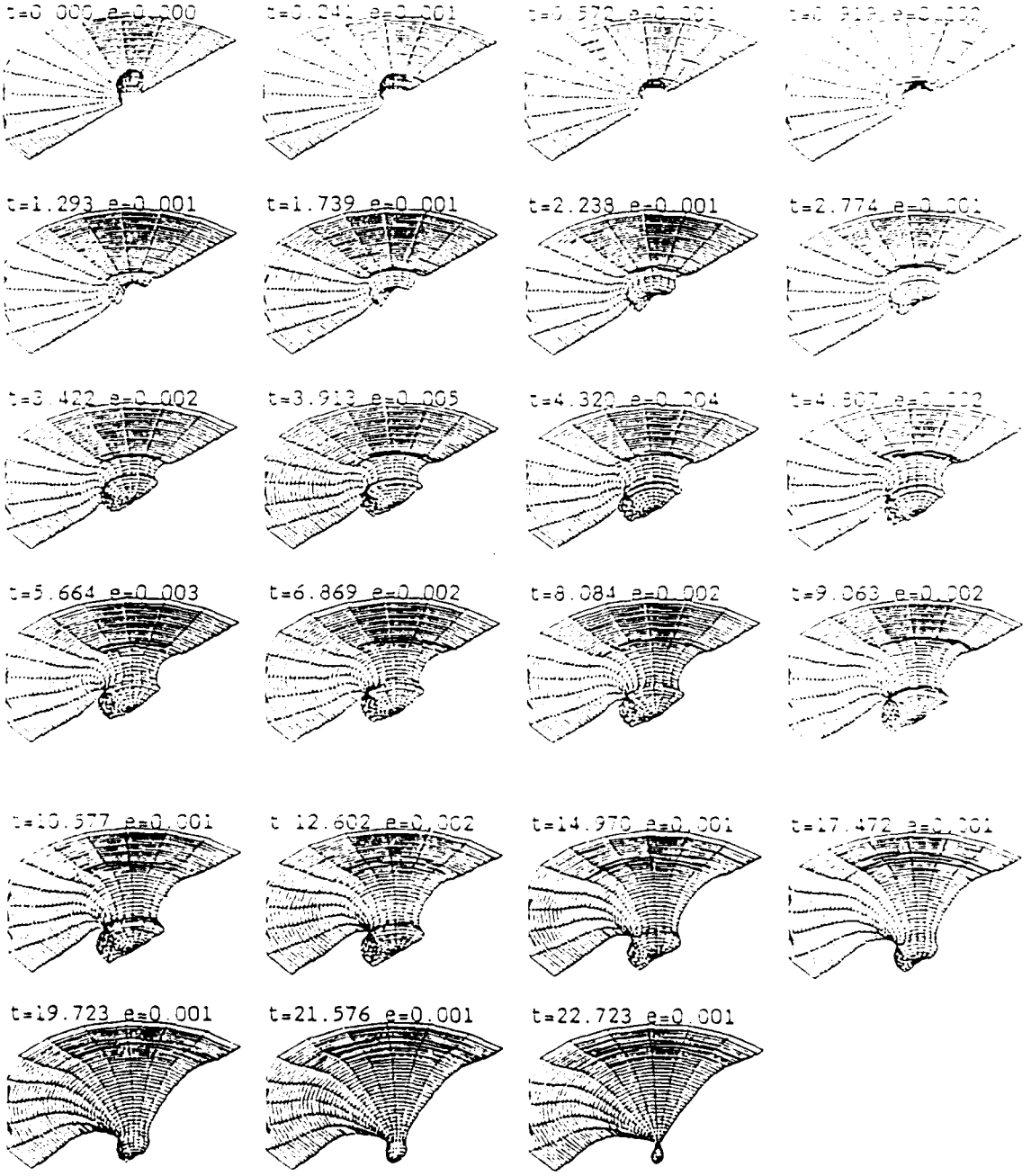
t=0.000 e=0.000
t=0.241 e=0.001
t=0.570 e=0.001
t=0.919 e=0.000
t=1.293 e=0.001
t=1.739 e=0.001
t=2.238 e=0.001
t=2.774 e=0.001
t=3.422 e=0.002
t=3.913 e=0.005
t=4.320 e=0.004
t=4.807 e=0.002
t=5.664 e=0.003
t=6.869 e=0.002
t=8.084 e=0.002
t=9.063 e=0.002
t=10.577 e=0.001
t 12.602 e=0.002
t=14.970 e=0.001
t=17.472 e=0.001
t=19.723 e=0.001
t=21.576 e=0.001
t=22.723 e=0.001

Figure 1B

BIOGRAPHICAL SKETCH OF THE AUTHOR

Full name: Hugh Charles Pumphrey

Date of Birth: 21 September 1964

Parents: Dr N. W. J. Pumphrey and Mrs R. Pumphrey

High school: Helsby County High School, Helsby, Warrington, Cheshire, England, 1976-1983. "O" levels 1981, "A" levels 1983

University: Jesus College, Cambridge, England, 1983-1986, B.A degree in Physics with first class honours, 1986.
University of Mississippi 1986-present. Ph.D Degree in Physics (expected) May 1989

Interests: The author enjoys sailing, camping and hiking and is interested in music. He plays the violin (badly) and has been a member of both the Helsby High School and the University of Mississippi orchestras. He also plays the guitar. He is keen on travel and has made a great effort to see as much of America as possible during his time on this side of the Atlantic.

Work experience: Has been involved in research since arriving at the University of Mississippi in 1986 and has in addition taught lab classes, recitation sessions and lectures.

Career objectives: The Author would like to work as a university lecturer as he enjoys both research and teaching.

Permanent Address: c/o Dr & Mrs N. W. J. Pumphrey,

120 Old Chester Road,

Helsby,

WARRINGTON

ENGLAND WA6 9PW

DISTRIBUTION LIST

1	Chief of Naval Research Office of Naval Research Department of the Navy Arlington, VA 22219 Attn: R. Fitzgerald (Code 1125UA)
2	Director Naval Research Laboratory Washington DC 20375 Attn: Library
3	Commander Space and Naval Warfare Systems Command Washington DC 20363-5101
4	Commander David Taylor Naval Ship Research and Development Center Target Physics Branch Bethesda MD 20084
5	Superintendent Naval Postgraduate School Monterey CA 93940 Attn: Steve Garret
6-10	Commanding Officer and Director Defense Technical Information Center Bldg. 5, Cameron Station 5010 Duke Street Alexandria VA 22314
11-20	Dr. L. A. Crum Associate Director of Basic Research National Center for Physical Acoustics University MS 38677
21-30	Dr. H. C. Pumphrey National Center for Physical Acoustics University MS 38677
31	Professor M. S. Longuet-Higgins Center for Studies of Nonlinear Dynamics LaJolla Institute 10280 N. Torrey Pines Road, Suite 260 LaJolla CA 92037

32 Professor J. E. Ffowcs Williams
Cambridge University Department of Engineering
Trumpington Street
Cambridge CB2 1PZ
United Kingdom

33 Dr. A. J. Walton
Cambridge University Physics Department
Cavendish Laboratory
Madingley Road
Cambridge CB3 0HE
United Kingdom

34 Dr. A. Prosperetti
Department of Mechanical Engineering
The Johns Hopkins University
Baltimore MD 21218

35 Dr. B. R. Kerman
Atmospheric Environment Service
4905 Dufferin Street
Downsview, Ontario, M3H 5T4
Canada

36 L. Bjørnø
Industrial Acoustics Laboratort
Technical University of Denmark
Building 425, DK-2800
LYNGBY, Denmark

37 P. Crowther
Marconi Underwater Systems Ltd.
Croxley Mill
WATFORD, Herts., WD1 8YR
United Kingdom

38 Dr. J. A. Nystuen
Code 68Ny
Department of Oceanography
Naval Postgraduate School
Monterey CA 93943

39 Dr. J. Rohr
Naval Ocean Systems Center
San Diego CA 92152

40 Dr. H. Medwin
Physics Department
Naval Postgraduate School
Monterey CA 93943

41 Dr. R. D. Hollet
SACLANT Undersea Research Centre
I19026 LaSpezia
Italy

42 Dr. D.M. Farmer
Institute of Ocean Sciences
P.O. Box 6000
SYDNEY, BC V8W 2Y2
Canada

43 Dr. O. M. Phillips
Dept. of Earth and Planetary Sciences
The Johns Hopkins University
Baltimore MD 21218

44 W. K. Melville
Massachusetts Institute of Technology
Cambridge MA 02139

45 Dr. E. C. Monahan
Marine Sciences Institute
University of Connecticut
Avery Point,
Groton CT 06340

46 Dr. S. A. Thorpe
Dept. of Oceanography
The University
SOUTHAMPTON SO9 5NH
United Kingdom

47 S. C. Ling
The Catholic University of America
Washington DC 20064

48 Dr. M. Y. Su
NORDA
NSTL MS 39529

49 Dr. S. T. McDaniel
The Pennsylvania State University
Applied Research Laboratory
University Park PA 16804

50 Dr. W. A. Kuperman
Naval Research Laboratory
Washington DC 20375

51 Dr. R. H. Mellen
Planning Systems Inc.
95 Trumbull Street
New London CT 06320

52 Dr. A. C. Kibblewhite
Department of Physics
University of Aukland
Private Bag
Auckland, New Zealand

53 Dr. W. M. Carey
Naval Underwater Systems Center
New London CT 06320

54 Dr. I. Dyer
Dept. of Ocean Engineering
Massachusetts Institute of Technology
Cambridge MA 02139

55 Dr. M. J. Buckingham
Royal Aircraft Establishment
FARNBOROUGH GU14 6TD
United Kingdom

56 Dr. D. Crighton
DAMTP
University of Cambridge
Cambridge
United Kingdom